MRI-BASED APPROACH FOR LONGITUDINAL MONITORING OF INTRALESIONAL THERAPY OF MSCS IN A LARGE ANIMAL MODEL OF TENDONITIS

by

ALEXANDRA MICHELLE SCHARF

(Under the Direction of JOHN PERONI and WILLIAM KISAALITA)

ABSTRACT

The goal of this dissertation was to establish a magnetic resonance imaging (MRI)-based tracking method for mesenchymal stem cells (MSCs) in ovine and equine models of tendonitis and to apply this method in a longitudinal assessment of cell tracking and tendon healing *in vivo*.

The first aim was designed to establish a labeling method using superparamagnetic iron oxide nanoparticles (SPIOs) in sheep, validate detection limits *in vitro* and *in vivo* at 3 Tesla (T), and follow out sheep after injection of labeled cells for 7 and 14 days. Labeled, ovine MSCs remained viable, proliferate, and undergo tri-lineage differentiation and remained detectable *in vitro* in cell numbers as low as 10,000. Cells remained detectable *in vivo* by MRI at 7 days, as confirmed by correlative histology for dually labeled SPIO+/GFP+ cells, but cells were not confirmed at 14 days.

The second aim was designed to establish a SPIO labeling method in the equine and to validate detection in a clinically relevant model of tendon injury at 1.5 T. Assays indicated no significant changes in cell viability, proliferation, migration, or tri-lineage differentiation due to the presence of SPIOs. Clusters of labeled cells were visible as signal voids in 6/6 subjects.

Coalescing regions of signal void were diffusely present in the peritendinous tissues. Greater than expected delocalization of cells was present and relatively few cells were retained within collagenous tendon compared to surrounding fascia.

The final aim was to non-invasively monitor cell migration and survival concurrent with healing in an ovine model of acute tendon injury over 28 weeks. SPIO-associated signal voids dropped off exponentially over the first 6 weeks, but remained present until 28 weeks. Quantitative MRI parameters including standard deviation (SD) of MRI signal intensity, signal to noise ratios (SNR), and signal difference to noise ratios (SDNR) decreased over time in all subjects. MSC-treated tendons had lower SD, SNR and SDNR than control and SPIO-MSC treated tendons at 28 weeks.

Overall, SPIO-labeling appears to be an effective and safe method to label MSCs, although some drawbacks are present. MSC treatment appears to improve tendon healing, but care should be taken when assessing SPIO-labeled cells concurrently with tendon quality.

INDEX WORDS: mesenchymal stem cells, magnetic resonance imaging, superparamagnetic iron oxide nanoparticles

MRI-BASED APPROACH FOR LONGITUDINAL MONITORING OF INTRALESIONAL THERAPY OF MSCS IN A LARGE ANIMAL MODEL OF TENDONITIS

by

ALEXANDRA MICHELLE SCHARF

BS, Cornell University, 2011

A Thesis Submitted to the Graduate Faculty of The University of Georgia in Partial Fulfillment of the Requirements for the Degree

DOCTOR OF PHILOSOPHY

ATHENS, GEORGIA

2016

MRI-BASED APPROACH FOR LONGITUDINAL MONITORING OF INTRALESIONAL THERAPY OF MSCS IN A LARGE ANIMAL MODEL OF TENDONITIS

by

ALEXANDRA MICHELLE SCHARF

Major Professor:	John Peroni
	William Kisaalita
Committee:	Shannon Holmes
	Timothy Foutz
	Johnna Temenoff

Electronic Version Approved:

Suzanne Barbour
Dean of the Graduate School
The University of Georgia
August 2016

DEDICATION

To my mom and dad for always pushing me harder and to all the horses that have kept me sane along the way.

ACKNOWLEDGEMENTS

Thank you to my major professor, John Peroni, for putting up with all of my antics and ideas and bringing many of them to life. What I have learned over the past 5 years goes beyond the limits of medicine. I hope one day I can be half the advisor you were to me.

To Jennifer Mumaw and Merrilee Thoreson, for helping me navigate the lab and all their guidance and friendship. Shannon Holmes and Jim Costley, for sharing their imaging knowledge and skills with me. To Mike Barletta, Jane Quandt, and their anesthesia team for helping make my sheep project possible. To all the UGA CVM faculty and staff for helping me organize these huge projects and making them a reality. And to my entire graduate committee for guiding me through this journey and sending me on to meet the next challenge.

To my sister Sam, Gillian Furqueron, Alaina Stumpf, and Shelbe Rice, for being the best friends anyone could ever ask for. I'm lucky I didn't have to do this alone.

To the Foster lab, especially Ashley Makela and Paula Foster, for their invaluable MRI expertise and great summer memories.

To those who have always given me horses to ride, especially Stephanie Parker-Cumming and Kristen Faircloth, and to those horses who put a smile on my face after many long days.

I am blessed beyond measure to be here. Thank you to everyone who has supported me and helped me achieve so much.

TABLE OF CONTENTS

Page

LIST OF TABLES

Page

LIST OF FIGURES

Page

CHAPTER 1

INTRODUCTION

Tendon injuries occur commonly in human and veterinary athletes alike, resolving with inferior biomechanical strength and predisposing patients to re-injury. Current treatment options fall short of success, allowing athletes to return only to low levels of performance and often, leaving them on the bench. Regenerative therapies have become increasingly prevalent in sports medicine and orthopedics, where many patients seek new options after conservative treatments have failed. Mesenchymal stem cells (MSCs) are adult-derived, multipotent cells, most commonly derived from the bone marrow or adipose tissue, that fall under the umbrella of regenerative medicine. MSCs are rapidly being tested across a wide range of diseases and medical conditions, from arthritis to organ transplantation, and thus far, have found great success. However, little is known about their persistence in the target tissue, migration through the body, or mechanism of action.

The first aim of this dissertation was to develop a safe, cell labeling method capable of tracking MSCs *in vivo* for both equine and ovine models of tendon injury using clinically available, magnetic resonance imaging (MRI) equipment. Chapter 3 describes the pursuit of this labeling system in an ovine model at 3 Tesla (T) over 14 days and chapter 4 describes the use of an equine model of tendonitis for cell tracking at 1.5 T where imaging was performed only immediately following injection.

The final aim of this dissertation was to monitor cell migration over time in a study using a conventional protocol for intra-lesional injection of MSCs for tendonitis and to assess the

efficacy of MSC therapy using a clinical MRI scanner. Chapter 5 combines the work and conclusions of the previous chapters, applying the cell labeling method to ovine MSCs, injecting iatrogenic injuries, and imaging sheep at 1.5 T to simultaneously monitor cell location and tendon healing at 2, 6 and 28 weeks.

CHAPTER 2

LITERATURE REVIEW

Tendon Injury Pathophysiology

Tendon injuries vary in their severity and capacity to heal, with important differences associated with chronicity, inflammation, and location. Flexor tendon injuries may result from chronic overuse, acute overload or traumatic tearing. These types of injuries occur in both veterinary, particularly equine, and human athletes. Participation in sports is the largest, predisposing factor, particularly in middle-aged males that participate in sports only on an occasional basis [1]. The most common locations for acute-type injuries are the digital flexor tendons of horses and the Achilles tendons of humans.

The flexor tendons are responsible for bearing weight during locomotion and at rest. In the forelimb, they rapidly transfer energy from muscle to bone, contributing up to 90% of the total work done by the distal forelimb at high speeds[2]. The collagen fibers within the tendon act as springs to store and release elastic strain energy, reducing the amount of work expended by the muscles [2]. The flexor tendons spanning the metacarpophalangeal joint, specifically the deep digital flexor tendon (DDFT) and superficial digital flexor tendon (SDFT), experience the highest forces. Forces transmitted to the SDFT have been measured over a range of 7 to 17 N/kg body mass from the walk to the gallop, respectively[2]. High forces are needed to stretch these tendons during the stance phase of locomotion[2], increasing the risk of injury upon impact. Horses naturally move at a pace that maximizes the utilization of strain energy, but when they are

pushed to faster paces, tendon loading and joint contact forces may lead to injury. In horses engaged in racing activities, the likelihood of tendon injury has been reported as high as 8 per 1000 race starts [3-5].

Flexor tendon injuries are associated with decreased performance and quality of life in equine patients, with re-injury rates in Thoroughbred racehorses reported to be as high as 53%[6-8]. A recent study reported 492/7993 veterinary events (6.2%) in flat-racing horses were tendon and ligament injuries, and of these most were moderate strains (42.7%)[9]. Although the majority of data relating to flexor tendon injury reflects injury rates in Thoroughbred racehorses[7; 10], National Hunt Horses[11; 12], or Standardbreds[10], it is widely recognized as one of the most common, career-debilitating injuries in all performance horses[13]. Racehorses[7; 8] and event horses[14] are most susceptible to injury of the SDFT; show jumpers to the DDFT[14]; and dressage horses to the suspensory ligament[14]. SDFT injuries are most commonly found in the mid-metacarpal region of the forelimb, although they frequently occur in the distal metacarpal region as well. Re-injury rates vary from 12.5 to 53% in different equestrian disciplines, with the most common issues arising in racing athletes[7; 8; 15]. During recovery, compensation with the contralateral limb puts these animals at high risk for secondary injury due to their large body size and unnatural stance[16]. Most horses never return to their previous level of performance and the high level of recurrence associated with this injury often leads to early retirement in elite competitors.

Mature tendon is primarily composed of water and collagen, allowing the tissue to be pliable and flexible while resisting extension. The collagen backbone is interspersed with fibroblast-like cells known as tenocytes as well as other non-collagenous proteins. Approximately one-third of the tendon is composed of type I collagen (ColI), which is arranged in a hierarchical structure. Subunits of tropocollagen are arranged into collagen fibrils that

overlap by a quarter length, creating the banding pattern that is commonly seen on electron microscopy[17]. Neighboring collagen fibrils are stabilized by crosslinking between lysine/hydroxylysine residues, which help assemble the larger tendon fascicles that can be seen on macroscopic tendon cross-sections[17]. This complex organization endows the tendon with high tensile strength, an essential characteristic for the high-performing athlete.

Non-collagenous proteins are also found in the tendon, but do not contribute significantly to the dry weight. Proteins such as cartilage oligomeric matrix protein (COMP) likely play a role in the early stages of fibrillogenesis[17]. Low COMP levels in tendon at skeletal maturity have been correlated with predisposition to tendon injury[18]. Heavily glycosylated proteins, known as proteoglycans help retain water in the tissue and resist compression. There are both large proteoglycans, including aggrecan, and smaller ones such as decorin and fibromodulin that associate with collagen fibrils. With consideration to the different groups of tendons, the weight-bearing flexor tendons demonstrate higher hydration, lower collagen content, and significantly higher levels of COMP at maturity[17].

The events leading to degenerative changes in flexor tendons may occur as a result of various events, including overuse, trauma, atrophy, and aging[19]. Tendon injuries often result when the collagen fibers exceed the physiological limit for strain, resulting in partial to complete tears. Exercise-based animal models indicate that repetitive mechanical loading leads to inflammatory and degenerative changes in tendon. Injection-based models that use collagenase or other inflammatory agents to initiate the injury indicate that biological factors like cytokines, matrix metalloproteinases (MMPs), and prostaglandins may be associated with tendon degeneration as well[20].

Subclinical, biochemical degeneration of the tendon matrix precedes physical defibrillation and clinical signs of tendon injury. A study performed on racehorses determined that changes in tendon ultra-structure occurred on days 1 and 2 post-race using dynamic echopatterns from ultrasound tissue characterization[21]. The ultrasound images appeared to have persistence of echogenic patterns associated with reversible remodeling and loosening of the tendon matrix, although no focal signs of injury were present[21]. As a result, the authors suggest that animals exposed to high mechanical loads within 72-hours after a competitive race may be at a high risk for tendon injury[21]. The tendon fibers become physically disrupted as damage progresses, often resulting in a core lesion of the SDFT in the mid-metacarpal region of the forelimb[22-24]. Tendonitis may also present itself as an increase in tendon diameter, fiber tearing, or disruption of the longitudinal, fiber pattern.

Current treatment options for tendinopathy

A variety of treatment methods have been implemented in the clinic and in the research setting in an attempt to ameliorate pain and improve tissue repair following flexor tendon injury. Traditional treatments such as the use of non-steroidal anti-inflammatory drugs (NSAIDs), cold therapy, and bandaging alleviate inflammatory symptoms that accompany the sub-acute phase of tendon injury. NSAIDs have been documented to have a negative impact on wound healing[25; 26] and should be discontinued as early as possible following the initial injury. Cold therapy and bandaging are effective in stimulating lymphatic drainage, reducing swelling, and providing support to the limb, but do not help restore structure to the tissue. Short-term pain management with corticosteroids is commonly implemented, but intermediate and long-term management is

not recommended and may actually correlate with increased pain [27] or predisposition to rupture [28] over time.

Sodium hylauronate (NaHA) is one of the most commonly implemented treatment methods, but has only shown moderate efficacy in the long-term. A study in a rat model of rotator cuff injury showed reduced expression of calcitonin gene-related peptide, a marker of inflammatory pain, and improvement in gait analysis following injection of steroid or hyaluronic acid injection, suggesting effective treatment[29]. Another study demonstrated improvement in tendon diameter, ultimate and yield strain, echogenicity and dry weight of transected tendons following surgical repair and treatment with NaHA[30]. In a study of re-injury rates following DDFT injury, 73% of horses receiving medical treatment with corticosteroid and NaHA injection of the navicular bursa returned to work, as compared to only 39% returning to work after rest alone[31]. Interestingly, only 15% of medically treated horses were sound at follow up, compared to 28% following rest alone, and 33% following medical treatment and rest[31]. Another study compared SDFT treatment with HA, β-aminoproprionitrile (BAPN), or polysulfated glycosaminoglycans (PSGAGs) and showed superior results following BAPN treatment[32]. Treatment with PSGAGs or NaHA or both resulted in re-injury rates greater than 42% whereas BPAN rates were only 16%[32]. A study in rabbits, however, suggests BAPN inhibits fibrosis and is predominated by smaller, mechanically weaker fibrils, and retards healing[33].

In a study of operative versus non-operative treatment in acute Achilles rupture, non-operative treatment resulted in re-rupture in 13.1% of patients under 40 years old whereas there were only 5.8% following surgical intervention[34]. However, surgical intervention is more involved for equine patients and has shown little success or benefit to them. In fact, surgery has

been shown to increase the likelihood of recurrent or new injuries, particularly in the contralateral limb [35] due to their uneven stance.

Newer methods of treatment include alternatives like extracorporeal shockwave and laser therapy. Extracorporeal shockwave therapy (EWST) has been investigated *in vitro,* demonstrating a moderate increase in tenocyte metabolism[36], which may translate to formation of smaller collagen fibrils, increased transforming growth factor (TGF)-β, and greater healing *in vivo*[37]. However, it is unknown if these results are clinically relevant and they are likely most useful in combination with other treatment regimens.

The low vascularity and cellularity of native tendon hampers an appropriate healing process and has contributed to the popularity of flexor tendon injury as a platform for testing biological treatments, specifically cell-based therapies. Current clinical and research therapies for tendinopathy include surgical manipulation and/or treatment with biological scaffolds[38; 39]; growth factors including bone morphogenic protein (BMP)-12[40-42] and human recombinant basic fibroblast growth factor (bFGF)[43]; platelet rich plasma (PRP)[44; 45] ; adipose or bone marrow-derived mesenchymal stem cells (MSCs)[46-48]; and other autologous preparations[38-42]. These therapies use blood and cell-based products to produce signaling molecules that can recruit endogenous cell populations and promote the assembly of appropriate extracellular matrix components needed to repair tendons. They are being explored for their potential to increase the proportion of type I collagen, fibril organization, and mechanical strength of healing tendons. Several studies now exist validating the use of MSCs for tendon repair, spanning investigations of iatrogenic[49; 50] and naturally occurring injuries[51; 52]. Extensive work in this field has demonstrated an increase in COMP [49], type I collagen[49; 53], increased longitudinal fiber orientation[49; 52], improved crimp pattern[52], decreased cellularity[52], decreased MMP activity[52],

decreased stiffness[52], and increased modulus[54] compared to untreated or placebo treated tendons. MSCs have also been demonstrated to reduce the rate of re-injury in racehorses returning to competition[51].

Stem Cells

Stem cells can be classified into 3 major categories: embryonic (ESCs), induced pluripotent stem cells (iPSCs), and adult-derived, MSCs. ESCs are pluripotent cells derived from the inner cell mass of the blastocyst. They are characterized by the ability to differentiate into any of the three somatic, germ-cell layers (endo-, meso-, and ectoderm). Human ESC lines were first established in 1998 and have since become a prominent area of research in regenerative medicine[55]. However, issues regarding the ethical derivation of human ESCs and the development of teratomas *in vivo* have hampered their translation into the clinic[56].

iPSCs are somatic cells that have been genetically reprogrammed into a pluripotent state. These cells can be derived from any adult tissue, including skin. In the lab, adult cells are transformed to a more primitive phenotype, characterized by the expression of Oct3/4, Sox2, c-Myc, and Klf4[57]. Once generated, these cells are indistinguishable from ESCs. The protocol to create iPSCs was first established in 2006[57]. After reprogramming the cells, the murine iPSCs were injected into murine blastocysts, successfully leading to embryonic development. Although this method circumvents the ethical challenges associated with ESCs, these cells are technically challenging to produce and have a very low yield[58]. Aberrant expression of the targeted genes may also lead to carcinogenesis.

MSCs are multipotent stromal cells that can be derived from nearly any adult tissue. As a multipotent cell type, they are able to differentiate into any cell type from their germ cell of

origin. Most commonly these cells are derived from the bone marrow or adipose tissue. The International Society for Cell Therapy has proposed characterizing MSCs by three primary criteria: adherence to plastic, multipotent differentiation potential, and specific surface antigen (Ag) expression[59]. Multipotency is most commonly demonstrated by differentiation into adipogenic, chrondrogenic, and osteogenic lineages *in vitro.* Surface Ag expression should include the positive expression of cluster of differentiation markers (CD)105, CD73, and CD90, as well as the absence of CD45, CD34, CD14 or CD11b, CD79α or CD19 and HLA class II in human MSCs [59]. Validation of these phenotypic characteristics in other species has been attempted by many research groups[60-63], but efforts have been slowed due to the limited availability of monocolonal antibodies in veterinary and lab animal species.

The clinical potential of MSCs has been widely accepted. The appeal of MSCs can be attributed to their ease of isolation and expansion, low immunogenicity, and ability to be cryopreserved and banked. Their combined multi-differentiation potential, anti-inflammatory action, and immunomodulating activity has led to discovery of their therapeutic benefits in diseases ranging from graft versus host disease[64] and organ transplantation[65] to chondral defects[66] and cutaneous wounds[67]. Additionally, MSCs secrete bioactive molecules that promote angiogenesis, attract other cell types, and decrease apoptosis and fibrosis[68; 69].

The trophic activity of MSCs results from both cell contact-dependent and independent events. MSCs are able to modulate cytokine production from T cell subsets, block the maturation and activation of antigen presenting cells, suppress T lymphocyte activation and proliferation, and stimulate the proliferation of T regulatory cells[68; 70-72]. MSCs also directly and indirectly promote secretion of interleukin (IL)-10 and TGF-β, two potent anti-inflammatory cytokines[68; 73], and play an active role in reducing cell apoptosis[74].

Comprehensive secretory protein profiles associated with MSCs have been carried out in numerous settings. MSCs are able to suppress fibroblast proliferation through TGF-β dependent pathways, which leads to an increase in secretion of molecules like prostaglandin E2 (PGE2)[75; 76]. PGE2 and hepatocyte growth factor (HGF) are well-documented anti-fibrotic factors. PGE2 has been reported to promote fibroblast apoptosis while inhibiting cell death in native tissue, suggesting a role for PGE2 in the reversal of fibroplasia[77; 78]. Studies suggest that insulin growth factor-1 (IGF-1) may also play a major role in reducing apoptosis of native tissue[79; 80] These properties make MSCs increasingly appealing for use in traumatic injury, especially when ischemia and inflammation are present.

Engraftment versus Paracrine Activity

As an increasing number of studies report low levels of long term, stem cell engraftment across a range of tissues, the importance of understanding the paracrine influence of stem cells has become paramount. Tumor necrosis factor (TNF)-α, vascular endothelial growth factor (VEGF), TGF-β, IL-1β, IL-2 and IL-10 have been implicated as key players in tendon inflammation and repair [81] Neutrophils and macrophages arrive at the site of injury within the first 24 hours post-injury [82]. Macrophages initially fulfill a pro-inflammatory role, secreting inflammatory mediators, which may even propagate cell damage. These macrophages are characterized as M1 macrophages and are associated with the expression of CD14, CD16, CD32, CD64, CD80 and CD86[83]. Over time, the macrophage phenotype can re-polarize to a less inflammatory, M2 macrophage associated with expression of the mannose receptor (MR) CD206 and CD163[83]. This usually occurs by 28 days[82], mediating re-organization of the collagenous extracellular matrix and deposition of collagen I in the presence of anti-inflammatory cytokines.

MSCs have been associated with the ability to modulate the production of many pro-inflammatory cytokines, decrease scar tissue deposition, and support the re-polarization of M1 to M2 macrophages. Uncontrolled immune cell activity can propagate inflammation, further tissue injury and produce tissue adhesions. Activated T cells regulate repair of the epitenon, particularly through the secretion of TGF-β and IL-2[84]. These cytokines promote cell-cell adhesion[84; 85], which can lead to deposition of excess scar tissue and the development of fibrous adhesions in the epitenon. MSCs can reduce hypertrophic scar formation through the reduction of IL-1β, IL-6, and TGF-β1[86]. Interestingly, different isoforms of TGF-β have been associated with different pro- and anti-inflammatory effects. The use of neutralizing antibodies to TGF-β1 and 2 or the addition of exogenous TGF-β3 in cutaneous wounds[87] and flexor tendon [88] models have been associated with decreased scar formation and improved range of motion. Stem cells have the potential to regulate this process and increase tissue organization and biomechanical integrity. The reduction in fibrosis is likely associated with a TGF-β3 dependent pathway[75] leading to a reduction in the TGF- β1/TGF-β3 ratio[89], and a decrease in release of TNF-α from activated macrophages[89].

Adipose-derived MSCs are capable of modulating the secretion of IL-1β and TNF-α in the presence of tendon fibroblasts and pro-inflammatory macrophages[90]. This effect is mediated over several days *in vitro* and suggests that a short, resident period is required for MSCs to mediate a potent, anti-inflammatory effect. TNF-α is a catabolic cytokine associated with the induction of apoptotic cell tissue and is up regulated in acute and chronically injured tenocytes[91]. It is also heavily secreted by pro-inflammatory, M1 macrophages. TNF-α leads to degradation of the tendon extracellular matrix (ECM) by down regulating collagen I, up regulating MMPs, and increasing expression of IL-1 and -6[92]. TNF-α is maintained at high concentrations through the

activity of an auto-amplification loop[92]. In a model of rat rotator cuff repair, a TNF-α blockade demonstrated improved biomechanical strength and limited improvements in histological integrity[93]. Stem cell therapeutics offer these benefits in conjunction with those mediated by other growth factors, leading to more significant improvements in repair.

MSCs have been associated with the up-regulation of potent anti-inflammatory factors such as IL-10 and IL-2. IL-10 is capable of suppressing activated macrophages, reducing active concentrations of TNF-α and IL-1 within hours[94], and has been associated with ECM turnover and the production of collagen by fibroblasts[95]. The overexpression of IL-10 in tendon has been shown to increased biomechanical strength in tendon injury[96].

Attempts to track cells *in vivo* have been attempted with both histological and imaging methods. Methods include labeling cells by genetically transducing cells to express green fluorescent protein (GFP) [50; 97]; exogenously labeling cells with fluorescent dyes like DiI[98]; tracking male cells in a female recipient[99]; and labeling with radionuclides for nuclear scintigraphy[100; 101] or paramagnetic[102; 103] or superparamagnetic[104; 105] nanoparticles for MRI. Current knowledge of stem cell migration in tendon lesions is limited. Although GFP-tracking[50; 97] has been performed, these studies provide a limited perspective that is only able to demonstrate the position and localization of these cells at one time point, and often only in two dimensions. Guest et al. (2008) demonstrated that some of the one million cells initially injected into the surgically-induced tendon lesion remained at day 10 and 34, and some cells were found engrafted to the surrounding, healthy tissue[50]; however, this study spanned a short time period and did not draw any conclusions with respect to tendon healing. In a follow-up study, Guest et al. (2010) showed that of an injected MSC population, less than 5% of the original MSC population could be detected in the lesion after day 10[97]. Again, analysis was not done with

respect to overall tissue repair or regeneration. A study by Pacini et al. (2007) demonstrated a significant increase in tendon tissue density at 30 days following injection of over 1 million stem cells into naturally occurring SDFT lesions[106]. Overall, studies indicate that MSCs are capable of improving tendon healing (Table 2.1), but further work tracking the migration and mechanism of MSCs in tendons is essential to optimizing this therapeutic treatment.

Stem Cell Delivery: Where and When

Musculoskeletal injuries are characterized by three primary stages of repair: inflammation, repair, and remodeling. The first, inflammatory phase lasts up to 1-week post injury and accompanies acute trauma. During this stage, red blood cells, leukocytes, and platelets infiltrate the site to release growth factors and help clear necrotic debris. During the repair phase, there is an influx of macrophages and continued fibroblast proliferation. Fibroblasts actively synthesize and deposit collagen and other components of the ECM to increase structural integrity at the site of injury. Macrophages shift to a reparative phenotype and help to recruit more endogenous cells. Tenocytes begin to deposit new ECM, primarily composed of collagen III. The third and most important is the maturation or remodeling phase. The remodeling phase focuses on reduction of excess extracellular matrix and contraction of the wound. At this time, collagen fibers are cross-linked, albeit often haphazardly, to stabilize the tissue and increase tensile strength. The tissue matrix is remodeled in a load-dependent manner, allowing longitudinal deposition of collagen I fibrils along axes of strain. If left unchecked, the repair process leads to deposition of fibrous tissue with an increased proportion of collagen III fibers, decreased cross-linking, and disruption of the crimp pattern [107-109]. If excessive ECM is produced, the remodeling phase is associated

with high volume scar tissue formation, and contributing to decreased biomechanical strength and range-of-motion[23].

There is increasing evidence that the outcome of MSC treatment may be associated with the timing of injection. Different characteristics of MSCs may influence the 3 stages of wound healing in different ways. It is important to evaluate the effects of timing at both the molecular and macroscopic level.

A handful of studies have demonstrated successful implantation of MSCs with therapeutic benefits following immediate, systemic administration of MSCs at the time of injury[110-114]. In a full-thickness skin wound model, systemic MSC administration resulted in a decrease in pro-inflammatory activity and decreased Th17 cell expansion [110]. In another corneal model, immediate systemic administration of MSCs was able to suppress corneal opacity[111], reduce inflammation[111; 112], and enhance epithelial repair [112]. Therapeutic injections homed to the injured tissue and increased paracrine factors in the bloodstream, resulting in increased regeneration of the injured tissue[111; 112]. Although long-term integration of MSCs was not observed, the immediate, paracrine effects, including increased secretion of TNF-α stimulated gene/protein (TSG)-6, were pronounced[111].

Corneal injuries and superficial wounds are not associated with profound, systemic inflammation, which may allow MSCs to exert a therapeutic effect at earlier time points than in those injuries associated with a more potent pro-inflammatory response. During peak inflammation MSCs may be overwhelmed by inflammatory stimulus. MSC injections must be performed with care around this time as they have demonstrated the ability to differentiate into a pro-inflammatory cell type[115; 116]. A recent study suggests this is due to the presence of toll-like receptors (TLRs) on MSCs[117]. Short-term, low-level exposure of TLR-4 agonists like IL-4 may

move the MSCs towards a pro-inflammatory phenotype. In contrast, exposure to a TLR3 agonist such as LPS predisposes the cells to an anti inflammatory phenotype.

The inflammatory cascade in wounded tissue is characterized by infiltration and activation of leukocytes and macrophages. Transplanted MSCs may provide therapeutic benefit through direct cell-cell contact with macrophages, as they can activate a tolerogenic response and up regulate therapeutic molecules. In co-culture, MSCs have been shown to stimulate the transition from a pro-inflammatory M1 phenotype to an anti-inflammatory M2 phenotype in macrophages[118]. Several studies have demonstrated the correlation between higher proportions of M2 macrophages and improved healing following direct injection *in vivo*[110; 119; 120]. M2 macrophages show increased secretion of IL-10 as well as reduction of IL-1β, IL-12, and macrophage inflammatory protein (MIP)-1α[118]. These experiments suggest M2 macrophages not only reduce pro-inflammatory cytokines in the environment, but also inhibit Th1 activation and promote phagocytic activity. The timing of injection of MSCs is critical when considering the modulation of macrophage phenotype.

Several studies in myocardial infarction and spinal cord injury have investigated the role of stem cell transplantation times. Park et al. (2011) implanted MSCs into a canine model of spinal cord injury (SCI) and found that cells implanted one week post-injury demonstrated greater clinical improvement, neuronal regeneration and reduction in fibrosis than those implanted 12 hours or two weeks post injury[121]. Interestingly, cells injected the same day of the injury showed no difference as compared to controls[121]. In myocardial infarction, MSCs demonstrate superior results as compared to controls when injected at one week post-injury, including decreased scar formation and increased functional performance, and superior cell homing and survival as compared to earlier and later time points[122; 123]. These data suggest that

cell transplantation may not be beneficial during times of peak inflammation. One author proposed that the oxidative load of inflammatory cells in the initial stages of disease may have been harmful to the MSCs and counteracted their therapeutic effect[122]. Myocardial infarction and spinal cord injury are both characterized by development of excessive scar tissue when left untreated and provide critical insight into the timing of injections. In the above studies, successful MSC therapy is most often correlated with injection 1-2 weeks post-injury, when a large population of macrophages is present.

It is also prohibitive to inject MSCs after too much time has lapsed. Cells injected late in the remodeling phase may require surgical intervention and debridement to remove excess fibrous scar tissue if a therapeutic effect is expected[71; 119; 122; 124]. MSCs can moderate matrix production and formation of granulation tissue, but once scar tissue has been formed their therapeutic efficacy is significantly reduced. Studies of SCI have shown that cell injections are most effective when injected 1-2 weeks post-injury when compared to later time points[119; 124]. Although cells persisted for equal time[119], only animals injected at 1-2 weeks showed significant functional and structural tissue repair[119; 124]. Interestingly, neural progenitors demonstrated neural differentiation and favorable cytokine profiles *in vivo* regardless of the time of injection[119]. However, cell distribution patterns were distinct when injected at 4+ weeks due to the formation of scar tissue. MSC therapy alone may be of limited value in chronic disease processes where scar tissue is abundant and excision of scar tissue prior to treatment is likely recommended.

Cell Tracking and MRI

The opportunity for longitudinal tracking of cell dynamics *in vivo* holds great promise for regenerative cell therapies, particularly for MSCs. Recent developments in magnetic resonance imaging (MRI) technology including superparamagnetic and paramagnetic contrast agents (CAs), specialized radiofrequency coils, and high field magnets have prompted researchers to pursue MRI-mediated cell tracking methods (Table 2.2). Unlike other imaging methods, MRI is able to provide high resolution, cell-tracking data in the context of both soft- and hard-tissue contrast.

Two major CAs that have been exploited for cell tracking purposes are superparamagnetic iron oxide nanoparticles (SPIONs) and paramagnetic gadolinium (Gd) chelates. SPIONs were originally formulated for imaging the reticuloendothelial system (RES) following administration of an IV bolus. Kupffer cells in normal RES tissue phagocytose the particles, but lesions that lack healthy Kupffer cells do not. As a result, SPIONs can be used to enhance lesion detection, particularly in the spleen and liver.

MRI contrast agents have magnetic properties that interfere with the spin of nearby protons resulting in conspicuous signal accumulation on MR images. Iron (Fe) and Gd are both naturally occurring, paramagnetic materials. They have unpaired electrons that create magnetic susceptibility, meaning that the magnetic field is much stronger where the material is located. This results in changes in T1 and T2 relaxation rates and resulting changes in T1 and T2 contrast on MRI. Relaxivity is a critical parameter for choosing an intracellular CA, describing its ability to change the T1 and T2 relaxation rates ($1/T_1$, $1/T_2$) of surrounding hydrogen protons. Super-paramagnetic materials have a net magnetic moment of zero without the application of an external magnetic field. Once the external field is applied, they act like a paramagnetic material,

except with a much larger, or "super" susceptibility. Superparamagnetic materials are usually much smaller and exist only on the nanoscale.

The binding of plasma proteins can also influence relaxivity, which may lead to small differences based on individual cell types or scanners[125]. Relaxivity may also be influenced by the location of nanoparticles within the cell. This is particularly relevant when choosing a labeling protocol, where some methods may lead to sequestration in the lysosome or leave the particles free in the cytosome.

Superparamagnetic Iron Oxide Nanoparticles

SPIONs consist of a monocrystalline or polycrystalline iron oxide core enveloped in a polymer coating that protects the particle from early oxidation and improves biocompatibility and solubility [126; 127]. SPIONs are ideal for cell tracking as they are non-toxic, do not emit ionizing radiation, and are readily available (Feridex®, Berlex Inc, Montville NJ, USA; Endorem®, Guerbet, Aulnay-sous-Bois, France; Resovist®, Bayer Schering Pharma AG, Berlin, Germany; Feraheme®, AMAG Pharmaceuticals, Waltham MA, USA) [128]. For cell labeling, SPIONs can be conjugated to the cell surface or internalized through endocytosis. When surface labeling is used, iron content tends to be lower and the immune system is able to rapidly clear the labeled cells. Intracellular labeling protocols are more common for stem cell tracking studies. For intracellular labeling, viral transfection or other cumbersome labeling protocols are not required. SPIONs are introduced into target cells by endocytosis, with or without addition of transfection agent[129], and compartmentalized into cell endosomes. Transfections have been done with solutions up to 100 μg SPIONs/mL in adherent cells without inducing apoptosis [126; 128; 130-132]. Human MSCs remain viable with iron concentrations of up to 23 pg/cell [132].

SPIONs are catabolized by the cell's natural, metabolic pathways for iron. Past research has shown that SPIONs do not alter cell viability, proliferation, differentiation, gene expression, or cytokine secretion in various cell types[133-136]. A few studies have shown impairment of chondrogenic differentiation potential[131; 137], but a study by van Buul et al. (2011) demonstrated no effect on pellet size, GAG deposition, or collagen II production following chondrogenic induction after incubation with Endorem®[105]. These results indicate that specific SPIONs may have differing effects on treated cells. Additional optimization of SPION treatment in specific cell types is warranted to ascertain specific effects on differentiation pathways or targeted tissues. A review by Mahmoudi, et al. (2012) highlights the potential for iron toxicity when treating cells with high concentrations of SPIONs[138]. Side effects may include altered mitochondrial activity, production of reactive oxygen species (ROS), and disruption of the actin cytoskeleton. SPIONs also accumulate in endosomes, which may align along the magnetic field produced by the MR unit and deform the intracellular environment[139]. The red-brown color associated with high SPION concentrations may also interfere with some assays that rely on absorbance and results must be interpreted carefully and compared to appropriate controls.

On MRI, SPIONs create a large dipolar magnetic field gradient that affects the spin of protons in the nearby environment[140]. This appears as a hypointense, or dark, area of signal known as a "susceptibility artifact" on T2 and T2*-weighted (T2w, T2*w) images. This is particularly beneficial for imaging in tissues characterized by bright signal intensity on T2w images, such as the brain. However, these signals may be hard to differentiate from other low signals such as hemorrhage, micro air bubbles, or surgical implants[141].

Successful protocols have been developed to monitor immune cells[142-144], stem cells[135; 145-149], and carcinogenic[150-152] cell migration with SPIONs in a variety of animal models. SPION-

derived MRI signal has been detected *in vivo* on a clinical MRI machine from 7-16 weeks following implantation[128; 153]. Using optimized equipment, SPION-labeled cells have even be detected at the single cell level[154]. Following injection of 300,000 MIRB-labeled cells, McFadden et al. (2011) demonstrated detection of single cell voids using a balanced steady state free precession (bSSFP) sequence on a 3 Tesla (T) MRI unit with optimized equipment[154].

One of the most notable shortcomings of SPION labeling is the inability to differentiate between viable and nonviable cells. Several recent efforts have attempted to overcome this obstacle. One effort bi-labeled MSCs with SPIONs and DiD for a multimodal approach to cell tracking using MRI and optical imaging, respectively[155]. Following intra-articular injection of viable and non-viable populations, no differences in signal intensity were appreciable by MRI or fluorescence. However, viable cell populations migrated into the adjacent inflamed ankle and their presence was confirmed by histology. It was hypothesized that viable cells could be differentiated based on their ability to migrate. Other studies have attempted to quantify changes in T1 and T2 relaxation in viable and non-viable cell populations[156; 157]. Unfortunately, signal of non-viable cells persisted for at least 15 days[156]. Interestingly, Gd-labeled signal from non-viable cells resolved within 2 hours post-transplantation[156]. Another study attempted to exploit compartmentalization of cells, assuming lysed cells would free SPIONs from lysosomal compartmentalization and lead to changes in T2w signal. This was successfully observed on T2w, but not T2*w sequences on 1.5 and 3 T clinical scanners[157].

An ideal CA will allow researchers to monitor changes in cell viability, although this has yet to be accomplished with confidence. In many cases, the development of a system to monitor cell migration in conjunction with cell viability is imperative, informing the degree of healing

conferred by direct differentiation and integration of injected cells as compared to the influence of paracrine factors and cell-cell interactions.

Additional shortcomings include the dilution of SPIONs upon cell division, spontaneous exocytosis, or release of nanoparticles into the environment following cell necrosis. Particles may become embedded in nearby tissue or taken up by macrophages where they will produce false positive signal on MRI. Once images have been acquired, if large numbers of labeled cells are present, blooming artifacts may interfere with monitoring local changes in tissue or lead to an overestimation of cell location.

The recent emergence of magnetic particle imaging (MPI) offers a boost in magnetization compared to conventional MR scanners as well as high contrast-to-noise ratios. Specialized MPI scanners generate positive contrast, as opposed to negative contrast, from SPION agents in T2 images, providing a new approach that may allow more precise localization of SPION-labeled cells.

Gadolium-based chelates

Gadolinium is a paramagnetic lanthanide that is also commonly used as a contrast agent for MRI. Gd chelates have numerous applications as an MR contrast media, including detection of tumors and for the detection of osteoarthritis or cartilage defects in joints. In tumors, macromolecular Gd complexes accumulate due to the tissue's hyperpermeability[158]. In cartilage, the positively charged Gd complex binds to the negatively charged proteoglycans, providing contrast visible on T1w images.

Gd is highly toxic as a free ion. Free Gd^{3+} interferes with calcium channels and protein-binding sites, demonstrating an LD_{50}=0.2 mmol kg^{-1} in mice[125]. It must be secured in a

macromolecular structure with high thermodynamic and kinetic stability before being used for any *in vivo* applications[139]. Gadolinium chelates are stable, soluble compounds that contain a Gd^{3+} metal ion coordinated to a polydentate ligand within a cyclic complex[158]. Two such chelates include gadolinium- diehtylenetriamine pentacetic acid (Gd-DPTA) and gadoteridol (Gd-HPDO3A), which are available as FDA-approved products (Magnevist®, Prohance®). These agents have a half life of 1-2 hours following intravascular injection and are predominantely eliminated through renal excretion[125].

On MRI, Gd agents shorten the T1 relaxation time of hydrogen protons, acting as a positive contrast media. Positive contrast cannot be obtained if the chelate is not in the proximity of a large number of hydrogen protons. The resulting T1 positive contrast, or bright signal, is particularly beneficial for tracking cells in tissues with inherent, low signal intensity. This signal is also less likely to be confused with signals originating from events such as hemorrhage that generate T2-weighted, negative contrast[140].

Intra-cellular labeling with Gd chelates and a Eu-containing analog[139; 158] have previously been shown by simple co-incubation, but modified protocols for uptake are often performed to increase the amount of Gd per cell due to the lower sensitivity of Gd contrast agents as compared to Fe. Protocols have included the use of transfection agents[141; 159-161], cationic liposomes[162; 163], or chemical modification of Gd complexes[164; 165] to increase sensitivity. Similar to SPIONs, Gd-complexes are retained in endocytotic vesicles that should protect the cell from any harmful effects[161].

In the last decade, a small number of researchers have successfully tracked cells *in vitro* and *in vivo* using Gd chelates, demonstrating intracellular uptake of Gd and positive MRI signal for up to 7 days on scanners down to 1.5 T[159-163; 165-169]. In a study by Shen et al.[141], neural stem

cells were dually labeled with Gd-DPTA and PKH26, a fluorescent dye, and were detectable as low as 5,000 cells immediately after labeling and $1x10^6$ cells remained detectable for up to 15 days *in vitro* on a 1.5 T MR scanner. In two consecutive studies by Loai et al.[167; 170], gadolinium oxide was used to label human aortic endothelial cells for detection at 7 T over a period of 7 days. The first study confirmed the biosafety of Gado *Cell Track* (BioPal, Inc) and the second assessed the ability to concurrently detect populations of Gd oxide and Fe oxide labeled cells. This study aimed to develop a detection method in which positive contrast could be used to identify one population and negative contrast to identify a second for up to 7 days in the same spatial location[167]. Another study used Gd after experiencing difficulty with SPIONs due to confounding signal loss in T2w images in a model of hemorrhagic spinal cord injury. This study demonstrated positive T1 signal in MSCs for up to 14 days and co-labeled with eGFP and Hoechst 33342 to confirm the results by histology[159].

Rationale for Presented Studies

MSC therapy is currently available in the clinic for human and veterinary patients, although little is known regarding the dose, duration of cell survival, degree of migration, or overall contribution to healing. This study will use SPION-labeled MSCs to investigate the answers to some of the above questions. The following studies were designed with the intention of validating a safe and reproducible method for labeling BM-derived MSCs with SPIONs for application in ovine and equine models of tendon injury with the potential to label cells in pre-clinical trials. Biosafety assays were conducted to demonstrate that the labeling protocols did not produce differences in any cellular characteristics, including viability, proliferation, differentiation and migration, as compared to unlabeled cells and could be used to image as few

as 100,000 cells *in vitro* at 1.5 and 3.0 T at the UGA College of Veterinary Medicine. Then, labeling protocols were applied to track and monitor MSCs in clinically relevant, veterinary models of acute tendonitis.

Species	Model	n	# of Cells	Type of Cells	Injection Volume	Time until Injection	Final Time Point	Measures of Healing	Ref
equine	N	12	$1x10^7$	autologous BM-MSCs in marrow supernatant	2 mL	average of 30 days	euthanized at 6mo	lower structural stiffness, improved histo and crimp pattern, lower cellularity, DNA, vascularity, water content, GAG, MMP13	52
equine	N	141	$10x10^6$	autologous BM-MSCs	1 mL x 2 injections	within 4 years	followed up for 2y	reduction of reinjury	51
equine	C	8	$3x10^6$	fdESCs in culture media	1.5 mL	1 week	8 weeks	improvement in tissue architecture, tendon size, tendon lesion size, fiber pattern	171
equine	C	22	$5.5x10^6$ BM-MSCs or $1.2x10^8$ BM-MNCs	autologous cultured BM MSCs or BMMNCs in fibrin glue or saline	calculated (CSA-1 x length of lesion)	3 weeks	21 weeks	increased COMP and Col1, low Col3, improved fiber pattern, improved ECM	49
equine	C	12	$10x10^6$	autologous BM-AdIGF-MSCs or BM MSCs	1 mL	5 days	8 weeks	improved histology, no change in gene expression	172
equine	N	13	$10x10^6$	autologous BM-MSCs	1 mL	4-10 week	n/a	n/a	173
equine	M	2	$1x10^6$	autologous and allogeneic MPCs	0.5 mL	7 days	10 and 34 days	no difference	50
equine	M	8	$1x10^6$	autologous and allogeneic MSCs or allogeneic ESCs	0.5 mL	7 days	3 months	n/a	97

ovine	C	30	1×10^8 BM-MNCs or 1×10^6 cBMSCs	BMMNCs or cBMSCs in fibrin glue	calculated	2 weeks	8 weeks	restoration of architecture and ECM, increased Col1 and COMP, low Col3	[174]
rat	C	81	1×10^6	human MSCs	0.1 mL	3 days	6 weeks	increased col1 and col3, improved ECM, neovascularization	[53]
rabbit	ST	57		BM-MSCs in fibrin carrier			12 weeks	improved biomechanical modulus	[54]
equine	C	5	10×10^6	AdMSCs in DMEM	1 mL	7 days	7 days	n/a	[175]
rabbit	ST	30	1×10^6	AdMSCs	0.1 mL	immediate	28 days	decrease in inflammation and increase in structural organization	[176]
rat	ST	78	1×10^6	BM-MSCs and TDSCs in DMEM	0.1 mL	immediate	4 weeks	increase in Col1, Col3, tenascin 3 and better density and fiber pattern	[177]
equine	N	11	average of 9.5×10^6	autologous BM-MSCs	<2.5 mL	variable	12 months	improved ultrasound and reduction in re-injury	[106]

Table 2.1. Timing of cell injections for tendon injury. C: collagenase, M: mechanical, N: natural, ST: sharp transection. AdMSCs: adipose derived-MSCs, cBMSCs: cultured bone marrow stromal cells, fdESCs: fetal derived ESCs, AdIGF-MSCs: IGF-1 enhanced MSCs, BM-MNCs: bone marrow mononuclear cells, MPCs: mesenchymal progenitor cells, TDSCs: tendon derived stem cells.

Contrast Agent	Model	Cell Type	Cell Number	Field Strength	Coil	Sequence	Ref
Gado CELL Track (Biopal, Inc) or Molday ION Rhodamine (Biopal, Inc)	*In vitro*	Normal human aortic endothelial cells and smooth muscle cells	250,000	7 T	B-GA12 gradient coil, 7.2 cm linear transmit coil, 4-channel murine phased-array receiver coil	T_1: 2D saturation-recovery rapid acquisition with relaxation enhancement (RARE) T_2: spin echo Carr-Purcell-Meiboom-Gill (CPMG) sequence	167
Gd-DTPA (Magnevist)/JetPEI (Polyplus Transfection)	Spinal cord injury in rat	Rat MSCs	1×10^6	3.0 T	Rat MRI coil	Spin echo T_1 weighted sequence	159
Gd-DTPA (Magnevist) and Effectene	*In vitro*	Rabbit neural stem cells	10^4 to 5×10^5	1.5 T	Circular surface coil with a diameter of 11 cm	T_1 weighted two-dimensional fast spin echo sequence and mixed-inversion recovery sequence for T_1 map	141
Gd-DTPA (Magnevist) or ferumoxide (Endorem)	Murine model of acute immunologic rejection	Human myoblasts	2×10^6	4 T	20 cm diameter 200 mT m^{-1} gradient insert, 28 mm inner diameter volume coil with quadrature polarization	Axial T_1-weighted spin echo, saturation recovery RARE imaging, T_2-weighted spin-echo sequences	178
PEGylated Gd_2O_3 or Molday ION Rhodamine B (Biopal Inc)	Murine glioma model	F98 rat glioma cells	3×10^5	1.0 T	RF mouse head coil	T_1-weighted 3D gradient echo or T_2*-weighted 3D gradient echo sequences	164
Gd-DTPA liposomes	subQ injection into hind limb	Rat MSCs	500,000	3.0 T	Unmodified gradients and custom surface coil with inner diameter of 2 cm	3D spoiled gradient recalled (SPGR) sequence with fat suppression	162
Gd_2O_3 ± protamine sulfate	*In vitro*	Murine Ba/F3 hematopoietic progenitors and human THP-1 monocytes	unknown	1.5 T	Head coil	T_1-weighted inversion recovery sequences with turbo spin echo acquisition and T_2–weighted multiecho spin echo sequences	179

Gadofluorine M	*In vitro*	U937 human monocytes	5 x 10^7	1.5 and 3 T	Standard circularly polarized quadrature knee coils	Coronal T_1 weighted spin echo 500/16 and 500/15 sequences	[165]
Gadolinium-DPTA:Rhodamine Dextran conjugate (GRID)	Rats with chronic brain damage follow middle cerebral artery occlusion	MHP36 neural stem cells	2 x 10^5	4.7 T	Quadrature birdcage RF coil with 63 mm internal diameter	Coronal T_1-weighted , T_2-weighted, and proton density-weighted spin echo sequences	[168]
GadofluorineM-Cy (Bayer Schering) or ferucarbotran	Cartilage defect in pig knee joint, *ex vivo*	hMSCs	5 x 10^5	3 T	Quadrature wrist coil	T_1 SE, T_2 fat-saturated fast spin echo (FSE), T_1 3D SPGR, T_2* gradient echo sequences	[169]
Fe_2O_3-PLL	Rat model for acute common carotid injury	Rat MSCs	6 x 10^6	7 T	Surface coil with 5 cm inner diameter	Multislice multiecho-proton density- (MSME-PD) T2 and 3D fast low angle shot (FLASH) sequences	[180]
Ferric oxide nanoparticles	Trochlear cartilage defect in minipig model	chondrocytes	5 x 10^7	3 T	Knee coil	T_2-weighted turbo spin echo (SET2WI) sequence	[181]
Micron-sized iron oxide (MPIO)	Murine model of spinal cord injury	Mouse MSCs	3 x 10^4	3 T	Custom built gradient coil, custom built solenoid RF coil (4 cm x 3 cm)	3D balanced steady state free precession (b-SSFP), 3D fast imaging employing steady state acquisition (FIESTA sequence)	[182]
MPIO	Mouse model of brain metastasis	Breast carcinoma cells	10^5	1.5 T	Custom built gradient coil (inner diameter: 12 cm, custom built solenoid mouse head RF coil (inner diameter: 1.5 cm)	3D FIESTA	[152]
Feridex with PLL	Murine model of chemically-induced diabetes	Pancreative islet cells	200-230 islets	3 T	Custom-built, high performance gradient coil insert	3D FIESTA	[183]
SPIO (Advanced Magnetics) and PLL	Mice with acute injury in the left	Adipose derived MSCs	10^6	3 T	Rodent receier coil	2D fast relaxation fast spin echo (FRFSE) T_2	[148]

	carotid					sequence	
Ferumoxide (Feridex) and protamine sulfate	Rat model of metastatic breast cancer	231BR breast ancer cells	10^6 or 3×10^6	3 T	Solenoid 4 cm RF receive only coil	T_2 weighted turbo spin echo and T_2* multi echo gradient sequence	[150]
Ferucarbotran (Resovist)	Antigen-induced osteoarthritis in rat	hMSCs	250,000	3 T	Circularly polarized Mayo BCID wrist coil	T_2-weighted axial spin echo and T_2*-weighted axial gradient echo sequences	[155]
Ferumoxytol (Feraheme)	Arthritic knee model in rat	Macrophages	Systemic/IV injection	7.0 T	Custom single-channel trasmit-receive partial birdcage radiofrequency coil with inner diameter of 2 cm	T_2-weighted fast spin-echo sequences	[144]

Table 2.2 Application of Fe and Gd-based contrast agents for cell tracking.

References

1. Raikin SM, Garras DN, Krapchev PV. 2013. Achilles tendon injuries in a United States population. Foot & ankle international / American Orthopaedic Foot and Ankle Society [and] Swiss Foot and Ankle Society 34:475-480.

2. Harrison SM, Whitton RC, Kawcak CE, et al. 2010. Relationship between muscle forces, joint loading and utilization of elastic strain energy in equine locomotion. The Journal of experimental biology 213:3998-4009.

3. Ely ER, Avella CS, Price JS, et al. 2009. Descriptive epidemiology of fracture, tendon and suspensory ligament injuries in National Hunt racehorses in training. Equine Vet J 41:372-378.

4. Parkin T, Rogers K, Stirk A. Risk factors for tendon strain injury during racing in Great Britain. Proceedings of the 16th International conference of racing analysts and veterinarians. Newmarket, UK: R and W Publications; p. 104.

5. Williams RB, Harkins LS, Hammond CJ, et al. 2001. Racehorse injuries, clinical problems and fatalities recorded on British racecourses from flat racing and National Hunt racing during 1996, 1997 and 1998. Equine Vet J 33:478-486.

6. Dyson SJ. 2004. Medical management of superficial digital flexor tendonitis: a comparative study in 219 horses (1992–2000). American Veterinary Journal 36:415-419.

7. Takahashi T, Kasashima Y, and, Ueno Y. 2004. Association between race history and risk of superficial digital flexor tendon injury in Thoroughbred racehorses. JAVMA 225.

8. Pinchbeck GL, Clegg PD, Proudman CJ, et al. 2004. Horse injuries and racing practices in National Hunt racehorses in the UK: the results of a prospective cohort study. Vet J 167:45-52.

9. Rosanowski SM, Chang YM, Stirk AJ, et al. 2016. Descriptive epidemiology of veterinary events in flat racing Thoroughbreds in Great Britain (2000 to 2013). Equine Vet J.

10. Genovese RL, Rantanen NW, Simpson BS, et al. 1990. Clinical experience with quantitative analysis of superficial digital flexor tendon injuries in Thoroughbred and Standardbred racehorses. Vet Clin North Am Equine Pract 6:129-145.

11. Avella CS, Ely ER, Verheyen KLP, et al. 2009. Ultrasonographic assessment of the superficial digital flexor tendons of National Hunt racehorses in training over two racing seasons. Equine Vet J 41:449-454.

12. Godwin EE, Young NJ, Dudhia J, et al. 2011. Implantation of bone marrow-derived mesenchymal stem cells demonstrates improved outcome in horses with overstrain injury of the superficial digital flexor tendon. Equine veterinary journal.

13. MURRAY RC, S. J. DYSON, C. TRANQUILLE a, et al. 2006. Association of type of sport and performance level with anatomical site of orthopaedic injury diagnosis. Equine Exercise Physiology 7:411-416.

14. Murray RC, Dyson SJ, Tranquille C, et al. 2006. Association of type of sport and performance level with anatomical site of orthopaedic injury diagnosis. Equine veterinary journal Supplement:411-416.

15. Dyson SJ. 2004. Medical management of superficial digital flexor tendonitis: a comparative study in 219 horses (1992–2000). American Veterinary Journal 36.

16. Meershoek LS, Lanovaz JL, Schamhardt HC, et al. 2002. Calculated forelimb flexor tendon forces in horses with experimentally induced superficial digital flexor tendinitis and the effects of application of heel wedges. American journal of veterinary research 63:432-437.

17. Smith RKW, and, Goodship AE. Tendon and ligament physiology.

18. Smith RK, Gerard M, Dowling B, et al. 2002. Correlation of cartilage oligomeric matrix protein (COMP) levels in equine tendon with mechanical properties: a proposed role for COMP in determining function-specific mechanical characteristics of locomotor tendons. Equine veterinary journal Supplement:241-244.

19. Zeugolis DI, Chan JCY, Pandit A. 2011. Tendons: Engineering of Functional Tissues. Tissue Eng:537-572.

20. Wang JH, Iosifidis MI, Fu FH. 2006. Biomechanical basis for tendinopathy. Clin Orthop Relat Res 443:320-332.

21. Docking SI, Daffy J, van Schie HT, et al. 2012. Tendon structure changes after maximal exercise in the Thoroughbred horse: use of ultrasound tissue characterisation to detect in vivo tendon response. Veterinary journal (London, England : 1997) 194:338-342.

22. Dowling BA, Dart AJ. 2005. Mechanical and functional properties of the equine superficial digital flexor tendon. Vet J 170:184-192.

23. Dowling BA, Dart AJ, Hodgson DR, et al. 2000. Superficial digital flexor tendonitis in the horse. Equine Vet J 32:369-378.

24. O'Sullivan CB. 2007. Injuries of the Flexor Tendons: Focus on the Superficial Digital Flexor Tendon. Clinical Techniques in Equine Practice 6:189-197.

25. Dimmen S, Engebretsen L, Nordsletten L, et al. 2009. Negative effects of parecoxib and indomethacin on tendon healing: an experimental study in rats. Knee surgery, sports traumatology, arthroscopy : official journal of the ESSKA 17:835-839.

26. Tsai WC, Hsu CC, Chen CP, et al. 2006. Ibuprofen inhibition of tendon cell migration and down-regulation of paxillin expression. J Orthop Res 24:551-558.

27. Coombes BK, Bisset L, Vicenzino B. 2010. Efficacy and safety of corticosteroid injections and other injections for management of tendinopathy: a systematic review of randomised controlled trials. Lancet 376:1751-1767.

28. Nichols AW. 2005. Complications associated with the use of corticosteroids in the treatment of athletic injuries. Clinical journal of sport medicine : official journal of the Canadian Academy of Sport Medicine 15:370-375.

29. Yamaguchi T, Ochiai N, Sasaki Y, et al. 2015. Efficacy of hyaluronic acid or steroid injections for the treatment of a rat model of rotator cuff injury. J Orthop Res 33:1861-1867.

30. Oryan A, Moshiri A, Meimandi Parizi AH, et al. 2012. Repeated administration of exogenous Sodium-hyaluronate improved tendon healing in an in vivo transection model. Journal of tissue viability 21:88-102.

31. Lutter JD, Schneider RK, Sampson SN, et al. 2015. Medical treatment of horses with deep digital flexor tendon injuries diagnosed with high-field-strength magnetic resonance imaging: 118 cases (2000-2010). Journal of the American Veterinary Medical Association 247:1309-1318.

32. Dyson SJ. 2004. Medical management of superficial digital flexor tendonitis: a comparative study in 219 horses (1992-2000). Equine Vet J 36:415-419.

33. Yamamoto E, Hata D, Kobayashi A, et al. 2002. Effect of beta-aminopropionitrile and hyaluronic acid on repair of collagenase-induced injury of the rabbit Achilles tendon. Journal of comparative pathology 126:161-170.

34. Gwynne-Jones DP, Sims M, Handcock D. 2011. Epidemiology and outcomes of acute Achilles tendon rupture with operative or nonoperative treatment using an identical functional bracing protocol. Foot & ankle international / American Orthopaedic Foot and Ankle Society [and] Swiss Foot and Ankle Society 32:337-343.

35. Gibson KT, Burbidge HM, Pfeiffer DU. 1997. Superficial digital flexor tendonitis in thoroughbred race horses: outcome following non-surgical treatment and superior check desmotomy. Australian veterinary journal 75:631-635.

36. Bosch G, Lin YL, van Schie HT, et al. 2007. Effect of extracorporeal shock wave therapy on the biochemical composition and metabolic activity of tenocytes in normal tendinous structures in ponies. Equine Vet J 39:226-231.

37. Caminoto EH, Alves AL, Amorim RL, et al. 2005. Ultrastructural and immunocytochemical evaluation of the effects of extracorporeal shock wave treatment in the hind limbs of horses with experimentally induced suspensory ligament desmitis. Am J Vet Res 66:892-896.

38. MacGillivray JD, Fealy S, Terry MA, et al. 2006. Biomechanical evaluation of a rotator cuff defect model augmented with a bioresorbable scaffold in goats. J Shoulder Elbow Surg 15:639-644.

39. Caliari SR, Harley BA. 2011. The effect of anisotropic collagen-GAG scaffolds and growth factor supplementation on tendon cell recruitment, alignment, and metabolic activity. Biomaterials 32:5330-5340.

40. Lee JY, Zhou Z, Taub PJ, et al. 2011. BMP-12 treatment of adult mesenchymal stem cells in vitro augments tendon-like tissue formation and defect repair in vivo. Plos One 6:e17531.

41. Jelinsky SA, Li L, Ellis D, et al. 2011. Treatment with rhBMP12 or rhBMP13 increase the rate and the quality of rat Achilles tendon repair. J Orthop Res 29:1604-1612.

42. Zumstein MA, Berger S, Schober M, et al. 2011. Leukocyte- and Platelet-Rich Fibrin (L-PRF) for Long-Term Delivery of Growth Factor in Rotator Cuff Repair: Review, Preliminary Results and Future Directions. Curr Pharm Biotechnol.

43. Fitzpatrick J, Bulsara M, Zheng MH. 2016. The Effectiveness of Platelet-Rich Plasma in the Treatment of Tendinopathy: A Meta-analysis of Randomized Controlled Clinical Trials. Am J Sports Med.

44. Haupt JL, Brandon P. Donnelly a, Nixon. AJ. 2006. Effects of platelet-derived growth factor-BB on the metabolic function and morphologic features of equine tendon in explant culture. AJVR.

45. Schnabel LV, Mohammed HO, Miller BJ, et al. 2007. Platelet rich plasma (PRP) enhances anabolic gene expression patterns in flexor digitorum superficialis tendons. J Orthop Res 25:230-240.

46. Nixon AJ, Dahlgren LA, Haupt JL, et al. 2008. Effect of adipose-derived nucleated cell fractions on tendon repair in horses with collagenase-induced tendinitis. Am J Vet Res 69:928-937.

47. Smith RK. 2008. Mesenchymal stem cell therapy for equine tendinopathy. Disabil Rehabil 30:1752-1758.

48. Uysal AC, Mizuno H. 2011. Differentiation of adipose-derived stem cells for tendon repair. Methods Mol Biol 702:443-451.

49. Crovace A, Lacitignola L, Rossi G, et al. 2010. Histological and immunohistochemical evaluation of autologous cultured bone marrow mesenchymal stem cells and bone marrow mononucleated cells in collagenase-induced tendinitis of equine superficial digital flexor tendon. Vet Med Int 2010:250978.

50. Guest DJ, Smith MR, Allen WR. 2008. Monitoring the fate of autologous and allogeneic mesenchymal progenitor cells injected into the superficial digital flexor tendon of horses: preliminary study. Equine Vet J 40:178-181.

51. Godwin EE, Young NJ, Dudhia J, et al. 2012. Implantation of bone marrow-derived mesenchymal stem cells demonstrates improved outcome in horses with overstrain injury of the superficial digital flexor tendon. Equine Vet J 44:25-32.

52. Smith RK, Werling NJ, Dakin SG, et al. 2013. Beneficial effects of autologous bone marrow-derived mesenchymal stem cells in naturally occurring tendinopathy. PLoS One 8:e75697.

53. Urdzikova ML, Sedlacek R, Suchy T, et al. 2014. Human multipotent mesenchymal stem cells improve healing after collagenase tendon injury in the rat. Biomed Eng Online 13:42.

54. Chong AK, Ang AD, Goh JC, et al. 2007. Bone marrow-derived mesenchymal stem cells influence early tendon-healing in a rabbit achilles tendon model. J Bone Joint Surg Am 89:74-81.

55. Smith AG. 2001. Embryo-derived stem cells: of mice and men. Annual review of cell and developmental biology 17:435-462.

56. Ezashi T, Yuan Y, Roberts RM. 2015. Pluripotent Stem Cells from Domesticated Mammals. Annual review of animal biosciences.

57. Takahashi K, Yamanaka S. 2006. Induction of pluripotent stem cells from mouse embryonic and adult fibroblast cultures by defined factors. Cell 126:663-676.

58. Medvedev SP, Shevchenko AI, Zakian SM. 2010. Induced Pluripotent Stem Cells: Problems and Advantages when Applying them in Regenerative Medicine. Acta naturae 2:18-28.

59. Dominici M, Le Blanc K, Mueller I, et al. 2006. Minimal criteria for defining multipotent mesenchymal stromal cells. The International Society for Cellular Therapy position statement. Cytotherapy 8:315-317.

60. De Schauwer C, Meyer E, Van de Walle GR, et al. 2011. Markers of stemness in equine mesenchymal stem cells: a plea for uniformity. Theriogenology 75:1431-1443.

61. Harting M, Jimenez F, Pati S, et al. 2008. Immunophenotype characterization of rat mesenchymal stromal cells. Cytotherapy 10:243-253.

62. Kisiel AH, McDuffee LA, Masaoud E, et al. 2012. Isolation, characterization, and in vitro proliferation of canine mesenchymal stem cells derived from bone marrow, adipose tissue, muscle, and periosteum. Am J Vet Res 73:1305-1317.

63. McCarty RC, Gronthos S, Zannettino AC, et al. 2009. Characterisation and developmental potential of ovine bone marrow derived mesenchymal stem cells. J Cell Physiol 219:324-333.

64. Munneke JM, Spruit MJ, Cornelissen AS, et al. 2015. The Potential of Mesenchymal Stromal Cells as Treatment for Severe Steroid-Refractory Acute Graft-Versus-Host Disease: A Critical Review of the Literature. Transplantation.

65. Saadi G, Fadel F, El Ansary M, et al. 2013. Mesenchymal stem cell transfusion for desensitization of positive lymphocyte cross-match before kidney transplantation: outcome of 3 cases. Cell proliferation 46:121-126.

66. Bornes TD, Adesida AB, Jomha NM. 2014. Mesenchymal stem cells in the treatment of traumatic articular cartilage defects: a comprehensive review. Arthritis research & therapy 16:432.

67. Hocking AM. 2012. Mesenchymal Stem Cell Therapy for Cutaneous Wounds. Advances in wound care 1:166-171.

68. Singer NG, Caplan AI. 2011. Mesenchymal stem cells: mechanisms of inflammation. Annu Rev Pathol 6:457-478.

69. Griffin MD, Elliman SJ, Cahill E, et al. 2013. Adult Mesenchymal Stromal Cell Therapy for Inflammatory Diseases: How Well are We Joining the Dots? Stem cells.

70. Le Blanc K, Ringden O. 2007. Immunomodulation by mesenchymal stem cells and clinical experience. J Intern Med 262:509-525.

71. Peroni JF, Borjesson DL. 2011. Anti-inflammatory and immunomodulatory activities of stem cells. Vet Clin North Am Equine Pract 27:351-362.

72. Stagg J, Galipeau J. 2013. Mechanisms of immune modulation by mesenchymal stromal cells and clinical translation. Current molecular medicine 13:856-867.

73. Nasef A, Chapel A, Mazurier C, et al. 2007. Identification of IL-10 and TGF-beta transcripts involved in the inhibition of T-lymphocyte proliferation during cell contact with human mesenchymal stem cells. Gene expression 13:217-226.

74. Yin F, Guo L, Meng CY, et al. 2014. Transplantation of mesenchymal stem cells exerts anti-apoptotic effects in adult rats after spinal cord ischemia-reperfusion injury. Brain Res 1561:1-10.

75. Wu Y, Peng Y, Gao D, et al. 2015. Mesenchymal stem cells suppress fibroblast proliferation and reduce skin fibrosis through a TGF-beta3-dependent activation. The international journal of lower extremity wounds 14:50-62.

76. Dong LH, Jiang YY, Liu YJ, et al. 2015. The anti-fibrotic effects of mesenchymal stem cells on irradiated lungs via stimulating endogenous secretion of HGF and PGE2. Scientific reports 5:8713.

77. Kendall RT, Feghali-Bostwick CA. 2014. Fibroblasts in fibrosis: novel roles and mediators. Frontiers in pharmacology 5:123.

78. Huang SK, White ES, Wettlaufer SH, et al. 2009. Prostaglandin E(2) induces fibroblast apoptosis by modulating multiple survival pathways. Faseb j 23:4317-4326.

79. Imberti B, Morigi M, Tomasoni S, et al. 2007. Insulin-like growth factor-1 sustains stem cell mediated renal repair. Journal of the American Society of Nephrology : JASN 18:2921-2928.

80. Huat TJ, Khan AA, Pati S, et al. 2014. IGF-1 enhances cell proliferation and survival during early differentiation of mesenchymal stem cells to neural progenitor-like cells. BMC neuroscience 15:91.

81. Yuksel S, Gulec MA, Gultekin MZ, et al. 2016. Comparison of the Early-Period Effects of Bone Marrow-Derived Mesenchymal Stem Cells and Platelet-Rich Plasma on Achilles Tendon Ruptures in Rats. Connective tissue research.

82. Marsolais D, Cote CH, Frenette J. 2001. Neutrophils and macrophages accumulate sequentially following Achilles tendon injury. J Orthop Res 19:1203-1209.

83. Dakin SG, Werling D, Hibbert A, et al. 2012. Macrophage sub-populations and the lipoxin A4 receptor implicate active inflammation during equine tendon repair. PLoS One 7:e32333.

84. Wojciak B, Crossan JF. 1994. The effects of T cells and their products on in vitro healing of epitenon cell microwounds. Immunology 83:93-98.

85. Chang J, Most D, Stelnicki E, et al. 1997. Gene expression of transforming growth factor beta-1 in rabbit zone II flexor tendon wound healing: evidence for dual mechanisms of repair. Plastic and reconstructive surgery 100:937-944.

86. Liu S, Jiang L, Li H, et al. 2014. Mesenchymal stem cells prevent hypertrophic scar formation via inflammatory regulation when undergoing apoptosis. J Invest Dermatol 134:2648-2657.

87. Shah M, Foreman DM, Ferguson MW. 1995. Neutralisation of TGF-beta 1 and TGF-beta 2 or exogenous addition of TGF-beta 3 to cutaneous rat wounds reduces scarring. J Cell Sci 108 (Pt 3):985-1002.

88. Chang J, Thunder R, Most D, et al. 2000. Studies in flexor tendon wound healing: neutralizing antibody to TGF-beta1 increases postoperative range of motion. Plastic and reconstructive surgery 105:148-155.

89. Qi Y, Jiang D, Sindrilaru A, et al. 2014. TSG-6 released from intradermally injected mesenchymal stem cells accelerates wound healing and reduces tissue fibrosis in murine full-thickness skin wounds. J Invest Dermatol 134:526-537.

90. Manning CN, Martel C, Sakiyama-Elbert SE, et al. 2015. Adipose-derived mesenchymal stromal cells modulate tendon fibroblast responses to macrophage-induced inflammation in vitro. Stem Cell Res Ther 6:74.

91. Gaida JE, Bagge J, Purdam C, et al. 2012. Evidence of the TNF-alpha system in the human Achilles tendon: expression of TNF-alpha and TNF receptor at both protein and mRNA levels in the tenocytes. Cells Tissues Organs 196:339-352.

92. John T, Lodka D, Kohl B, et al. 2010. Effect of pro-inflammatory and immunoregulatory cytokines on human tenocytes. J Orthop Res 28:1071-1077.

93. Gulotta LV, Kovacevic D, Cordasco F, et al. 2011. Evaluation of tumor necrosis factor alpha blockade on early tendon-to-bone healing in a rat rotator cuff repair model. Arthroscopy 27:1351-1357.

94. Bogdan C, Paik J, Vodovotz Y, et al. 1992. Contrasting mechanisms for suppression of macrophage cytokine release by transforming growth factor-beta and interleukin-10. J Biol Chem 267:23301-23308.

95. Reitamo S, Remitz A, Tamai K, et al. 1994. Interleukin-10 modulates type I collagen and matrix metalloprotease gene expression in cultured human skin fibroblasts. The Journal of clinical investigation 94:2489-2492.

96. Ricchetti ET, Reddy SC, Ansorge HL, et al. 2008. Effect of interleukin-10 overexpression on the properties of healing tendon in a murine patellar tendon model. J Hand Surg Am 33:1843-1852.

97. Guest DJ, Smith MR, Allen WR. 2010. Equine embryonic stem-like cells and mesenchymal stromal cells have different survival rates and migration patterns following their injection into damaged superficial digital flexor tendon. Equine Vet J 42:636-642.

98. Odintsov B, Chun JL, Berry SE. 2013. Whole body MRI and fluorescent microscopy for detection of stem cells labeled with superparamagnetic iron oxide (SPIO) nanoparticles and DiI following intramuscular and systemic delivery. Methods Mol Biol 1052:177-193.

99. An J, Beauchemin N, Albanese J, et al. 1997. Use of a rat cDNA probe specific for the Y chromosome to detect male-derived cells. Journal of andrology 18:289-293.

100. Spriet M, Buerchler S, Trela JM, et al. 2015. Scintigraphic tracking of mesenchymal stem cells after intravenous regional limb perfusion and subcutaneous administration in the standing horse. Vet Surg 44:273-280.

101. Sole A, Spriet M, Galuppo LD, et al. 2012. Scintigraphic evaluation of intra-arterial and intravenous regional limb perfusion of allogeneic bone marrow-derived mesenchymal stem cells in the normal equine distal limb using (99m) Tc-HMPAO. Equine Vet J 44:594-599.

102. Pan H, Lan J, Luo X, et al. 2014. Biologic properties of gadolinium diethylenetriaminepentaacetic acid-labeled and PKH26-labeled human umbilical cord mesenchymal stromal cells. Cytotherapy 16:74-83.

103. Nolte IS, Gungor S, Erber R, et al. 2008. In vitro labeling of glioma cells with gadofluorine M enhances T1 visibility without affecting glioma cell growth or motility. Magn Reson Med 59:1014-1020.

104. Yang Y, Zhang J, Qian Y, et al. 2013. Superparamagnetic Iron Oxide is Suitable to Label Tendon Stem Cells and Track Them In Vivo with MR Imaging. Ann Biomed Eng.

105. van Buul GM, Kotek G, Wielopolski PA, et al. 2011. Clinically translatable cell tracking and quantification by MRI in cartilage repair using superparamagnetic iron oxides. Plos One 6:e17001.

106. Pacini S, Spinabella S, Trombi L, et al. 2007. Suspension of bone marrow-derived undifferentiated mesenchymal stromal cells for repair of superficial digital flexor tendon in race horses. Tissue Eng 13:2949-2955.

107. Birch HL, Bailey AJ, Goodship AE. 1998. Macroscopic 'degeneration' of equine superficial digital flexor tendon is accompanied by a change in extracellular matrix composition. Equine Vet J 30:534-539.

108. Patterson-Kane JC, Firth EC. 2009. The pathobiology of exercise-induced superficial digital flexor tendon injury in Thoroughbred racehorses. The Veterinary Journal 181:79-89.

109. Khan KM, Cook JL, Bonar F, et al. 1999. Histopathology of common tendinopathies. Update and implications for clinical management. Sports medicine (Auckland, NZ) 27:393-408.

110. Zhang QZ, Su WR, Shi SH, et al. 2010. Human gingiva-derived mesenchymal stem cells elicit polarization of m2 macrophages and enhance cutaneous wound healing. Stem cells 28:1856-1868.

111. Roddy GW, Oh JY, Lee RH, et al. 2011. Action at a distance: systemically administered adult stem/progenitor cells (MSCs) reduce inflammatory damage to the cornea without engraftment and primarily by secretion of TNF-alpha stimulated gene/protein 6. Stem cells 29:1572-1579.

112. Lan Y, Kodati S, Lee HS, et al. 2012. Kinetics and function of mesenchymal stem cells in corneal injury. Investigative ophthalmology & visual science 53:3638-3644.

113. Rojas M, Parker RE, Thorn N, et al. 2013. Infusion of freshly isolated autologous bone marrow derived mononuclear cells prevents endotoxin-induced lung injury in an ex-vivo perfused swine model. Stem Cell Res Ther 4:26.

114. Curley GF, Ansari B, Hayes M, et al. 2013. Effects of intratracheal mesenchymal stromal cell therapy during recovery and resolution after ventilator-induced lung injury. Anesthesiology 118:924-932.

115. Carrion F, Nova E, Luz P, et al. 2011. Opposing effect of mesenchymal stem cells on Th1 and Th17 cell polarization according to the state of CD4+ T cell activation. Immunology letters 135:10-16.

116. Bunnell BA, Betancourt AM, Sullivan DE. 2010. New concepts on the immune modulation mediated by mesenchymal stem cells. Stem Cell Res Ther 1:34.

117. Waterman RS, Tomchuck SL, Henkle SL, et al. 2010. A new mesenchymal stem cell (MSC) paradigm: polarization into a pro-inflammatory MSC1 or an Immunosuppressive MSC2 phenotype. PLoS One 5:e10088.

118. Abumaree MH, Al Jumah MA, Kalionis B, et al. 2013. Human placental mesenchymal stem cells (pMSCs) play a role as immune suppressive cells by shifting macrophage differentiation from inflammatory M1 to anti-inflammatory M2 macrophages. Stem Cell Rev 9:620-641.

119. Nishimura S, Yasuda A, Iwai H, et al. 2013. Time-dependent changes in the microenvironment of injured spinal cord affects the therapeutic potential of neural stem cell transplantation for spinal cord injury. Molecular brain 6:3.

120. Cho DI, Kim MR, Jeong HY, et al. 2014. Mesenchymal stem cells reciprocally regulate the M1/M2 balance in mouse bone marrow-derived macrophages. Experimental & molecular medicine 46:e70.

121. Park SS, Byeon YE, Ryu HH, et al. 2011. Comparison of canine umbilical cord blood-derived mesenchymal stem cell transplantation times: Involvement of astrogliosis, inflammation, intracellular actin cytoskeleton pathways, and neurotrophin. Cell Transplant.

122. Hu X, Wang J, Chen J, et al. 2007. Optimal temporal delivery of bone marrow mesenchymal stem cells in rats with myocardial infarction. Eur J Cardiothorac Surg 31:438-443.

123. Jiang CY, Gui C, He AN, et al. 2008. Optimal time for mesenchymal stem cell transplantation in rats with myocardial infarction. Journal of Zhejiang University Science B 9:630-637.

124. Keirstead HS, Nistor G, Bernal G, et al. 2005. Human embryonic stem cell-derived oligodendrocyte progenitor cell transplants remyelinate and restore locomotion after spinal cord injury. The Journal of neuroscience : the official journal of the Society for Neuroscience 25:4694-4705.

125. Zhou Z, Lu ZR. 2013. Gadolinium-based contrast agents for magnetic resonance cancer imaging. Wiley Interdiscip Rev Nanomed Nanobiotechnol 5:1-18.

126. Mahmoudi M, Hosseinkhani H, Hosseinkhani M, et al. 2011. Magnetic Resonance Imaging Tracking of Stem Cells in Vivo Using Iron Oxide Nanoparticles as a Tool for the Advancement of Clinical Regenerative Medicine. Chemical Reviews 111:253-280.

127. Laconte L, Nitin N, Bao G. 2005. Magnetic nanoparticle probes. Materials Today 8:32-38.

128. Farrell E, Wielopolski P, Pavljasevic P, et al. 2008. Effects of iron oxide incorporation for long term cell tracking on MSC differentiation in vitro and in vivo. Biochemical and Biophysical Research Communications 369:1076-1081.

129. Arbab AS, Yocum GT, Wilson LB, et al. 2004. Comparison of transfection agents in forming complexes with ferumoxides, cell labeling efficiency, and cellular viability. Mol Imaging 3:24-32.

130. McFaddena C, C. L. Malletta, Foster aPJ. 2011. Labeling of multiple cell lines using a new iron oxide agent for cell tracking by MRI. Contrast Media Mol Imaging.

131. Farrell E, Wielopolski P, Pavljasevic P, et al. 2009. Cell labelling with superparamagnetic iron oxide has no effect on chondrocyte behaviour. Osteoarthritis and Cartilage 17:961-967.

132. Hsiao JK, Tai MF, Chu HH, et al. 2007. Magnetic nanoparticle labeling of mesenchymal stem cells without transfection agent: cellular behavior and capability of detection with clinical 1.5 T magnetic resonance at the single cell level. Magn Reson Med 58:717-724.

133. Ferreira L, Karp JM, Nobre L, et al. 2008. New Opportunities: The Use of Nanotechnologies to Manipulate and Track Stem Cells. Cell Stem Cell 3:136-146.

134. Frank J, Miller B, Arbab A, et al. 2003. Clinically Applicable Labeling of Mammalian and Stem Cells by Combining Superparamagnetic Iron Oxides and Transfection Agents. Radiology.

135. Ko IK, Song H-T, Cho E-J, et al. 2006. In vivo MR Imaging of Tissue-engineered Human Mesenchymal Stem Cells Transplanted to Mouse: a Preliminary Study. Annals of Biomedical Engineering 35:101-108.

136. Addicott B, Willman M, Rodriguez J, et al. 2011. Mesenchymal stem cell labeling and in vitro MR characterization at 1.5 T of new SPIO contrast agent: Molday ION Rhodamine-B. Contrast Media Mol Imaging 6:7-18.

137. Kostura L, Kraitchman DL, Mackay AM, et al. 2004. Feridex labeling of mesenchymal stem cells inhibits chondrogenesis but not adipogenesis or osteogenesis. NMR in Biomedicine 17:513-517.

138. Mahmoudi M, Hofmann H, Rothen-Rutishauser B, et al. 2012. Assessing the in vitro and in vivo toxicity of superparamagnetic iron oxide nanoparticles. Chemical Reviews 112:2323-2338.

139. Aime S, Barge A, Cabella C, et al. 2004. Targeting cells with MR imaging probes based on paramagnetic Gd(III) chelates. Curr Pharm Biotechnol 5:509-518.

140. Xu C, Mu L, Roes I, et al. 2011. Nanoparticle-based monitoring of cell therapy. Nanotechnology 22:494001.

141. Shen J, Cheng LN, Zhong XM, et al. 2010. Efficient in vitro labeling rabbit neural stem cell with paramagnetic Gd-DTPA and fluorescent substance. Eur J Radiol 75:397-405.

142. Raynal I, Prigent P, Peyramaure S, et al. 2004. Macrophage endocytosis of superparamagnetic iron oxide nanoparticles: mechanisms and comparison of ferumoxides and ferumoxtran-10. Investigative radiology 39:56-63.

143. Oude Engberink RD, Van der Pol SMA, Dopp EA, et al. 2007. Comparison of SPIO and USPIO for in Vitro Labeling of Human Monocytes: MR Detection and Cell Function. Radiology 243.

144. Khurana A, Nejadnik H, Gawande R, et al. 2012. Intravenous ferumoxytol allows noninvasive MR imaging monitoring of macrophage migration into stem cell transplants. Radiology 264:803-811.

145. Yang CY, Hsiao JK, Tai MF, et al. 2011. Direct labeling of hMSC with SPIO: the long-term influence on toxicity, chondrogenic differentiation capacity, and intracellular distribution. Mol Imaging Biol 13:443-451.

146. Terrovitis J, Stuber M, Youssef A, et al. 2008. Magnetic resonance imaging overestimates ferumoxide-labeled stem cell survival after transplantation in the heart. Circulation 117:1555-1562.

147. Schmidtke-Schrezenmeier G, Urban M, Musyanovych A, et al. 2011. Labeling of mesenchymal stromal cells with iron oxide-poly(L-lactide) nanoparticles for magnetic resonance imaging: uptake, persistence, effects on cellular function and magnetic resonance imaging properties. Cytotherapy 13:962-975.

148. Qin JB, Li KA, Li XX, et al. 2012. Long-term MRI tracking of dual-labeled adipose-derived stem cells homing into mouse carotid artery injury. Int J Nanomedicine 7:5191-5203.

149. Li YG, Wei JN, Lu J, et al. 2011. Labeling and tracing of bone marrow mesenchymal stem cells for tendon-to-bone tunnel healing. Knee Surg Sports Traumatol Arthrosc.

150. Song HT, Jordan EK, Lewis BK, et al. 2009. Rat model of metastatic breast cancer monitored by MRI at 3 tesla and bioluminescence imaging with histological correlation. J Transl Med 7:88.

151. Kosaka N, Bernardo M, Mitsunaga M, et al. 2012. MR and optical imaging of early micrometastases in lymph nodes: triple labeling with nano-sized agents yielding distinct signals. Contrast Media Mol Imaging 7:247-253.

152. Heyn C, Ronald JA, Ramadan SS, et al. 2006. In vivo MRI of cancer cell fate at the single-cell level in a mouse model of breast cancer metastasis to the brain. Magn Reson Med 56:1001-1010.

153. Li SC, Tachiki LML, Luo J, et al. 2010. A Biological Global Positioning System: Considerations for Tracking Stem Cell Behaviors in the Whole Body. Stem Cell Reviews and Reports 6:317-333.

154. McFadden CD, C L Mallett, and PJ Foster. 2011. Labeling of multiple cell lines using a new iron oxide agent for cell tracking by MRI. Contrast Media Mol Imaging 6:514-522.

155. Sutton EJ, Henning TD, Boddington S, et al. 2010. In vivo magnetic resonance imaging and optical imaging comparison of viable and nonviable mesenchymal stem cells with a bifunctional label. Mol Imaging 9:278-290.

156. Guenoun J, Ruggiero A, Doeswijk G, et al. 2013. In vivo quantitative assessment of cell viability of gadolinium or iron-labeled cells using MRI and bioluminescence imaging. Contrast Media Mol Imaging 8:165-174.

157. Henning TD, Wendland MF, Golovko D, et al. 2009. Relaxation effects of ferucarbotran-labeled mesenchymal stem cells at 1.5T and 3T: discrimination of viable from lysed cells. Magn Reson Med 62:325-332.

158. Tripathi L, Kumar P, Singh R. 2009. Role of chelates in magnetic resonance imaging studies. Journal of cancer research and therapeutics 5:148-153.

159. Liu Y, He ZJ, Xu B, et al. 2011. Evaluation of cell tracking effects for transplanted mesenchymal stem cells with jetPEI/Gd-DTPA complexes in animal models of hemorrhagic spinal cord injury. Brain Res 1391:24-35.

160. Rudelius M, Daldrup-Link HE, Heinzmann U, et al. 2003. Highly efficient paramagnetic labelling of embryonic and neuronal stem cells. European journal of nuclear medicine and molecular imaging 30:1038-1044.

161. Shyu WC, Chen CP, Lin SZ, et al. 2007. Efficient tracking of non-iron-labeled mesenchymal stem cells with serial MRI in chronic stroke rats. Stroke 38:367-374.

162. Guenoun J, Koning GA, Doeswijk G, et al. 2012. Cationic Gd-DTPA liposomes for highly efficient labeling of mesenchymal stem cells and cell tracking with MRI. Cell Transplant 21:191-205.

163. Guenoun J, Ruggiero A, Doeswijk G, et al. 2013. In vivo quantitative assessment of cell viability of gadolinium or iron-labeled cells using MRI and bioluminescence imaging. Contrast Media Mol Imaging 8:165-174.

164. Faucher L, Tremblay M, Lagueux J, et al. 2012. Rapid synthesis of PEGylated ultrasmall gadolinium oxide nanoparticles for cell labeling and tracking with MRI. ACS Appl Mater Interfaces 4:4506-4515.

165. Henning TD, Saborowski O, Golovko D, et al. 2007. Cell labeling with the positive MR contrast agent Gadofluorine M. European radiology 17:1226-1234.

166. Anderson SA, Lee KK, Frank JA. 2006. Gadolinium-fullerenol as a paramagnetic contrast agent for cellular imaging. Investigative radiology 41:332-338.

167. Loai Y, Ganesh T, Cheng HL. 2012. Concurrent dual contrast for cellular magnetic resonance imaging using gadolinium oxide and iron oxide nanoparticles. International journal of molecular imaging 2012:230942.

168. Modo M, Mellodew K, Cash D, et al. 2004. Mapping transplanted stem cell migration after a stroke: a serial, in vivo magnetic resonance imaging study. NeuroImage 21:311-317.

169. Nejadnik H, Henning TD, Do T, et al. 2012. MR imaging features of gadofluorine-labeled matrix-associated stem cell implants in cartilage defects. PLoS One 7:e49971.

170. Loai Y, Sakib N, Janik R, et al. 2011. Human Aortic Endothelial Cell Labeling with Positive Contrast Gadolinium Oxide Nanoparticles for Cellular Magnetic Resonance Imaging at 7 Tesla. Mol Imaging.

171. Watts AE, Yeager AE, Kopyov OV, et al. 2011. Fetal derived embryonic-like stem cells improve healing in a large animal flexor tendonitis model. Stem Cell Res Ther 2:4.

172. Schnabel LV, Lynch ME, van der Meulen MC, et al. 2009. Mesenchymal stem cells and insulin-like growth factor-I gene-enhanced mesenchymal stem cells improve structural aspects of healing in equine flexor digitorum superficialis tendons. J Orthop Res 27:1392-1398.

173. Becerra P, Valdes Vazquez MA, Dudhia J, et al. 2013. Distribution of injected technetium(99m)-labeled mesenchymal stem cells in horses with naturally occurring tendinopathy. J Orthop Res 31:1096-1102.

174. Crovace A, Lacitignola L, Francioso E, et al. 2008. Histology and immunohistochemistry study of ovine tendon grafted with cBMSCs and BMMNCs after collagenase-induced tendinitis. Vet Comp Orthop Traumatol 21:329-336.

175. Carvalho Ade M, Badial PR, Alvarez LE, et al. 2013. Equine tendonitis therapy using mesenchymal stem cells and platelet concentrates: a randomized controlled trial. Stem Cell Res Ther 4:85.

176. Vieira MH, Oliveira RJ, Eca LP, et al. 2014. Therapeutic potential of mesenchymal stem cells to treat Achilles tendon injuries. Genetics and molecular research : GMR 13:10434-10449.

177. Al-Ani M, Xu K, Sun Y, et al. 2015. Study of Bone Marrow Mesenchymal and Tendon-Derived Stem Cells Transplantation on the Regenerating Effect of Achilles Tendon Ruptures in Rats. Stem cells international 2015:984146.

178. Baligand C, Vauchez K, Fiszman M, et al. 2009. Discrepancies between the fate of myoblast xenograft in mouse leg muscle and NMR label persistency after loading with Gd-DTPA or SPIOs. Gene Ther 16:734-745.

179. Hedlund A, Ahren M, Gustafsson H, et al. 2011. Gd(2)O(3) nanoparticles in hematopoietic cells for MRI contrast enhancement. Int J Nanomedicine 6:3233-3240.

180. Cao AH, Shi HJ, Zhang Y, et al. 2009. In vivo tracking of dual-labeled mesenchymal stem cells homing into the injured common carotid artery. Anat Rec (Hoboken) 292:1677-1683.

181. Chen J, Wang F, Zhang Y, et al. 2012. In Vivo Tracking of Superparamagnetic Iron Oxide Nanoparticle Labeled Chondrocytes in Large Animal Model. Annals of Biomedical Engineering.

182. Gonzalez-Lara LE, Xu X, Hofstetrova K, et al. 2011. The use of cellular magnetic resonance imaging to track the fate of iron-labeled multipotent stromal cells after direct transplantation in a mouse model of spinal cord injury. Mol Imaging Biol 13:702-711.

183. Kriz J, Jirak D, White D, et al. 2008. Magnetic resonance imaging of pancreatic islets transplanted into the right liver lobes of diabetic mice. Transplant Proc 40:444-448.

CHAPTER 3

SUPERPARAMAGNETIC IRON OXIDE NANOPARTICLES AS A MEANS TO TRACK MESENCHYMAL STEM CELLS IN A LARGE ANIMAL MODEL OF TENDON INJURY[1]

[1] Scharf, AM, SP Holmes, M Thoreson, J Mumaw, A Stumpf, and J Peroni. 2015. *Contrast Media & Molecular Imaging*, 10:388-397. Reprinted here with permission of the publisher.

Abstract

Purpose: The goal of this study was to establish a SPIO-based cell tracking method in an ovine model of tendonitis and to determine if this method may be useful for further study of cellular therapies in tendonitis *in vivo*.

Procedures: Functional assays were performed on labeled and unlabeled cells to ensure no significant changes were induced by intracellular SPIOs. Following biosafety validation, tendon lesions were mechanically (n=4) or chemically (n=4) induced in 4 sheep and scanned *ex vivo* at 7 and 14 days to determine the presence and distribution of intralesional cells.

***Results*:** Ovine MSCs labeled with 50 μg SPIOs/mL remain viable, proliferate, and undergo tri-lineage differentiation ($p<0.05$). Labeled ovine MSCs remained detectable *in vitro* in concentrated cell numbers as low as 10,000 and in volumetric distributions as low as 100,000 cells/mL. Cells remained detectable by MRI at 7 days, as confirmed by correlative histology for dually labeled SPIO+/GFP+ cells. Histological evidence at 14 days suggested that SPIO particles remained embedded in tissue, providing MRI signal, although cells were no longer present.

Conclusions: SPIO labeling has proven to be an effective method for cell tracking for a large animal model of tendon injury for up to 7 days post-injection. The data obtained in this study justifies further investigation into the effects of MSC survival and migration on overall tendon healing and tissue regeneration.

Keyworks:

MRI, SPIO, cell tracking, MSC

Introduction

Over the last decade, discoveries in stem cell research have led to the integration of regenerative medicine approaches into traditional orthopedic treatment regimens in both human and veterinary medicine. The injection of mesenchymal stem cells (MSCs) and stem cell-derived products in the treatment of tendon and ligament injuries has led to notable improvements in tissue repair [1-4]. Furthermore, studies conducted in humans and animals have shown that stem cell-based therapies improve the organization, composition and biomechanics of injured soft tissues [4-10]. Despite these promising results, the biological events that underpin the interactions between injected MSCs and the host tissue are still poorly understood. The development of reliable animal models will greatly aid the study of disease progression and the mechanisms of healing affected by stem cell therapies [11-15]. In this study, we employ an ovine model of tendinopathy to elucidate the localization of MSCs after intralesional treatment.

In addition to their regenerative properties, MSCs contribute to healing via a paracrine effect that results in modulation of inflammatory and immune responses and activation and proliferation of progenitor cells present in native tissue [16-18]. As a result, therapeutic effects of MSCs have been observed even when relatively low numbers of cells engraft or incorporate into damaged tissues [19; 20]. Tracking MSCs following injection into damaged tissues is vital to understanding whether tissue healing is primarily attributed to the direct integration of injected cells; a localized, signaling cascade induced by these cells; or a combination of these effects.

Nanotechnology-based cell tracking methods provide non-toxic, non-invasive, clinically applicable solutions for long term monitoring of cells post-injection [21; 22]. These nanotechnologies may expedite the translation of stem cell therapies from the laboratory into the clinic, but not without extensive preliminary work demonstrating their biosafety and detection limits. The

overall goal of this study is to validate the use of magnetic resonance imaging (MRI) to track migration patterns of MSCs labeled with superparamagnetic iron oxide (SPIO) in an ovine model of tendonitis.

SPIOs are a negative contrast agent, producing dark regions or signal voids on MRI images obtained using T2 or T2*-weighted pulse sequences. They are particularly effective at generating image contrast in tissues characterized by high signal intensity, such as the brain [23]. SPIO particles offer several advantages over other contrast agents, such as bioluminescent labels, quantum dots and radionuclides because they are non-toxic, biodegradable, and do not emit ionizing agents [22; 24]. They can be endocytosed by stem cells using simple co-incubation protocols, after which they remain detectable for a period of weeks [21; 24-26]. To date, SPIO nanoparticle labels have been used as MRI contrast agents in several studies involving MSCs [27-30]. The detection of SPIO-labeled cells has been accomplished in pancreatic islet transplants [31], myocardial dysfunction [32], cancers [33], spinal cord and brain injuries [34; 35], and articular cartilage defects [36].

The overall goal of this study was to establish a SPIO-based cell tracking method in an ovine model of tendonitis that can be used to more accurately understand the *in vivo* behavior of MSCs introduced within a tendon injury. The hypotheses underlying the current study were that ovine MSCs labeled with up to 50 μg of Molday ION™ SPIO nanoparticles/mL will remain viable, proliferate, and undergo tri-lineage differentiation, and that these labeled ovine MSCs will be detectable both *in vitro* and *ex vivo* using a clinical, high field MRI unit for up to 14 days post-injection.

Materials and Methods

All experiments were performed in triplicate using 3 biological replicates of cryopreserved bone marrow derived ovine MSCs cultured under passage 10. Cells were maintained in culture at 37 °C and 5% CO_2, grown to 70% confluency in MSC culture medium (low glucose Dulbecco's Modified Eagle Medium (DMEM), 10% Fetal Bovine Serum, 1% L-glutamine, 50 U/mL penicillin, 50 μg/mL streptomycin), and treated with either 25 or 50 μg/mL Molday ION C6Amine (Biopal, Inc.) SPIOs overnight unless otherwise noted. Untreated cells were prepared identically and used for all experiments. Prior to use in the experiments, incubation medium was aspirated from the plates, and the cells washed with PBS and harvested with 0.25% Trypsin-EDTA (Invitrogen). Cells were fixed with 4% paraformaldehyde, incubated for 10 minutes with Prussian Blue reagents (Biopal, Inc), and positive staining was confirmed with light microscopy (Leica).

Cell Labeling Efficiency, Iron Content, and Viability following SPIO treatment

For all experiments, cells were grown to 70% confluency, labeled overnight with SPIO nanoparticles and harvested for analysis. Cell labeling efficiency was evaluated in cells treated with 25 or 50 μg Molday ION Coumarin™/mL by flow cytometry. Molday ION Coumarin™ is the fluorescent equiavalent of Molday C5Amine™ (Biopal, Inc). Flow cytometry was performed on a HyperCyan (Beckman Coulter) machine with FACSDiva software. For iron content, cells were labeled with 25 μg Molday C6Amine™/mL, harvested, counted, and digested in dilute nitric acid for analysis by MS-OES performed by the Center for Applied Isotope Studies at the University of Georgia. For cell viability, cells were labeled with 25, 50, or 100 μg Molday C6Amine™/mL. A Trypan Blue (cellgro®) exclusion assay was performed for viability according to the manufacturer's protocol.

Metabolic Activity and Proliferation

For proliferation assays, cells were plated in flat bottom, 96-well plates at a density of 28,000 cells/cm^2. Once they reached 50% confluency, the cells were treated with 25 or 50 μg/mL Molday ION C6Amine, rinsed and used for the following two assays. An alamarBlue® (Invitrogen) assay was performed according to the manufacturer's protocol and read on a microplate reader at 12, 24 and 48 hours post-treatment. The Click-iT® Edu (Invitrogen) assay was performed according to the manufacturer's microplate assay protocol.

Tri-Lineage Differentiation

For osteogenic and adipogenic differentiation experiments, cells were plated in flat bottom, 96-well plates at a density of 28,000 cells/cm^2 and cultured in complete MSC medium for 24 hours. Undifferentiated cells cultured for 24 hours in MSC culture medium were used as controls for all differentation assays.

Osteogenic induction cultures were replenished with Hyclone® AdvanceSTEM™ osteogenic medium every 2-3 days for 28 days. Osteogenic differentiation was determined using Calcium Liquicolor® Test (Stanbio). Briefly, calcium was extracted from the differentiated cultures with 0.6N HCl overnight at 4 degrees. The supernatant was combined at a ratio of 1:20 in an equal portion mixture of the color and base reagents from the calcium liquicolor test and read on a plate reader at 550 nm.

Adipogenic induction cultures were replenished with Hyclone® AdvanceSTEM™ adipogenic medium for 14 days then switched to an adipogenic medium consisting of DMEM, 10% FBS, 5% rabbit serum, 0.5 μM dexamethasone, 60 μM indomethacin, 0.5 mM IBMX, 1 μM insulin, and 50 U/ml penicillin, 50 μg/ml streptomycin for the remaining 14 days with medium changes

every 2-3 days. Adipogenic cells were fixed with 4% paraformaldehyde and stained with Oil Red O to identify lipid deposits.

For chondrogenic differentiation, cells were plated in conical bottom, 96-well plates without culture treatment at 100,000 cells/well, centrifuged at 500 x g for 10 minutes, and replenished with Hyclone® AdvanceSTEM™ chondrogenic medium every 2-3 days for 28 days. For quantification of viable cells following differentiation, a neutral red uptake assay was preformed as described [37] with minor variations. Briefly, chondrogenic pellets were incubated with 40 μg/mL neutral red in MSC culture medium for 2 hours and rinsed with PBS. The neutral red was extracted from the chondrogenic pellets during fixation with 100% methanol at -20°C for 10 minutes. The methanol was transferred to a flat bottom plate and read on a plate reader at 550 nm. The fixed chondrogenic pellets were then stained with 0.2% Alcian Blue in 0.1 M HCl overnight, extracted with 0.1 mL 6 M guanidine/HCl for 2 hours, and read at 650 nm in a flat bottom plate.

MRI Phantom Study

A preliminary study was performed to establish the sensitivity and limits of MRI detection of SPIO treated MSCs. In this study, phantoms were designed using Lab-Tek™ chamber slides filled with 1 mL layers of 1% agar containing either 10,000; 100,000; 500,000; or 1 million cells separated by a 1mL layer of cell-free 1% agar. Five 3-mm wells were also made in a chamber slide filled with 1% agar solution to scan concentrated cell suspensions containing the same cell numbers. Mean signal intensities (MSI) of labeled cells were measured using a circular ROI of 0.065 cm^2 and a rectangular ROI of 0.065 cm^2 in four slices using Osirix software. SNR was calculated by dividing the MSI by the standard deviation of the background noise. Sidak's

multiple comparison test was used in addition to Tukey's multiple comparison test to compare the difference between equal cell numbers at different treatment levels.

In Vivo Experiments

GFP fluorescence

To ensure cells were co-localized with SPIOs detectable by MRI, cells were dually labeled with nanoparticles and green fluorescent protein (GFP). To generate GFP positive cells, ovine MSCs were plated in 6-well plates at 32,000 cells/cm^2 and allowed to adhere overnight. The following day the cells were transduced with a lentiviral vector containing eGFP with a CAG promoter described in Pfeifer, Ikawa et al [38]. The plasmid for the lentiviral eGFP was obtained from addgene (plasmid 14857). The transduction was performed at 10 molecules of infection in the presence of 8 μg/ml polybrene. To enhance the transduction efficiency, the plates were centrifuged at 100 X g for 90 minutes at room temperature. The MSCs were sorted using MoFlo XDP (Beckman Coulter) to obtain a pure population of GFP positive cells and cryopreserved for future use.

Sheep Model

All work performed in this study was done in accordance with the University of Georgia Institutional Animal Care and Use committee guidelines. Deep digital flexor tendon (DDFT) lesions were created in four sheep using opposite front and hind limbs. Sheep were sedated with 0.25 mg/kg midazolam and 0.1 mg/kg butorphanol, administered intravenously and restrained in lateral recumbency. The lateral and medial aspects of one metatarsal and one metacarpal region were clipped and aseptically prepared. The limbs were desensitized with a ring block performed using 5 ml of 2% lidocaine infused subcutaneously just distal to the carpus or tarsus. Mechanically-induced lesions were made in one forelimb and chemically induced lesions were

made in one hind limb of all 4 sheep. Mechanical lesions were created using a curved 16 gauge 8.89 cm Weiss Epidural needle with a Tuohy tip placed under ultrasonographic guidance within the core of the deep digital flexor tendon. This needle was manipulated to separate tendon fibers longitudinally. Chemical lesions were induced via the injection of 400 IU collagenase 1A (Sigma) dissolved in 0.5 mL saline under ultrasonagraphic guidance within the core of the deep digital flexor tendon.

Three days later, cryopreserved GFP+, P6 or P7 ovine allogeneic, ovine MSCs were treated with 25 ug/mL C6Amine Molday ION overnight. The following day, cells were harvested, recipient sheep were sedated as described above, and the skin overlying their tendons aseptically prepared. The labeled cells were suspended in PBS at a concentration of 500,000 cells/ml and injected under ultrasonographic guidance through a 20-gauge needle according to the schedule in Table I. Sheep received a dose of either 500,000 or 1 million cells. The sheep were evaluated daily for changes in body temperature, heart and respiratory rates and lameness for the duration of the study.

Ex Vivo *Magnetic Resonance Imaging*

Sheep were sacrificed at either 7 or 14 days following the injections of MSCs (Table I). Tendon imaging was performed immediately following euthanasia and tendon excision to minimize tissue degradation. MRI was performed using a GE HDX 3.0T Signa twin gradient MRI unit with 15.0 M4 software. All imaging was performed with an 8-channel wrist coil. All samples were imaged using a fast imaging employing steady state acquisition (FIESTA) pulse sequence, acquired in transverse and sagittal planes. The FIESTA imaging parameters were as follows: TR = 10.7 ms; TE = 5.3 ms; flip angle, 20°; receiver bandwidth 31.25 kHz; isotropic resolution of 0.3 mm. The acquisition time was approximately 30 minutes. T2-weighted fast spin echo (FSE)

images were acquired in the sagittal plane to define the extent of tendonitis. A measurement from the proximal limit of the sesamoid bone to the proximal limit of signal void was made with Osirix image visualization program (Pixmeo, Geneva, Switzerland) in DICOM (Digital Imaging and Communication in Medicine) format and used as a reference to cut 4 cm tendon sections for histology.

Correlative Histology

A 4 cm length of tendon was excised, embedded in OCT compound (Tissue-Tek®), and longitudinally sectioned on a cryostat (Leica) at 10 or 20 μm. Sections were serially collected from the tendons and mounted on glass slides. Slides of varying depth/regions from all tendons were fixed with 4% paraformaldehyde, incubated with Prussian Blue reagents (Biopal, Inc) for 10 minutes to evaluate the presence of iron nanoparticles, and counterstained with Nuclear Fast Red to visualize tissue morphology with light microscopy. For all slides staining positive for Prussian Blue, serially located slides were fixed with acetone, incubated with a rabbit polyclonal anti-GFP antibody at a concentration of 1:500 in 1% BSA, then incubated with a donkey anti-rabbit Alexa Flour 594-conjugated secondary antibody (1:1000; Invitrogen), counterstained with DAPI (Biotium) at 0.1 μg/ml and mounted with fluorescent mounting medium (Diagnostic Biosystems) to assess the location of GFP+ cells with fluorescent microscopy.

Statistical Analysis

One-way analysis of variance (ANOVA) was performed between groups, followed by Tukey's multiple comparison tests at a significance level of 0.05 as compared to control using Prism software. Three ovine cell lines were analyzed at each time point with measurements performed in triplicate. Error is reported in figures as standard error of the mean.

Results

Cell Labeling Efficiency, Iron Content, and Viability following SPIO treatment

SPIO particles at both 25 and 50 μg/mL were endocytosed by MSCs and appeared to be perinuclear in location (Figure 3.1). Analysis of Trypan Blue exclusion data demonstrated that the viability of ovine MSCs did not vary from 97% following treatments at 25 or 50 μg/mL, but showed a significant decrease to 93% ($p<0.05$) following treatment at 100 μg/mL, compared to 99% in untreated cells (Figure 3.2A). Labeling efficiency of the ovine MSCs was 95% and 94% after treatment with 25 and 50 μg/mL, respectively (Figure 3.2B). Iron content was determined to be 9.58 ± 2.79 pg/cell.

Metabolic Activity and Proliferation

The metabolic activity and proliferative capacity of MSCs were not significantly different than that of untreated cells at either concentration ($p<0.05$, Figure 3.3).

Tri-Lineage Differentiation

There was no appreciable difference in the ability of untreated and treated cells to undergo osteogenic (Figure 3.4) and adipogenic differentiation (Figure 3.5). All cells underwent osteogenic and chondrogenic differentiation as compared to undifferentiated control cells ($p<0.0001$, Figure 3.4 and 3.6). In contrast, cells in both treatment groups showed a significant reduction in chondrogenic differentiation when compared to untreated cells ($p<0.05$, Figure 3.6).

MRI Phantom Study

Phantom models indicated that MR signal intensity decreased with increasing labeled cell numbers. Cell concentrations as low as 100,000 cells/mL were readily detected at this image resolution in the larger, 1 mL volumetric model for both treatment groups (Figure 3.7B and D, $p<0.0001$). The more concentrated cell suspensions demonstrated significant MR signal in cells

labeled with 25 or 50 μg/mL with cell numbers greater than or equal to 10,000 cells (Figure 3.7A and C). However, significant differences were seen between cell treatment groups at the lowest concentration of 10,000 cells in both concentrated cells and in cell suspensions ($p<0.0001$). At the highest cell concentration tested (1,000,000 cells/mL), characteristic magnetic dipole moments induced by the SPIO particles were most evident.

Ex Vivo *Magnetic Resonance Imaging*

All chemical and mechanical lesions were detectable at 7 and 14 days. Collagenase lesions were detectable as large areas of diffuse, hyperintense signal (Figure 3.8A) whereas mechanical lesions were detectable as small, focal, linear areas of disruption within the flexor tendon (Figure 3.8B). In dorsal plane FIESTA MR images of ovine deep digital flexor tendons, spherical signal voids, as well as coalescing regions of signal void, were present in subjectively greatest quantity near the site of injection on both days 7 and 14 (Figure 3.9A and B). Smaller foci of signal void were present throughout the visible area of tendon disruption, indicating that migration of the labeled MSCs away from the initial location of injection had occurred. These areas were easiest to localize within chemically induced tendon injuries. The signal voids seen within or near the tendon sheath were suspected to be associated with injection or reflux of cells along the shaft of the needle.

Correlative Histology

Histological tissue sections corresponding to tendon measurements, as mapped on MRI, stained positive for Prussian Blue and showed distribution patterns similar to those seen in MR images (Figure 3.9). Tissue sections harvested on day 7 (Figure 3.10A) also stained positive for GFP at or near the location of SPIO particles, suggesting that cells remained viable and that the particles likely remained within cells at this time. Less staining for GFP cells was noted on day 14 (Figure

3.10B) and often no GFP+ stain was visible on serially located slides that stained positive for Prussian Blue.

Discussion

This study is the first to establish a clinically relevant method for robust detection of cell numbers as low as 500,000 in a large animal model of tendon injury. SPIO labeling has been applied to numerous cell-tracking studies; however, there is little available data demonstrating the ability to detect and track cells. Specifically MSC detection and tracking was achieved using a clinical strength magnet without the use of expensive, equipment modifications, such as magnets with field strength greater than 3 Tesla [39] or modified gradient coils [24; 31; 35]. There is also little published data comparing the variability of SPIO uptake and cytotoxicity between species or cell lines, even though several papers have been published acknowledging the potential for cytotoxicity following the uptake of dextran-coated nanoparticles [40; 41].

The SPIOs adopted for the MSC tracking method used in the current study were dextran-coated iron oxide-based superparamagnetic contrast reagents with a colloidal size of 35 nm (BioPal, Inc). These particles are designed for cell labeling and tracking and require neither viral nor chemical transfection reagents. Cells labeled with 25 μg/mL Molday ION™ nanoparticles remained viable, proliferated, and underwent tri-lineage differentiation similar to untreated cells. These results are in agreement with many studies conducted in MSCs of different species [21; 27; 35; 42]. In our study, chondrogenic differentiation was appreciably different between treated and untreated cells, although treated MSCs still retained the ability to form cartilage. Conflicting results can be found in the literature regarding the ability of SPIO-treated cells to undergo chondrogenic differentiation [36; 39; 42-44]. These data suggest that it is particularly important to assay

the effects of SPIO particles on individual cell lines if applications for cartilage regeneration are of interest. If these limitations are due to changes in the production of extracellular matrix or interference with the actin cytoskeleton, it is unlikely that SPIOs can be justified as a means to track cell migration *in vivo*.

Phantom models were constructed and used to optimize MRI sequences for detection. Within the agar gel mold, the intracellular nanoparticles create a region of magnetic susceptibility that is clearly visible using FIESTA pulse sequences. The FIESTA sequences generate images with T2 and T1 properties. It is a sequence widely employed for the detection of SPIOs as it provides high-resolution images with high contrast and high signal-to-noise ratio and is able to discriminate hemorrhage [31; 34; 45]. The signal voids generated by SPIOs in FIESTA images often extend beyond the voxel in which the SPIO-labeled cells are contained and create a blooming effect with notable dipoles if SPIO numbers are large enough. A decrease in signal intensity was noticed in both agar gel phantoms and used to establish the limit of cell detection as 100,000 cells/mL in a 1 mL volumetric distribution and 10,000 cells when concentrated. Blooming signal voids were clearly visible in all tendon specimens containing labeled cells up to day 14 post-injection, indicating that nanoparticles can be identified successfully using a 3T MR scanner and an 8-channel wrist coil. Although tendon is characterized by low signal intensity in T2-weighted images, the characteristic fiber disruption and edema present in tendonitis produce a favorable contrast for SPIO detection. The collagenase model of tendonitis provided a superior model for cell tracking as compared to the mechanical model due to the presence of large and diffuse areas of hyperintense signal. The distribution of nanoparticles in MR images correlated well to corresponding histological sections stained with Prussian Blue, confirming that the signal voids originated from nanoparticles as opposed to other phenomena, such as hemorrhage. Similar

results were obtained recently in a study of tendon stem cells conducted by Yang et al. [26] successfully demonstrating negative MRI signal and Prussian Blue staining for up to 3 weeks post-injection *in vivo*. This study, however, did not confirm the co-localization of cells, but only the continued presence of nanoparticles.

Recent studies have expressed concern regarding the fate of the iron nanoparticles post-injection [22; 35; 46-48]. SPIOs may be expelled by the host cells during cell lysis or apoptosis and taken up by macrophages in the host tissue [22; 46]. Wang et al. noted that SPIO-labeled cells may exocytose the SPIOs once the cells localize *in vivo*, recognizing the SPIO as unwanted material [49]. As a result, many studies have adopted dual labeling strategies, incorporating GFP [50; 51] or quantum dots [52] into the cell of interest, in addition to SPIO nanoparticles. In this study, SPIO+/GFP+ cells were injected into tendons to establish co-localization of nanoparticles and injected cells. GFP+ cells were definitively present at day 7, while little to no GFP+ cells remained detectable at day 14. GFP expression is only maintained in viable cells. In this study, the co-localization of nanoparticles and GFP+ cells at day 7 followed by the persistence of nanoparticles and absence of GFP+ cells at day 14 suggests that the MSCs persist for only a short time before undergoing cell death. It is unlikely that cell death is correlated with SPIO labeling; many studies, including this one, have demonstrated low cytotoxicity of SPIO particles in labeled cells [21; 22; 24; 25; 27; 28; 53-56]. Previous studies have also demonstrated the persistence of the SPIO label following cell division [22; 33], so all daughter cells should retain the SPIO and GFP labels. It is most likely that the majority of injected cells do not survive, which has similarly been reported following intra-lesional injection [19; 20] and regional limb perfusion [50]. However, these studies do not conclude if low cell retention is due to cell migration or cell death. It is possible that the tendon microenvironment does not provide adequate nutrient and oxygen supply to support large cell

populations such as those routinely injected for cell therapies and is unlikely to enable long-term cell retention as a result.

The clinical importance of cell survival must be taken into account and studied further to understand the overall effects MSCs have on the healing process. For instance, multiple injections at regular intervals may provide greater benefit to the patient as compared to a single injection. To confirm the results of this study, further data regarding cell survival *in vivo* paired with additional cell tracking technologies must be collected. Numerous studies have reported that SPIOs can be taken up by local immune cells [47; 49; 57-59] and/or persist after cell death [47; 49; 57; 60]. For this reason, it is essential to pair SPIO-imaging strategies with additional cell tracking protocols, such as GFP labeling. One of the limitations of this study was that we were unable to quantify the extent of cell death post-injection. If the majority of cell migration is expected to take place within the first 7 days, it appears likely that all labeled cells remain labeled and viable at this time.

The positive detection of nanoparticles seen at 3 T both in agar gel phantoms and in ovine tendon provide encouraging data that MRI-based SPIO cell tracking can provide an effective means of detecting cells in numbers as low as 10,000 cells in focused regions *in vitro* and 500,000 cells *in vivo*. This is likely to be sufficient in equine and/or human tendon where clinical protocols inject between 10 and 30 million cells per lesion.

Conclusion

SPIO labeling has proven to be an effective method for cell tracking for a large animal model of tendon injury for up to 7 days post-injection. The continual development of this technology will result in a longitudinal cell tracking method that will enable researchers to analyze data regarding

cell location, distribution, and rates of disappearance over time in the musculoskeletal system of large animals. This technology can be used to determine whether or not cells have reached their target and how long they remain in these locations, as well as to monitor and optimize route of delivery, preferred sites of engraftment, and dosing schedules. The application of MRI-based cell tracking should facilitate the field of regenerative medicine, elucidating new aspects of MSC behavior.

Day 7	Sheep 1 LF: 500 000	Sheep 1 RH: 500 000
	Sheep 2 RF: 1 million	Sheep 2 LH: 1 million
Day 14	Sheep 3 LF: 500 000	Sheep 3 RH: 500 000
	Sheep 4 RF: 1 million	Sheep 4 LH: 1 million

Table 3.1 Schedule for sheep treatments.

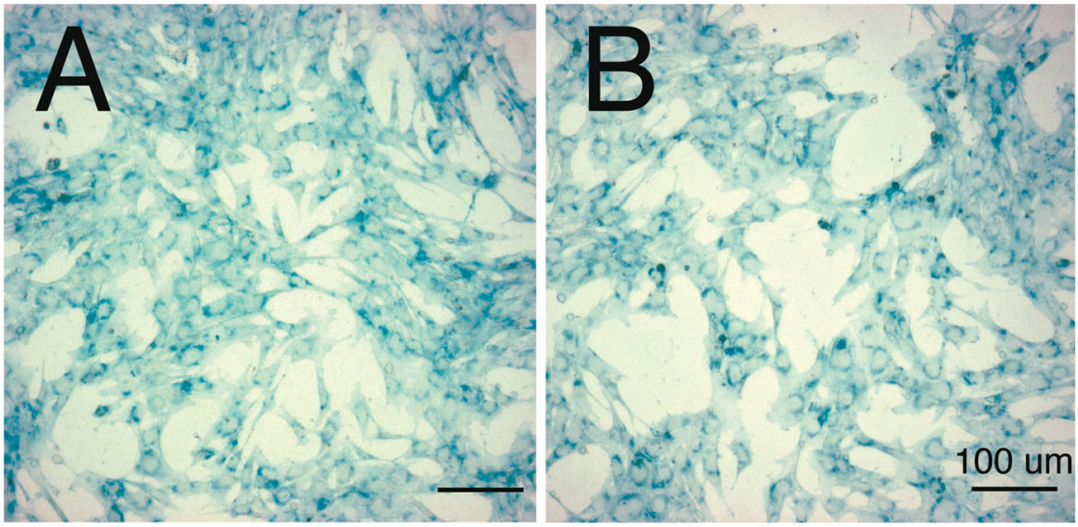

Figure 3.1. Light microscopy of SPIO-labeled cells. Following treatment with A) 25 and B) 50 μg/mL and Prussian Blue staining.

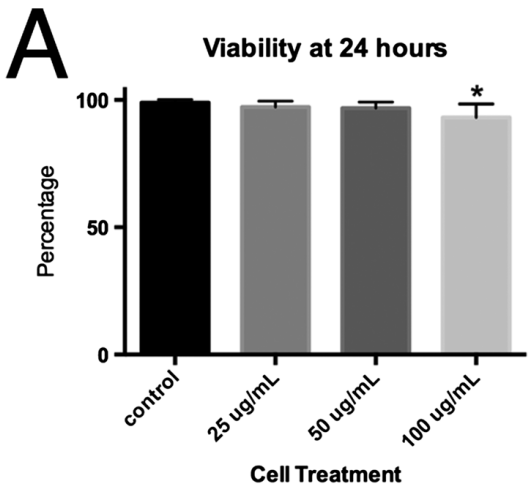

Test details	Mean 1	Mean 2
control vs. 25 ug/mL	98.94	97.38
control vs. 50 ug/mL	98.94	96.94
control vs. 100 ug/mL	98.94	93.27

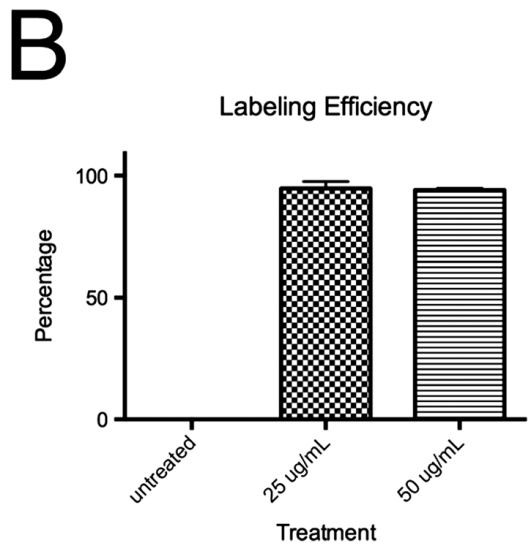

Figure 3.2. Viability and labeling efficiency. Representative A) trypan blue exclusion data for cell viability and B) flow cytometry data for labeling efficiency (Coumarin+) in treated versus untreated cells (*$p<0.05$).

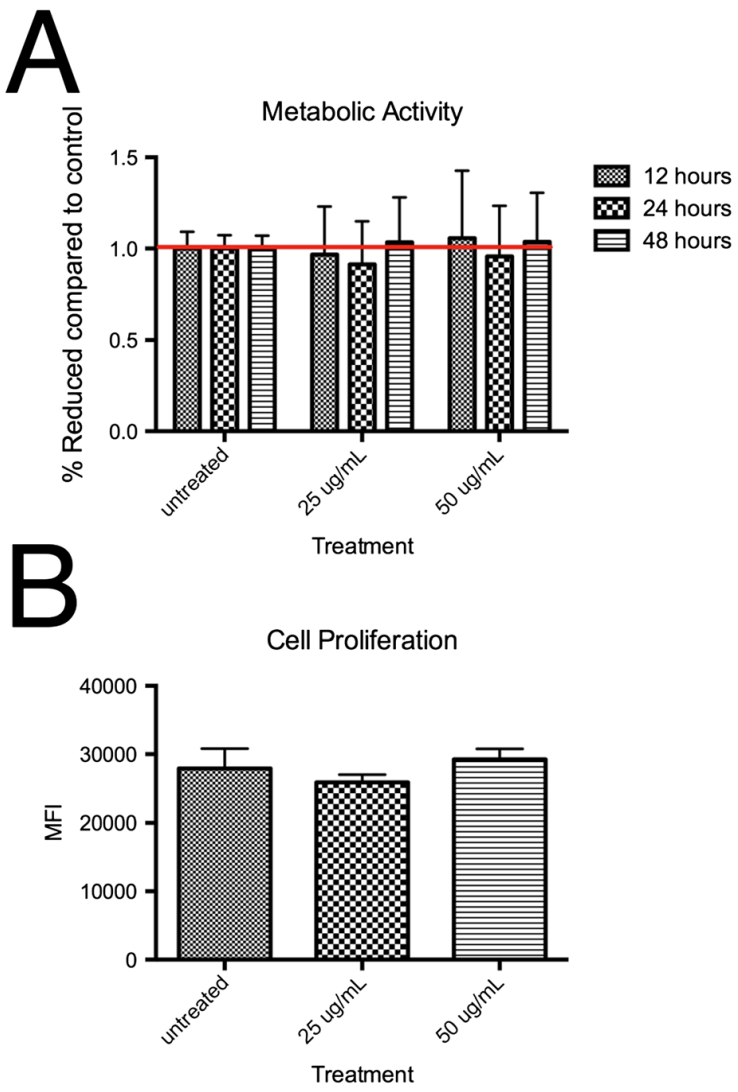

Figure 3.3. Cell metabolism and proliferation. Representative of A) percent reduction of media as compared with untreated cells (baseline = 1.0) at 12, 24, and 48 hours for alamarBlue assay and B) mean fluorescence intensity (MFI) following Click-iT Edu assay, respectively. No significant differences were seen between treated and untreated cells for either assay.

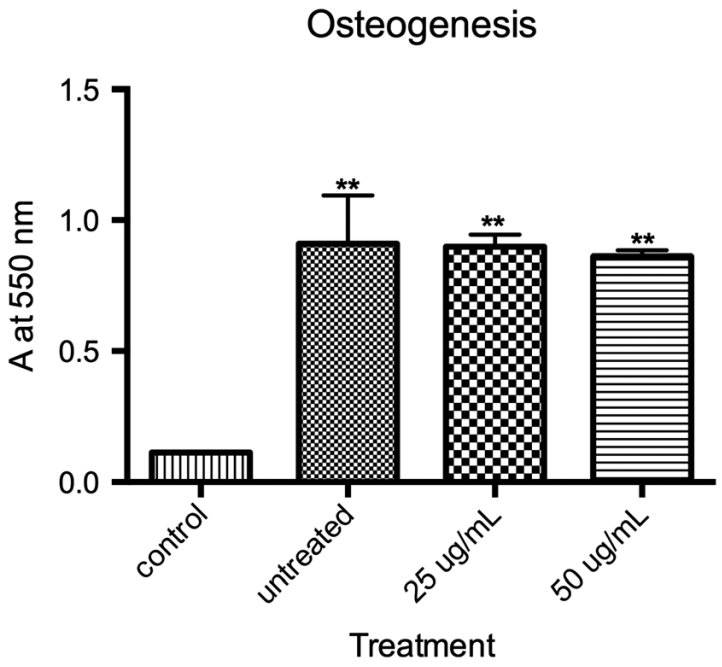

Figure 3.4. Osteogenesis. Calcium extraction results as measured by absorbance using Stanbio® Calcium Liquicolor Test in undifferentiated (control), untreated, and treated cells (**p<0.0001).

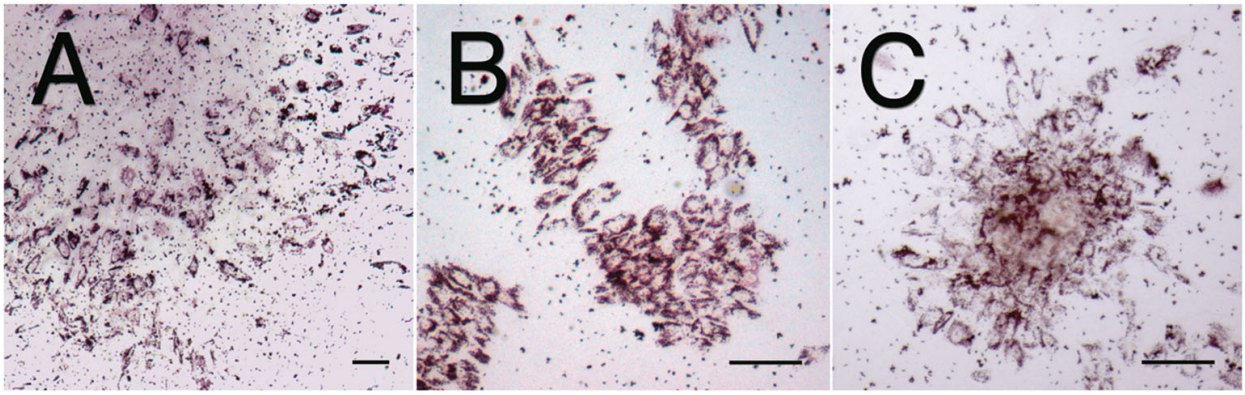

Figure 3.5. Adipogenesis. Staining following 28 day differentiation as demonstrated by Oil Red O staining in A) untreated, B) cells treated at 25 and C) 50 μg/mL.

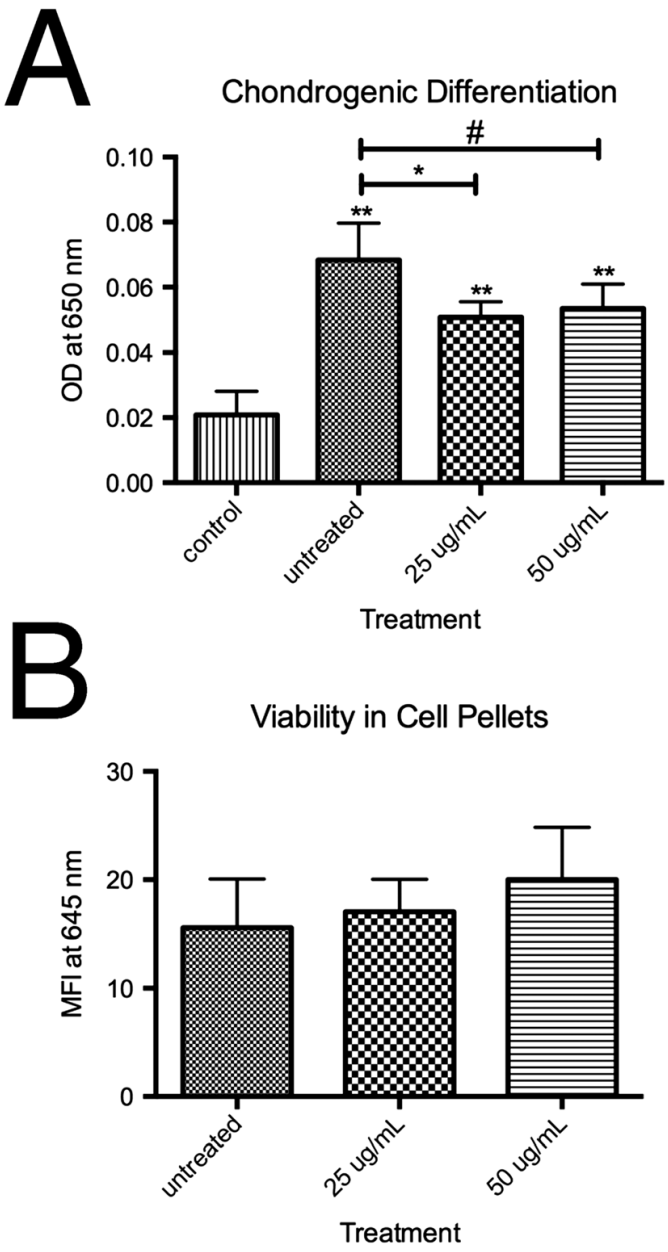

Figure 3.6. Chondrogenic differentiation and viability in cell pellets. A) Chondrogenic differentiation in micromass cell pellets as demonstrated by alcian blue staining and subsequent extraction in undifferentiated (control), untreated, and treated cells. Differentiation was significantly different in treated versus untreated cells at both treatment levels. (B) Viability of cell pellets using neutral red dye uptake assay and subsequent extraction. (**$p<0.0001$, *$p<0.001$, #$p<0.01$).

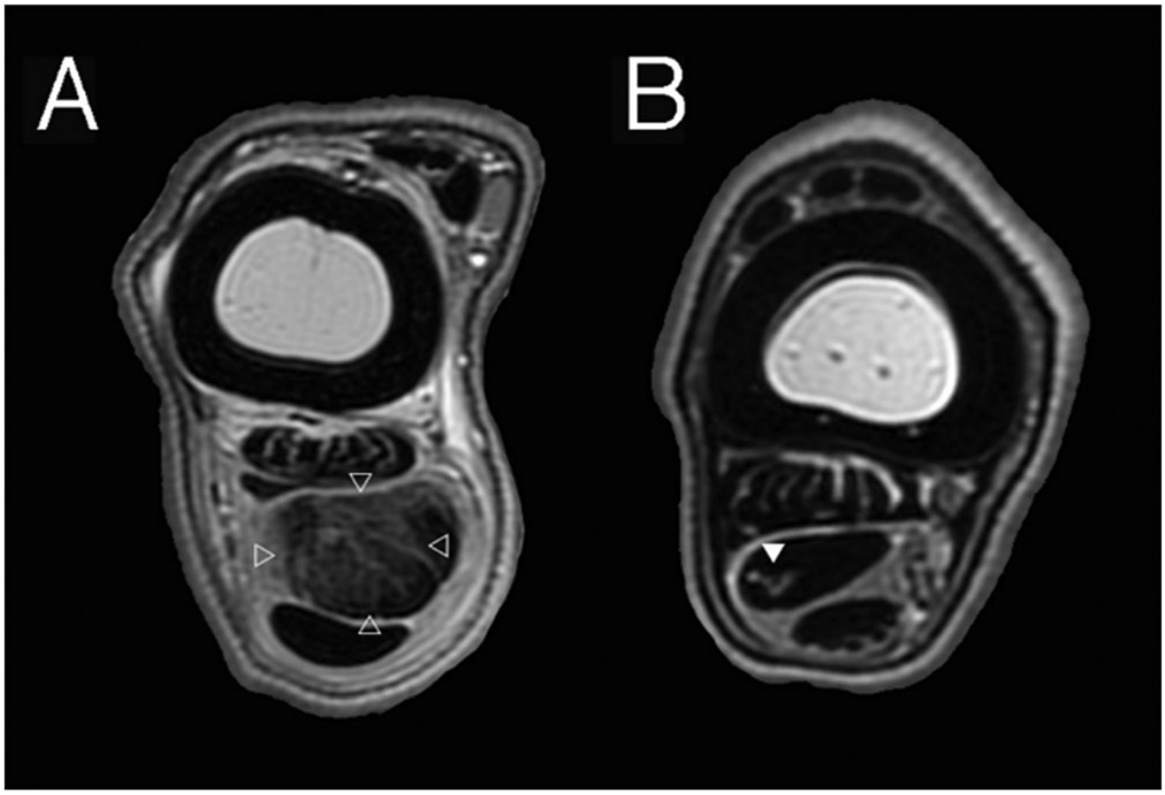

Figure 3.7. Axial MR images of DDFT lesions. Induced by A) collagenase (open arrowheads) and B) mechanical means (white arrowhead).

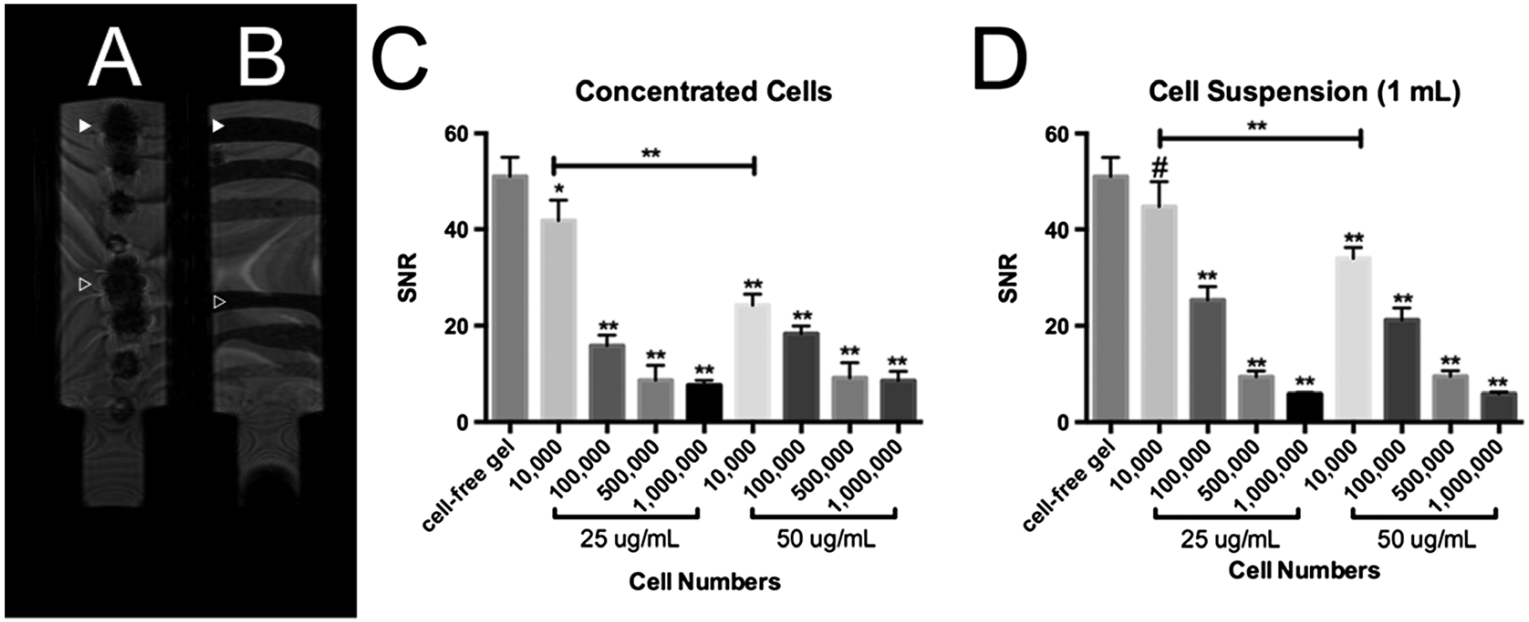

Figure 3.8. FIESTA MRI and SNR of cell phantoms. A), B) FIESTA MR image of cell agar gel phantoms showing A) concentrated cell pellets and B) volumetric cell suspensions in 1 mL agar gel in the following numbers: 50 μg/mL (from top to bottom, white arrow), 1,000,000; 500,000; 100,000; and 10,000 cells; 25 μg/mL (open arrow), 1,000,000; 500,000; 100,000; and 10,000 cells. C), D) SNR values correspond to C) the concentrated cell pellets in A) and D) cells suspended in 1 mL of gel in B). (**$p<0.0001$, *$p<0.001$, #$p<0.01$).

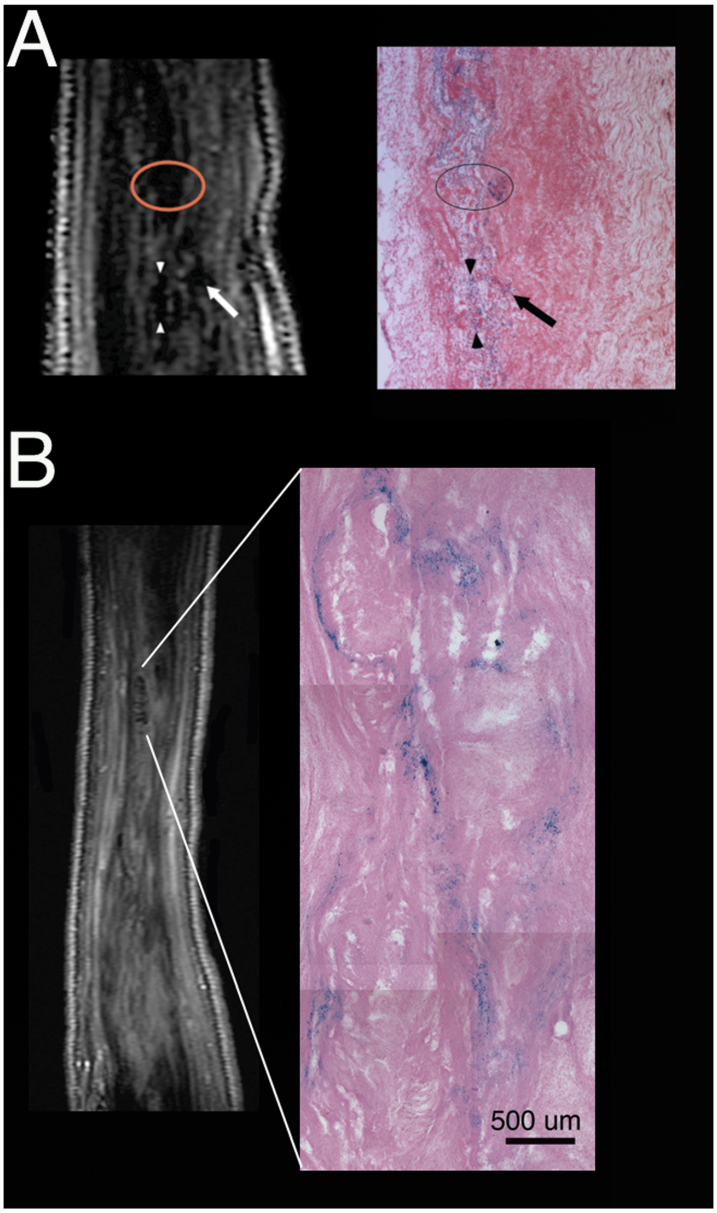

Figure 3.9. Dorsal FIESTA MRI and corresponding histology. A) Magnified portion of dorsal plane FIESTA image of the DDFT with spatially matched 4x magnification image of tendon lesion 7 days following injection of cells. The distribution of labeled MSCs at the site of implantation is similar, with the low signal intensity area of labeled MSCs surrounding a more organized blood clot that appears as intermediate signal. There are areas of coalescing MSC aggregates at the distal extent of the site of implantations (oval). There are also conspicuous accumulations of labeled MSCs that have migrated distal to the site of implantation are focused in areas of greater tendon disruption (arrowheads and arrow). More diffusely distributed labeled MSCs are also noted. B) Similar image shown 14 days following injection of cells. Similar patterns are seen in the MSCs identified on the Prussian blue-stained areas of tendonitis as compared with both MR images.

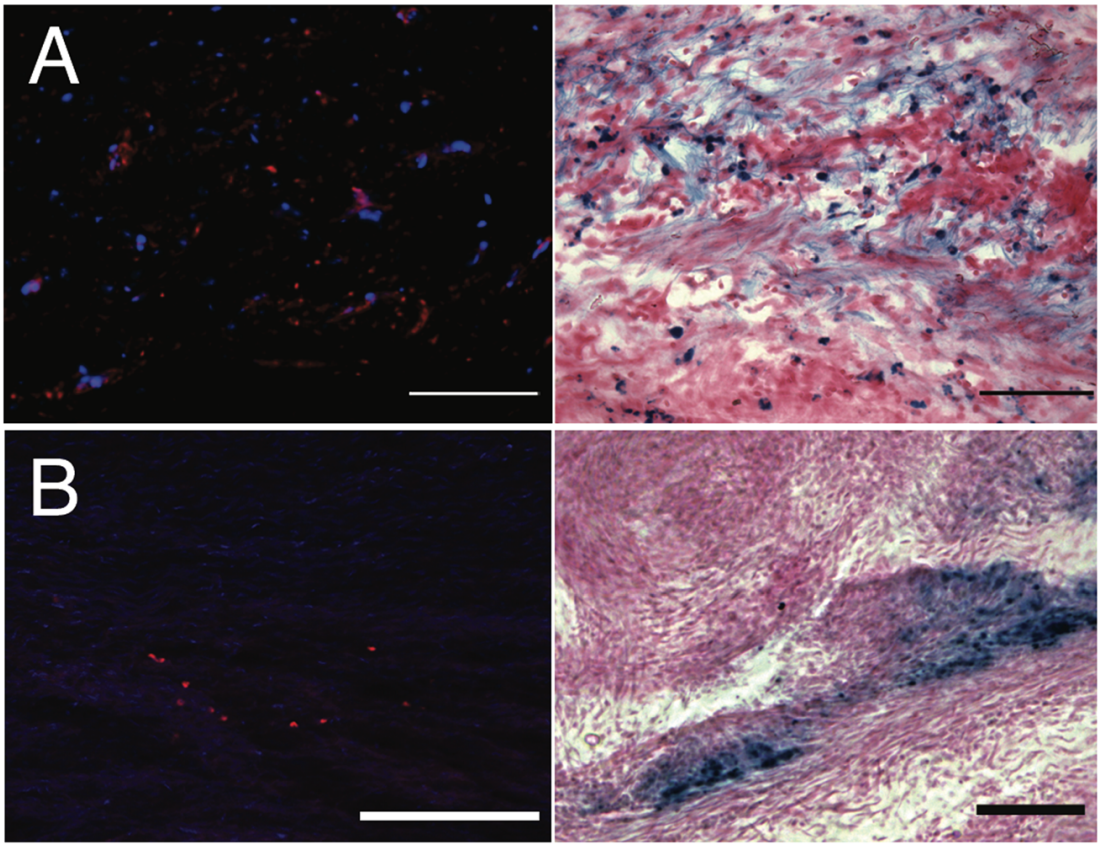

Figure 3.10. Tendon histology and GFP cells. (Left) GFP+ (red) cells and cell nuclei (blue) demonstrating presence of injected cells in host tissue and (right) SPIO particles (blue) and host tissue (red) demonstrating presence of SPIOs in host tissue on A) day 7 and B) day 14. Images were taken from similar areas of tendon on subsequent slides to investigate co-localization of GFP+ cells and SPIO nanoparticles. Scale bar 100 μm.

References

1. Dyson SJ. 2004. Medical management of superficial digital flexor tendonitis: a comparative study in 219 horses (1992–2000). American Veterinary Journal 36:415-419.

2. Avella CS, Ely ER, Verheyen KLP, et al. 2009. Ultrasonographic assessment of the superficial digital flexor tendons of National Hunt racehorses in training over two racing seasons. Equine Vet J 41:449-454.

3. Genovese RL, Rantanen NW, Simpson BS, et al. 1990. Clinical experience with quantitative analysis of superficial digital flexor tendon injuries in Thoroughbred and Standardbred racehorses. Vet Clin North Am Equine Pract 6:129-145.

4. Godwin EE, Young NJ, Dudhia J, et al. 2011. Implantation of bone marrow-derived mesenchymal stem cells demonstrates improved outcome in horses with overstrain injury of the superficial digital flexor tendon. Equine Vet J.

5. Bullough R, Finnigan T, Kay A, et al. 2008. Tendon repair through stem cell intervention: cellular and molecular approaches. Disabil Rehabil 30:1746-1751.

6. Crovace A, Lacitignola L, Rossi G, et al. 2010. Histological and immunohistochemical evaluation of autologous cultured bone marrow mesenchymal stem cells and bone marrow mononucleated cells in collagenase-induced tendinitis of equine superficial digital flexor tendon. Vet Med Int 2010:250978.

7. Fortier LA, Smith RK. 2008. Regenerative medicine for tendinous and ligamentous injuries of sport horses. Vet Clin North Am Equine Pract 24:191-201.

8. Frisbie DD, Smith RK. 2010. Clinical update on the use of mesenchymal stem cells in equine orthopaedics. Equine Vet J 42:86-89.

9. Qiu Y, Lim JJ, Scott L, Jr., et al. 2011. PEG-based hydrogels with tunable degradation characteristics to control delivery of marrow stromal cells for tendon overuse injuries. Acta Biomater 7:959-966.

10. Watts AE, Yeager AE, Kopyov OV, et al. 2011. Fetal derived embryonic-like stem cells improve healing in a large animal flexor tendonitis model. Stem Cell Res Ther 2:4.

11. Bosch G, Lameris MC, van den Belt AJ, et al. 2010. The propagation of induced tendon lesions in the equine superficial digital flexor tendon: an ex vivo study. Equine Vet J 42:407-411.

12. Pacini S, Spinabella S, Trombi L, et al. 2007. Suspension of bone marrow-derived undifferentiated mesenchymal stromal cells for repair of superficial digital flexor tendon in race horses. Tissue Eng 13:2949-2955.

13. Schramme M, Hunter S, Campbell N, et al. 2010. A surgical tendonitis model in horses: technique, clinical, ultrasonographic and histological characterisation. Vet Comp Orthop Traumatol 23:231-239.

14. Bruns J, Kampen J, Kahrs J, et al. 2000. Achilles tendon rupture: experimental results on spontaneous repair in a sheep-model. Knee Surg Sports Traumatol Arthrosc 8:364-369.

15. Crovace A, Lacitignola L, Francioso E, et al. 2008. Histology and immunohistochemistry study of ovine tendon grafted with cBMSCs and BMMNCs after collagenase-induced tendinitis. Vet Comp Orthop Traumatol 21:329-336.

16. Gebler A, Zabel O, Seliger B. 2012. The immunomodulatory capacity of mesenchymal stem cells. Trends Mol Med 18:128-134.

17. Hegyi B, Sagi B, Kovacs J, et al. 2010. Identical, similar or different? Learning about immunomodulatory function of mesenchymal stem cells isolated from various mouse tissues: bone marrow, spleen, thymus and aorta wall. Int Immunol 22:551-559.

18. Peroni JF, Borjesson DL. 2011. Anti-inflammatory and immunomodulatory activities of stem cells. Vet Clin North Am Equine Pract 27:351-362.

19. Guest DJ, Smith MR, Allen WR. 2008. Monitoring the fate of autologous and allogeneic mesenchymal progenitor cells injected into the superficial digital flexor tendon of horses: preliminary study. Equine Vet J 40:178-181.

20. Guest DJ, Smith MR, Allen WR. 2010. Equine embryonic stem-like cells and mesenchymal stromal cells have different survival rates and migration patterns following their injection into damaged superficial digital flexor tendon. Equine Vet J 42:636-642.

21. Addicott B, Willman M, Rodriguez J, et al. 2011. Mesenchymal stem cell labeling and in vitro MR characterization at 1.5 T of new SPIO contrast agent: Molday ION Rhodamine-B. Contrast Media Mol Imaging 6:7-18.

22. Mahmoudi M, Hosseinkhani H, Hosseinkhani M, et al. 2011. Magnetic Resonance Imaging Tracking of Stem Cells in Vivo Using Iron Oxide Nanoparticles as a Tool for the Advancement of Clinical Regenerative Medicine. Chemical Reviews 111:253-280.

23. Shen J, Cheng LN, Zhong XM, et al. 2010. Efficient in vitro labeling rabbit neural stem cell with paramagnetic Gd-DTPA and fluorescent substance. Eur J Radiol 75:397-405.

24. McFadden CD, C L Mallett, and PJ Foster. 2011. Labeling of multiple cell lines using a new iron oxide agent for cell tracking by MRI. Contrast Media Mol Imaging 6:514-522.

25. Hsiao JK, Tai MF, Chu HH, et al. 2007. Magnetic nanoparticle labeling of mesenchymal stem cells without transfection agent: cellular behavior and capability of detection with clinical 1.5 T magnetic resonance at the single cell level. Magn Reson Med 58:717-724.

26. Yang Y, Zhang J, Qian Y, et al. 2013. Superparamagnetic Iron Oxide is Suitable to Label Tendon Stem Cells and Track Them In Vivo with MR Imaging. Ann Biomed Eng.

27. Farrell E, Wielopolski P, Pavljasevic P, et al. 2008. Effects of iron oxide incorporation for long term cell tracking on MSC differentiation in vitro and in vivo. Biochemical and Biophysical Research Communications 369:1076-1081.

28. Frank J, Miller B, Arbab A, et al. 2003. Clinically Applicable Labeling of Mammalian and Stem Cells by Combining Superparamagnetic Iron Oxides and Transfection Agents. Radiology.

29. Ko IK, Song H-T, Cho E-J, et al. 2006. In vivo MR Imaging of Tissue-engineered Human Mesenchymal Stem Cells Transplanted to Mouse: a Preliminary Study. Annals of Biomedical Engineering 35:101-108.

30. Ferreira L, Karp JM, Nobre L, et al. 2008. New Opportunities: The Use of Nanotechnologies to Manipulate and Track Stem Cells. Cell Stem Cell 3:136-146.

31. Kriz J, Jirak D, White D, et al. 2008. Magnetic resonance imaging of pancreatic islets transplanted into the right liver lobes of diabetic mice. Transplant Proc 40:444-448.

32. Kraitchman DL, Kedziorek DA, Bulte JW. 2011. MR imaging of transplanted stem cells in myocardial infarction. Methods Mol Biol 680:141-152.

33. Heyn C, Ronald JA, Ramadan SS, et al. 2006. In vivo MRI of cancer cell fate at the single-cell level in a mouse model of breast cancer metastasis to the brain. Magn Reson Med 56:1001-1010.

34. Heyn C, Ronald JA, Mackenzie LT, et al. 2006. In vivo magnetic resonance imaging of single cells in mouse brain with optical validation. Magn Reson Med 55:23-29.

35. Gonzalez-Lara LE, Xu X, Hofstetrova K, et al. 2011. The use of cellular magnetic resonance imaging to track the fate of iron-labeled multipotent stromal cells after direct transplantation in a mouse model of spinal cord injury. Mol Imaging Biol 13:702-711.

36. van Buul GM, Kotek G, Wielopolski PA, et al. 2011. Clinically translatable cell tracking and quantification by MRI in cartilage repair using superparamagnetic iron oxides. Plos One 6:e17001.

37. Repetto G, del Peso A, Zurita JL. 2008. Neutral red uptake assay for the estimation of cell viability/cytotoxicity. Nat Protoc 3:1125-1131.

38. Pfeifer A, Ikawa M, Dayn Y, et al. 2002. Transgenesis by lentiviral vectors: lack of gene silencing in mammalian embryonic stem cells and preimplantation embryos. Proc Natl Acad Sci U S A 99:2140-2145.

39. Heymer A, Haddad D, Weber M, et al. 2008. Iron oxide labelling of human mesenchymal stem cells in collagen hydrogels for articular cartilage repair. Biomaterials 29:1473-1483.

40. Singh N, Jenkins GJ, Asadi R, et al. 2010. Potential toxicity of superparamagnetic iron oxide nanoparticles (SPION). Nano Rev 1.

41. Mahmoudi M, Hofmann H, Rothen-Rutishauser B, et al. 2012. Assessing the in vitro and in vivo toxicity of superparamagnetic iron oxide nanoparticles. Chemical Reviews 112:2323-2338.

42. Kostura L, Kraitchman DL, Mackay AM, et al. 2004. Feridex labeling of mesenchymal stem cells inhibits chondrogenesis but not adipogenesis or osteogenesis. NMR in Biomedicine 17:513-517.

43. Farrell E, Wielopolski P, Pavljasevic P, et al. 2009. Cell labelling with superparamagnetic iron oxide has no effect on chondrocyte behaviour. Osteoarthritis and Cartilage 17:961-967.

44. Foldager CB, Pedersen M, Ringgaard S, et al. 2011. Chondrocyte gene expression is affected by very small iron oxide particles-labeling in long-term in vitro MRI tracking. J Magn Reson Imaging 33:724-730.

45. Heyn C, Bowen CV, Rutt BK, et al. 2005. Detection threshold of single SPIO-labeled cells with FIESTA. Magn Reson Med 53:312-320.

46. Liu W, Frank JA. 2009. Detection and quantification of magnetically labeled cells by cellular MRI. Eur J Radiol 70:258-264.

47. Guenoun J, Ruggiero A, Doeswijk G, et al. 2013. In vivo quantitative assessment of cell viability of gadolinium or iron-labeled cells using MRI and bioluminescence imaging. Contrast Media Mol Imaging 8:165-174.

48. Xu C, Mu L, Roes I, et al. 2011. Nanoparticle-based monitoring of cell therapy. Nanotechnology 22:494001.

49. Wang YX, Wang HH, Au DW, et al. 2008. Pitfalls in employing superparamagnetic iron oxide particles for stem cell labelling and in vivo MRI tracking. Br J Radiol 81:987-988.

50. Sole A, Spriet M, Galuppo LD, et al. 2012. Scintigraphic evaluation of intra-arterial and intravenous regional limb perfusion of allogeneic bone marrow-derived mesenchymal stem cells in the normal equine distal limb using (99m) Tc-HMPAO. Equine Vet J 44:594-599.

51. Chen J, Wang F, Zhang Y, et al. 2012. In Vivo Tracking of Superparamagnetic Iron Oxide Nanoparticle Labeled Chondrocytes in Large Animal Model. Ann Biomed Eng 40:2568-2578.

52. Kosaka N, Bernardo M, Mitsunaga M, et al. 2012. MR and optical imaging of early micrometastases in lymph nodes: triple labeling with nano-sized agents yielding distinct signals. Contrast Media Mol Imaging 7:247-253.

53. Arbab AS, Yocum GT, Kalish H, et al. 2004. Efficient magnetic cell labeling with protamine sulfate complexed to ferumoxides for cellular MRI. Blood 104:1217-1223.

54. Delcroix GJ, Jacquart M, Lemaire L, et al. 2009. Mesenchymal and neural stem cells labeled with HEDP-coated SPIO nanoparticles: in vitro characterization and migration potential in rat brain. Brain Res 1255:18-31.

55. Ramaswamy S, Schornack PA, Smelko AG, et al. 2011. Superparamagnetic iron oxide (SPIO) labeling efficiency and subsequent MRI tracking of native cell populations pertinent to pulmonary heart valve tissue engineering studies. NMR in Biomedicine:n/a-n/a.

56. Thu MS, Bryant LH, Coppola T, et al. 2012. Self-assembling nanocomplexes by combining ferumoxytol, heparin and protamine for cell tracking by magnetic resonance imaging. Nat Med 18:463-467.

57. Berman SC, Galpoththawela C, Gilad AA, et al. 2011. Long-term MR cell tracking of neural stem cells grafted in immunocompetent versus immunodeficient mice reveals distinct differences in contrast between live and dead cells. Magn Reson Med 65:564-574.

58. Raynal I, Prigent P, Peyramaure S, et al. 2004. Macrophage endocytosis of superparamagnetic iron oxide nanoparticles: mechanisms and comparison of ferumoxides and ferumoxtran-10. Investigative radiology 39:56-63.

59. Luciani N, Wilhelm C, Gazeau F. 2010. The role of cell-released microvesicles in the intercellular transfer of magnetic nanoparticles in the monocyte/macrophage system. Biomaterials 31:7061-7069.

60. Terrovitis J, Stuber M, Youssef A, et al. 2008. Magnetic resonance imaging overestimates ferumoxide-labeled stem cell survival after transplantation in the heart. Circulation 117:1555-1562.

CHAPTER 4

MRI-BASED ASSESSMENT OF INTRALESIONAL DELIVERY OF BONE MARROW-DERIVED MESENCHYMAL STEM CELLS IN A MODEL OF EQUINE TENDONITIS[1]

[1] Scharf, AM, SP Holmes, M Thoreson, J Mumaw, A Stumpf, and J Peroni. Submitted to *Stem Cells International,* 06/06/2016.

Abstract

Ultrasound-guided intra-lesional injection of mesenchymal stem cells (MSCs) is held as the benchmark for cell delivery in tendonitis. The primary objective of this study was to investigate the immediate cell distribution following intra-lesional injection of MSCs. Unilateral superficial digital flexor tendon (SDFT) lesions were created in the forelimb of six horses and injected with $10x10^6$ MSCs labeled with superparamagnetic iron oxide nanoparticles (SPIOs) under ultrasound guidance. Assays were performed to confirm no significant changes in cell viability, proliferation, migration, or tri-lineage differentiation due to the presence of SPIOs. Limbs were imaged on a 1.5T clinical MRI scanner pre and post-injection to determine the extent of tendonitis and detect SPIO MSCs.

Clusters of labeled cells were visible as signal voids in 6/6 subjects. Coalescing regions of signal void were diffusely present in the peritendinous tissues. Although previous reports have determined that local injury retains cells within a small radius of the site of injection, our study shows greater than expected delocalization and that relatively few cells retained within collagenous tendon compared to surrounding fascia. Further work is needed if this is a reality *in vivo* and to determine if directed intra-lesional delivery of MSCs is as critical as presently thought.

Keywords:

MRI, SPIO, cell tracking, MSC

Introduction

The incidence of athletic, overuse injury continues to rise with the popularity of recreational and competitive sports in both human and veterinary patients. At this time, over 50 US clinical trials investigating the effects of biological therapeutics including platelet rich plasma or stem cells on tendon or ligament injury are active or have recently been completed in humans. (Clinicaltrials.gov). A comprehensive review of tendinopathies in the equine and human athlete has shown striking similarities and concluded that the horse provides a robust preclinical model for translational therapies [1]. The use of mesenchymal stem cells (MSCs) for tendon therapy in the horse has shown encouraging results, including superior tissue organization, composition and mechanics compared to untreated controls[2-6]. Direct, intra-lesional injection of MSCs under ultrasound guidance is held as the benchmark for MSCs therapy in tendonitis [3; 4; 6-8], although little is known about the efficacy of this delivery technique.

Current tracking studies rely heavily on post-mortem histological validation [9-11] or utilize low resolution imaging modalities such as nuclear scintigraphy [12; 13] and low-field magnetic resonance imaging [14; 15]. Such studies report low cell retention and survival in tendon following injection of MSCs, reporting <25% cells total retained after the first 24 hours [12; 13] and fewer than 5% of the original bolus after 10 days as confirmed by histology [11]. However, little is known about the discrete localization of cells post-injection or their ability to migrate into injured tissues over time.

This study represents part of an effort to establish a model of tendon injury that can be paired with nanotechnology-based cell tracking methods to track MSCs following ultrasound-guided injection into damaged tissues [16]. Superparamagnetic iron oxide nanoparticles (SPIOs) have the ability to image and monitor cells using MRI. SPIOs are non-toxic at low

concentrations, biodegradable, do not emit ionizing agents, and are readily endocytosed by adherent cells in culture [17-20]. At this time, SPIOs have safely been implemented as an intracellular label for stem cell studies in the liver [21], heart [22], spinal cord and brain [19; 23], and articular cartilage [24] to study spatial distribution and migration post-implantation using MRI over periods of time ranging from weeks to months [18; 25-27].

The major aims of this study were to validate the safety of labeling equine BM-derived MSCs with SPIOs and to investigate the immediate distribution of cells following ultrasound-guided, intra-lesional injection of MSCs into an established model of iatrogenic, flexor tendon injury in the horse [28; 29]. This model was chosen to reflect the environment associated with acute tendon injury and provide reproducible areas of tissue contrast on MRI that could be used to enhance intra-lesional detection of SPIOs. The hypotheses of this research were that (i) equine BM-MSCs would be unaltered by SPIO labeling, (ii) that SPIOs labeled MSCs could be tracked immediately after injection in an equine tendonitis model and (iii) MSCs would be localized within the tendon lesion following ultrasound-guided injection.

Materials and Methods

In Vitro *Validation*

All experiments were performed in triplicate using cryopreserved, bone marrow derived equine mesenchymal stem cells from 3 horses below passage 10. Cells were cryopreserved in 10% (v/v) DMSO in cell culture medium and thawed for 1 minute in a 37°C water bath. Cells were diluted in 10 mL MSC culture medium (low glucose Dulbecco's Modified Eagle Medium (DMEM), 10% Fetal Bovine Serum, 1% L-glutamine, 50 U/mL penicillin, 50 μg/mL streptomycin), centrifuged, and plated for culture at 10,000 cells/cm^2. Cells were maintained in culture at 37°C

and 5% CO_2 in MSC culture medium. At 70% confluency, MSCs were treated with 25 μg/mL Molday ION C6Amine (Biopal, Inc.) suspended in 0.1 mL/cm^2 MSC culture medium for 4 or 16 hours, as noted. Untreated cells were used as a control. Following treatment, cells were trypsinized, centrifuged, and manually counted for use in the following assays.

Cell Viability following SPIO treatment

For cell viability, cells were labeled with SPIOs as described above for 4 or 16 hours. Cells were harvested and evaluated immediately post treatment and 24 hours following completion of treatment. A Trypan Blue (Cellgro®) exclusion assay was performed for viability according to the manufacturer's protocol. Results were analyzed with one-way analysis of variance (ANOVA) and Dunnett's multiple comparisons test using untreated cells as the control. Bonferroni's multiple comparison test was used to compare cells immediately post treatment to cells after 24 hours of recovery.

Iron Content and Cell Proliferation

For qualitative assessment, cells were fixed with 4% paraformaldehyde over ice for 10 minutes, incubated for 10 minutes with Prussian Blue reagents (Biopal, Inc), and Prussian Blue-positive, intracellular deposits of SPIOs were confirmed with light microscopy. For quantitative assessment, cells were harvested, counted, and digested in dilute aqueous nitric acid for analysis by inductively coupled plasma-mass spectrometry with a VG Plasmaquad 3 (VG Instruments) to determine iron content. To measure proliferation, cells were plated in flat bottom, 96-well plates and the CyQuant® (Life Technologies) assay was performed according to the manufacturer's microplate protocol and analyzed at 0, 24, 48, and 72 hours. Results were analyzed with two-way ANOVA using Dunnett's multiple comparisons test and untreated cells as the control.

Tri-Lineage Differentiation

For osteogenic and adipogenic differentiation experiments, SPIO-labeled cells were plated in flat bottom, 96-well plates at a density of 28,000 cells/cm^2 and cultured in MSC culture medium for 24 hours. Fresh MSCs (undifferentiated) were included as controls for all experiments. Osteogenic induction cultures were replenished with Hyclone® AdvanceSTEM™ osteogenic medium every 2-3 days for 28 days. Osteogenic differentiation was determined using Calcium Liquicolor® Test (Stanbio) according to their protocol. Calcium was extracted from the differentiated cultures with 0.6N HCl overnight at 4°C. The supernatant was combined at a ratio of 1:20 in an equal portion mixture of the color and base reagents from the calcium liquicolor test and read on a plate reader at 550 nm (Biotek Synergy 4).

Adipogenic induction cultures were replenished with Hyclone® AdvanceSTEM™ adipogenic medium for 14 days then switched to an adipogenic medium modified from Gimble et al. (2006) consisting of DMEM, 10% FBS, 5% rabbit serum, 0.5 μM dexamethasone, 60 μM indomethacin, 0.5 mM IBMX, 1 μM insulin, and 50 U/ml penicillin, 50 μg/ml streptomycin for the remaining 14 days with medium changes every 2-3 days [30]. Adipogenic cells were fixed with 4% paraformaldehyde for 10 minutes over ice and stained with Oil Red O to identify lipid deposits.

For chondrogenic differentiation, 100,000 cells/well were plated in conical bottom, 96-well plates, centrifuged for 10 minutes, and replenished with Hyclone® AdvanceSTEM™ chondrogenic medium every 2-3 days for 28 days. Chondrogenic pellets were fixed with methanol, stained with 0.2% Alcian Blue in 0.1 M HCl overnight, extracted with 0.1 mL 6 M guanidine/HCl for 2 hours, and read at 650 nm in a plate reader (Biotek Synergy 4).

Scratch Test

The scratch test was modified from the protocol outlined by Liang et al. [31]. Cells were plated at confluency in a 24-well plate. A p200 pipet tip was used to scratch a line through the cells. Light microscopy images were taken at 0, 8, 16, and 24 hours. Image analysis was performed using ImageJ. Distance was measured between 3 sets of cells per well per time point. Results were analyzed with a two-way ANOVA repeated measures analysis and Bonferroni's multiple comparisons test at a significance level of 0.05.

Inflammatory Modulation and Cytokine Production

Equine peripheral blood mononuclear cells (PBMCs) were obtained by collecting 60 mL of peripheral blood from a healthy horse into a syringe with ethylenediaminetetraacetic acid (EDTA) as an anticoagulant. Blood was layered onto Histopaque-1077 and centrifuged at 20°C for 30 min, and the PBMC layer was removed by aspiration. Cells were washed twice in phosphate buffered saline (PBS), resuspended in monocyte media (RPMI-1641 with 10% equine serum, 50 U/mL penicillin, and 50 μg/mL streptomycin) at $4x10^6$/mL, and plated. PBMCs were incubated for 2 hours, after which non-adherent cells were washed off and adherent PBMCs were harvested for the following assays.

To assess the ability of MSCs to modulate the inflammatory response, 100,000 MSCs were plated in 12-well transwell plates and allowed to adhere for approximately 12 hours. At this time, MSC media was exchanged for 1.5 mL monocyte media/well. Next, 400,000 monocytes were added to each upper transwell in 0.5 mL monocyte media supplemented with 50 ng/mL *E. Coli* LPS and allowed to incubate for 16 hours overnight. Monocytes +/- LPS without MSCs were used as controls. Supernatant was collected and used for analysis by ELISA for production of interleukin-10 (IL-10, abcam®) and prostaglandin E_2 (PGE_2, Enzo® Life Sciences) according

to manufacturer's protocols. An ELISA for tumor necrosing factor-α (TNF-α) was performed as previously described by Sun et al [32]. ELISA plates were coated with anti-equine TNF-α polyclonal antibody overnight, washed, and incubated with samples. Plates were washed again, incubated with anti-equine TNF-α biotin-labeled polyclonal antibody, washed, incubated with avidin-horseradish peroxidase, washed again, incubated with a peroxidase substrate (ABTS®) and read at 405 nm on a plate reader (Biotek Synergy 4).

MRI Study

MRI was performed using a Siemens Symphony with TIM technology 1.5T MRI unit with B17 software. All imaging was performed with limb centered in a 15-channel knee coil with receiver bandwidth of 130 kHz. Proton density (PD), true fast imaging with steady-state free precession (TRUFI) sequences, T2*, and multiecho spin-echo (MSE) T2-weighted sequences were acquired for cell phantoms and all subjects (Table 1). Analysis was performed with Osirix DICOM software and ImageJ.

In Vitro *Phantom Study*

A preliminary study was performed to establish the sensitivity and limits of MRI detection of SPIO labeled MSCs. Cell phantoms were prepared by suspending 0.01, 0.1, 0.25, 0.5 and $1x10^6$ cells in 200 μL of 1% agar in the wells of a 96-well plate. Mean signal intensities (MSI) of labeled cells were measured using a circular ROI of 8.44 mm^2 on 4 contiguous slices acquired from TRUFI images. Signal to noise ratio (SNR) was calculated by dividing the MSI by the standard deviation of the background noise. A second study was performed in normal tendon. Tissue was collected from 1 horse euthanized for purposes unrelated to this study. 1, 5, 10, and $20x10^6$ cells were injected from proximal to distal into the SDFT and scanned as described above.

In vivo *MRI Analysis of Intralesional Cell Injection*

All work performed in this study was done in accordance with the University of Georgia Institutional Animal Care and Use committee guidelines. All horses were scheduled to be euthanized for reasons unrelated to this project.

Pilot Lesion

An iatrogenic lesion was made in the forelimb of one horse scheduled for anesthesia and subsequent euthanasia. While under general anesthesia, the metacarpal region was circumferentially clipped and aseptically prepared. The limb was desensitized with a ring block performed using 10 ml of 2% lidocaine infused subcutaneously just distal to the carpus. A 1 cm incision was made on the caudal aspect of the metacarpus and into the SDFT just above the proximal extent of the digital flexor tendon sheath. A 4.5mm Steinmann pin was inserted within the SDFT and advanced 5 cm 5 times, withdrawn, and the skin sutured. The horse was euthanized under general anesthesia. $10x10^6$ SPIO-labeled MSCs were injected into the lesion under ultrasound guidance and imaged as described above.

Model of Tendon Injury

Unilateral SDFT lesions were created in the forelimb of six horses. A protocol was modified from Schramme et al. [28] to perform the procedure with horses in standing. Horses were premedicated with i.v. flunixin meglumine (1.1mg/kg) and then sedated with a combination of detomidine hydrochloride (10 μg/kg) and butorphanol (20 μg/kg) administered intravenously. The limb was surgically prepped as described above. A 1 cm incision was made on the caudal aspect of the metacarpus and into the SDFT just above the proximal extent of the digital flexor tendon sheath. While holding the limb off the ground, a 4.5mm Steinmann pin was inserted within the SDFT and advanced 5 cm. The pin was extracted and replaced with a 5mm

arthroscopic burr. The burr was activated at 2500 rpm and inserted and withdrawn within the SDFT 5 times. The skin incision was closed with surgical staples and the forelimb was bandaged. Horses were maintained on stall rest and handwalked two times per day and subsequently euthanized 10 days following induction of the lesion. Cell injections and MRI were performed immediately following euthanasia and removal of the limb.

Cell preparation

Cryopreserved, BM-derived equine MSCs below passage 10 were thawed and plated 3-5 days prior to treatment for culture as described above. The day prior to imaging, cells were treated with 25 μg/mL C6Amine Molday ION suspended in MSC culture media for 4 hours. At the time of injection, cells were harvested and $10x10^6$ cells were counted. Cells were suspended in 0.25 to 0.75 mL PBS for injection, depending on the size of the lesion as determined by MRI and ultrasound.

Ex Vivo *Imaging*

Immediately following euthanasia, the injured forelimb was placed in a 15-channel knee coil with the palmar side up and imaged on a Siemens 1.5 T MRI scanner. PD images were acquired in the sagittal and transverse planes and a TRUFI was acquired in the dorsal plane prior to injection as described in Table 1. Next, the limb was removed from the scanner and placed on a flat surface in a horizontal position, with palmar side up for evaluation by ultrasound. This position was chosen to mimic cell injections performed on a non-weight bearing limb, with minimal tension on the flexor tendons so as to permit the largest volume of fluid within the core lesion. Cells were delivered via a 20-gauge needle placed into the lesion under ultrasound guidance using a 7.5 mHz probe connected to a Micromaxx Ultrasound System (SonoSite, Inc. 21919 30th Drive SE Bothell, WA 98021 USA). The cell bolus was not delivered unless the tip

of the needle could be verified within the core of the lesion on transverse and longitudinal planes. Following injection, limbs were returned to MRI and scanned with all sequences described in Table 1.

The extent of hypointense signal or signal void associated with SPIO-labeled MSC dispersion was measured using Osirix software on isotropic TRUFI images proximal and distal to the site of injection. The depth of signal into the subcutaneous tissue surrounding normal tendon was also measured. Relative pixel intensity (RPI) was measured on every other slice in T2* transverse images from the most proximal and distal aspects where signal voids could be observed. Histograms were generated on ImageJ to quantify the RPI from the distal aspect of the suspensory to the palmar surface of the limb. Histograms were also generated from the SDFT and deep digital flexor tendons (DDFT), which were subsequently subtracted from the total RPI to quantify the amount of RPI that was likely associated with SPIOs in the paratendinous fascia and subcutaneous tissues. Pixel values >100 were excluded from analysis.

Histology

Following MRI, 3.5-4.0 cm of affected area of the SDFT was excised at the site of injection, embedded in OCT compound (Tissue-Tek®), and longitudinally sectioned on a cryostat (Leica) at 12 μm. Sections were mounted, fixed with 4% paraformaldehyde, incubated with Prussian Blue reagents (Biopal, Inc) to evaluate the presence of iron nanoparticles, and counterstained with Nuclear Fast Red to visualize tissue morphology with light microscopy.

Statistical Analysis

Results were analyzed with one-way ANOVA and Bonferroni's multiple comparison tests at a significance level of 0.05 using Prism 6 software, unless otherwise noted above. Cells isolated

from 3 horses were analyzed at each time point with measurements performed in triplicate. Error is reported in figures as standard error (SE) of the mean.

Results

Cell Viability following SPIO treatment

Untreated MSCs and MSCs treated for 4 hours showed 97.35±0.36(SE) and 96.56±0.64% viability respectively (Figure 1). Viability of equine MSCs treated for 4 hours did not differ at 24 hours following treatment (Figure 1). MSCs showed a significant decrease in viability following treatment for 16 hours (74.53±4.11%, $p<0.0001$). Cells treated for 16 hours demonstrated an increase in viability 24 hours later (82.92±2.55%) as compared to viability immediately following treatment ($p<0.05$).

Iron Content and Cell Proliferation

Iron content was determined to be 3.99 ± 0.35 (SE) and 18.64 ± 1.25 (SE) pg/cell in cells treated for 4 and 16 hours, respectively. Untreated and treated MSCs demonstrated an increasing, linear relationship proliferative capacity over 72 hours post-treatment. Cell proliferation was not significantly different in untreated cells as compared to cells treated for 4 or 16 hours (Figure 2).

Tri-Lineage Differentiation

Due to the significant difference in viability between cells labeled for 4 versus 16 hours, only cells treated for 4 hours were used in the remaining experiments. Untreated and treated cells successfully demonstrated osteogenic ($p<0.0001$) and chondrogenic differentiation ($p<0.01$ untreated, $p<0.0001$ treated) as compared to undifferentiated control cells (Figure 3a,b). Additionally, treated and untreated cells both demonstrated adipogenic differentiated as assessed by oil red O staining of lipid vacuoles at 28 days post treatment (Figure 3c).

Scratch Test

The scratch test showed no significant difference between the ability of treated and untreated MSCs to close the distance of the wound gap over 24 hours (Figure 4).

Inflammatory Modulation and Cytokine Production

Treated and untreated MSCs successfully upregulated PGE2 ($p<0.0001$), downregulated TNFα ($p<0.0001$), and upregulated IL-10 production (ns) when co-cultured with PBMCs stimulated with LPS (Figure 5).

MRI Study

In Vitro *Study*

Phantom models indicated that MR signal intensity decreased with increasing labeled cell numbers. All cell concentrations were qualitatively discernible compared to cell free gel (CFG) on TRUFI and PD images showing distinct loss of signal (Figure 6a). The signal to noise ratio (SNR) for all cell concentrations were significantly different as compared to cell-free gel ($p<0.0001$), but only 10,000 ($p<0.0001$); 100,000 cells ($p<0.0001$); and 250,000 cells ($p<0.01$) were discernible from background (BG) signal (Figure 6b). Cells could not be visualized within normal tendon. Areas of hypointense signal were visible in the paratendinous fascia and subcutaneous tissues and were concentrated near sites of injection following injection into normal tendon (Figure 6c).

Pilot Study

Iatrogenic injury was localized and consisted of a focal area of fiber disruption and edema at the site of surgical incision in the transverse and sagittal plane. Although a small amount of contrast was produced, contrast was not evident more proximal to the site of surgical incision. The extent of cell delivery into the lesion could not be determined (Figure 7a). At this time, the model was

redesigned such that cells would be injected 10 days following surgery to allow edema to develop and more closely mimic clinical disease. Current studies routinely inject cells 1-2 weeks following iatrogenic injury, which supports the implementation of this timeframe [2; 10; 11; 14; 33; 34].

Ex Vivo *Imaging*

Prior to injection, tendon injuries were detectable as small, focal areas of hyperintensity localized to the SDFT in the transverse plane (Figure 8a,e) and were visible as longitudinal, linear segments of hyperintense signal in the dorsal plane (Figure 8b,f) in 5/6 subjects. The lesions were measured to be 5.41± 0.36(SE) cm in length, on average. On TRUFI images, clusters of labeled cells were visible as hypointense, signal voids in 6/6 subjects. Coalescing regions of signal void were diffusely present throughout the site of injury, in the paratendinous, subcutaneous, and fibrous scar tissues surrounding the SDF (Figure 8c, d, g, h). Cell retention within the lesions varied greatly, with 1/6 subjects demonstrating little to no cell retention within the lesion (Figure 8, f-h). Substantial leakage of labeled cells outside of the SDFT was observed. High numbers of low intensity pixel values likely associated with SPIO-labeled cells were quantifiable throughout the tissue surrounding the SDFT and DDFT in 6/6 subjects (Figure 9). Cells were located at 1.89± 0.33(SE) cm proximal and distal to the site of injection and were found at a depth 3.13± 0.40(SE) mm into the surrounding tissues.

Histology

Tendon lesions were grossly visible as areas of mechanical disruption with little to no fiber density. No scar tissue was present within the lesioned area. The margin surrounding the injury was delineated by dense irregular connective tissue with increased cellularity. The tissue surrounding the lesion was normal with no inflammatory cell infiltrate, and demonstrated crimp and fiber patterns characteristic of normal tendon. Prussian blue-positive, iron-containing cells

were detectable within the lesioned area and adherent to the bordering, dense, irregular connective tissue (Figure 10). Few Prussian-blue positive cells were located within the normal tendon tissue surrounding the lesion.

Discussion

With this study, we aimed to standardize a technique for safely loading equine BM-MSCs with SPIOs and to ensure that MSCs would not be functionally altered by SPIO labeling. A positive correlation was observed between time of incubation with SPIO-treated media and iron load per cell. A previous study demonstrated a linear relationship between SPIO concentration in media and iron load per cell [17]. Increasing time of incubation may provide a more economical alternative to increasing iron load per cell. Our data shows that a higher iron load of 19 pg/cell can be achieved by overnight incubation, but this was detrimental to cell viability. Care must be taken to avoid interference with cell migration and survival when performing cell-tracking studies. Subsequent imaging demonstrated robust detectability of clinically relevant cell numbers following only 4 hours of incubation in SPIO-treated media. To ensure maximum cell viability and functionality in future cell tracking studies, we employed a lower iron load of 4 pg/cell for labeling and tracking BM-MSCs although higher loads of 10-12 pg/cell have been validated in prior work [17]. Interestingly, even with this low iron burden, tri-lineage differentiation showed increased potential for chondrogenesis (ns) and decreased potential for osteogenesis (ns) and an increase in cell proliferation (ns) was noted in SPIO-labeled cells. Previous studies report similar conflicts in tri-lineage potential and the mechanism of action remains unclear [35-38]. Another study associated changes in cell proliferation with free Fe in the lysosome leading to an increase in cell

cycle progression [39]. As such, SPIO-labeled cells should be considered a feasible method for cell tracking *in vivo,* but care should be taken when interpreting results.

The second aim of this study was to establish a clinically relevant, reproducible model for cell detection and tracking in equine tendon injury. The model of iatrogenic injury described by Schramme et al. (2010) has been well characterized on several imaging modalities [28; 29]. However, pathologic tendon is characterized by heterogeneous areas of high and low signal intensity on T2-weighted images, which can be difficult to discern from SPIO-associated signal [14; 15]. Additionally, SPIOs are nearly undetectable in normal tendon and can only be differentiated in proximity to the subcutaneous tissues where their dipolar effect may disrupt normal tendon borders on MRI. A high field magnet can enhance this effect and is valuable in the interpretation of cell distribution in tissues with low contrast, like tendon. For this reason, we evaluated this model pre- and post-injection with a clinical dose of MSCs on a 1.5 T MRI scanner.

The animal model used in this study is most representative of acute, focal injury to the SDFT and can successfully be used to monitor a large bolus of labeled MSCs post-injection by MRI. The use of a mechanical model of injury enhanced detection of MSCs by providing soft tissue contrast within the lesion associated with the absence and disruption of collagen fibers and mild edema. The efflux of cells into the subcutaneous tissues was easily detectable due to the high signal intensity of the fat contrast associated with these surrounding areas. In the future, these cells can easily be tracked and monitored for cell survival and migration into the tendon, as determined by diminution of the hypointense signal and re-distribution within the tissues. Longer term *in vivo* tracking studies will also have to consider the effects of biomechanical tendon loads, motion and gravity on cell movement and distribution.

Our third objective was to characterize the distribution of cells at the time of injection. In contrast to our stated hypothesis, our data suggest that there is a substantial variation in cell distribution among study subjects even though the injection is performed with precise ultrasound triangulation technique. Post-injection T2*-weighted images in the transverse plane demonstrated heterogeneous and inconsistent cell localization within the tendon lesions when compared to pre-injection images and showed consistent leakage of the labeled cells into the tissue surrounding the SDFT, including the paratenon and subcutaneous tissues, in all subjects.

Histological evaluation confirmed that some cells were also retained within the core lesion. The histologic appearance of the lesioned areas suggests fluid filling that increases interstitial tissue pressure and causes cells to flow retrograde along the needle surface into the fascial layers surrounding the tendons. It is interesting to note that most equine studies suspend cells in a volume of 1-2 mL for injection into flexor tendon injuries [3; 4; 6; 7; 34], whereas we injected less than 1 mL and still observed poor intralesional cellular retention. The clinical presumption that the majority of a cell bolus is retained within the core-lesion is incorrect and further studies should be performed to investigate the degree to which cells migrate within the tendon post-injection and if healing is affected by the degree of cell delocalization.

Limitations

This study performed all imaging and injections post-mortem for economical and logistical reasons. Limbs were not injected in weight-bearing conformation, which is common practice in the clinic. However, it is possible that when the flexor tendons are in slack position there is less risk of iatrogenic damage from the incoming fluid and needle stick. If injections are performed in

standing, it seems reasonable to expect that cells will efflux distal to the needle injection as opposed to equi-distance proximal and distal to the location, due to the effects of gravity. The influence of circulation on cell viability within the tendon lesion will also have to be considered in future studies. It is possible that cells engrafted into the subcutaneous tissues may exhibit higher rates of survival than those in the lesion because of higher vascular perfusion and nutrient supply.

Due to the inherent low signal intensity of normal tendon, it is not possible to perform a quantitative evaluation of SPIO signal or to compare the ratio of cells within and surrounding the tendon lesion. However, the images provide a cohesive, albeit qualitative assessment regarding the distribution of MSCs following ultrasound-guided, intra-lesional tendon injections. Although this question has not been raised in the literature in the past, several studies have already begun to investigate cell migration and survival using histology or other methods [2; 10; 11; 14]. The delocalization of cells immediately following cell injection suggests *in vivo* imaging methods will be far superior for analyzing these data. Additionally, with wider cell distribution established here than expected or reported, changes in MSC administration may be needed. However, confirmation of cell location and in vivo effect on tendon repair, through tissue biopsy in large animal studies, is needed to better establish a protocol for cellular therapies.

Conclusion

Although previous reports have determined that local injury retains cells within a small radius of the site of injection, our study shows greater than expected delocalization and that relatively few cells are retained within collagenous tendon compared to surrounding fascia. The theories of MSC mechanism of action may need to consider greater contribution from MSCs outside of

collagenous tissue. The regional retention of MSCs may have important implications regarding the healing of injuries. Further work is needed if this is a reality *in vivo* and therefore to determine if directed intra-lesional delivery of MSCs is as critical as presently thought.

Competing Interests

The authors declare that there are no competing interests regarding the publication of this paper.

Acknowledgements

The authors would like to thank the American Quarter Horse Association, Morris Animal Foundation, and the University of Georgia Interdisciplinary Grant for their financial support of this project.

Sequence, plane	PD, sagittal	PD, transverse	TRUFI, sagittal and dorsal	T2*, transverse	MSE T2, sagittal
TR (ms)	1830	3020	11.8	695	400
TE (ms)	56	39	5	22.5	4.8, 13, 21.3, 29.6, 37.8
Slice thickness (mm)	2.5	3.0	0.3	2.5	2.5
Flip angle	150	180	28	30	60
FOV (cm)	16x16	15x15	11x16	12.2x15	11.4x14
Matrix size	320x320	320x320	352x512	260x320	260x320

Table 4.1. Parameters for MRI sequences acquired.

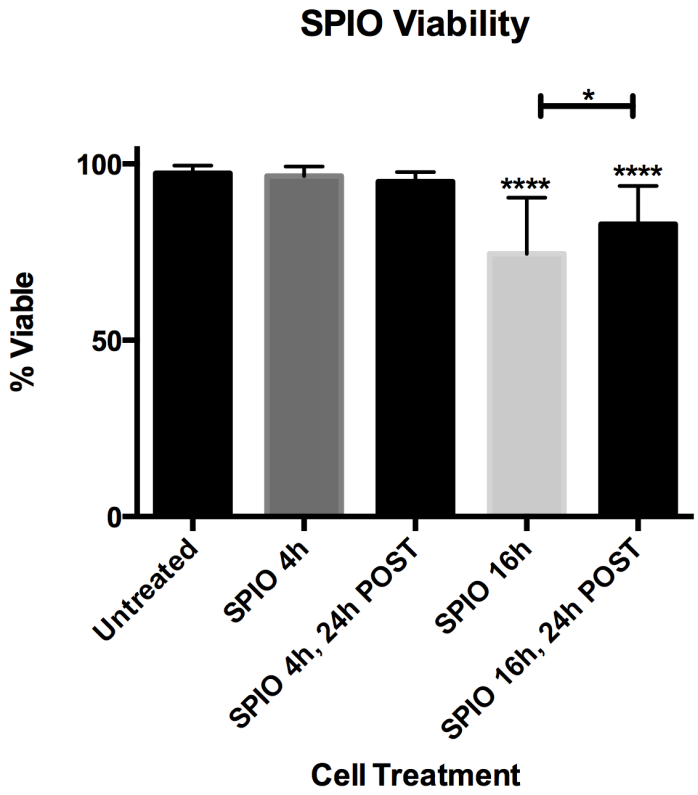

Figure 4.1. Cell viability. Shown after labeling with SPIOs for 4 or 16 hours as compared to untreated cells. Measurements were recorded immediately and 24 hours post-treatment (****$p<0.0001$, *$p<0.05$)

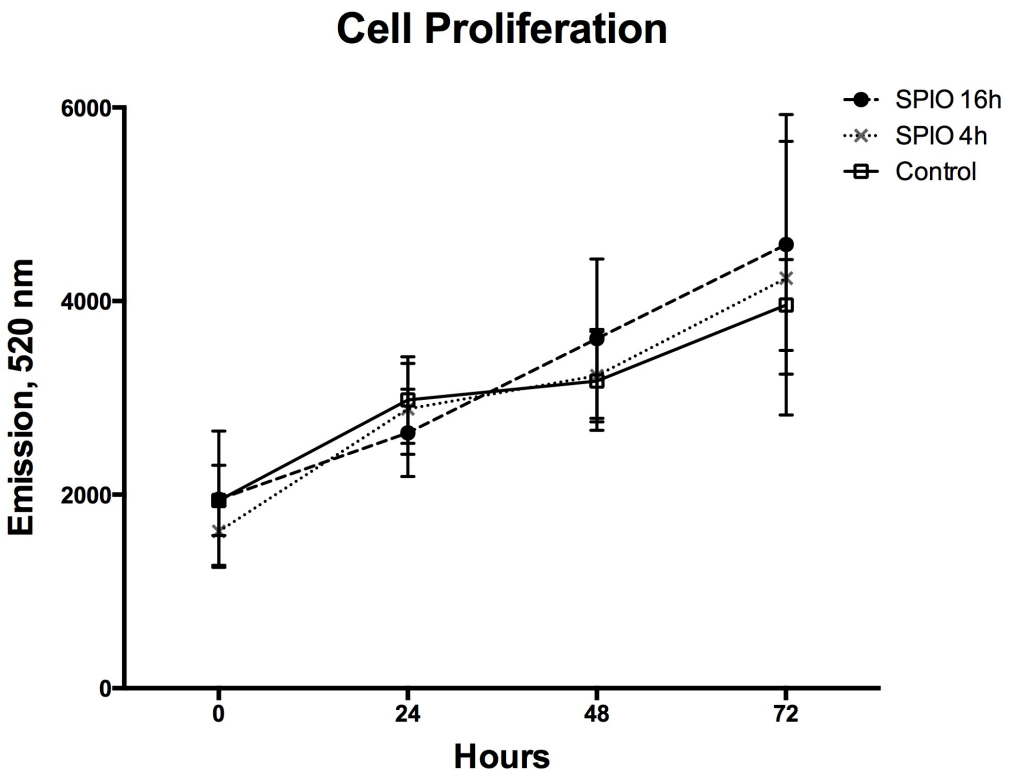

Figure 4.2. Cell proliferation. Shown over 72 hours after labeling with SPIOs for 4 or 16 as compared with untreated cells.

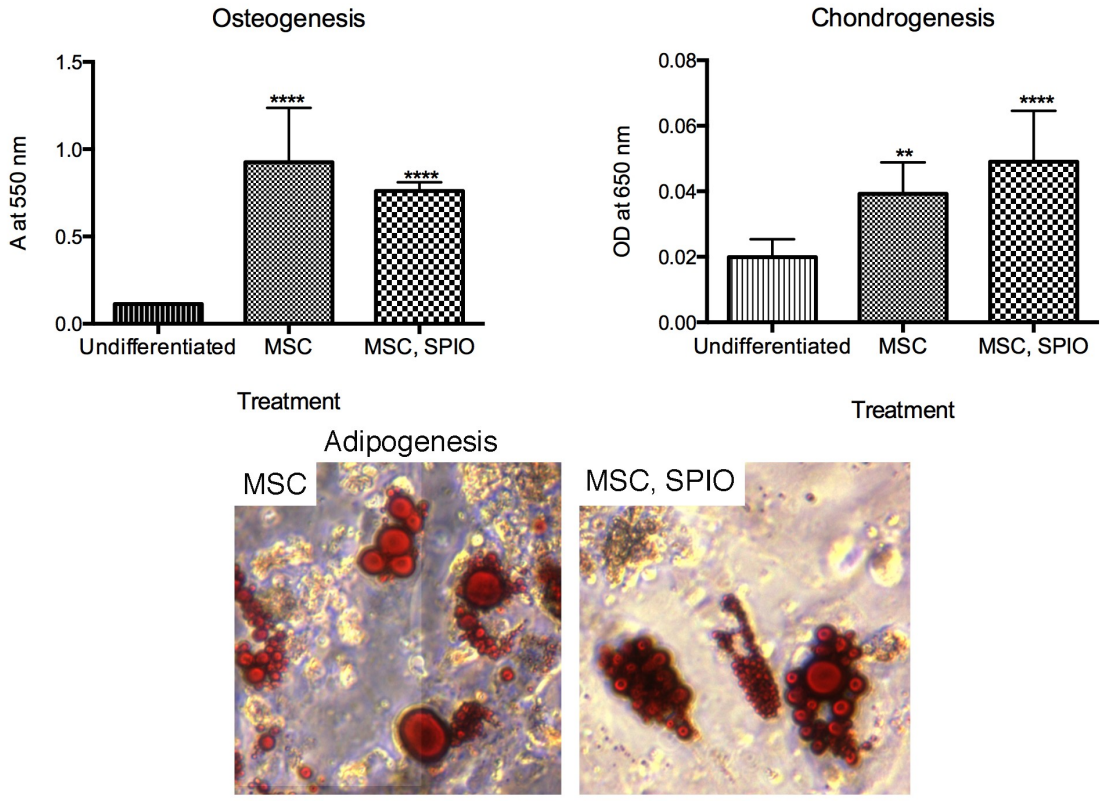

Figure 4.3. Tri-lineage differentiation. Data demonstrating A) osteogenesis as measured by Calcium production (****p<0.0001), B) chondrogenesis as measured by alcian blue uptake in cell pellets (**p<0.01, ****p<0.0001), and C) adipogenesis as noted by lipid deposition visualized with Oil Red O.

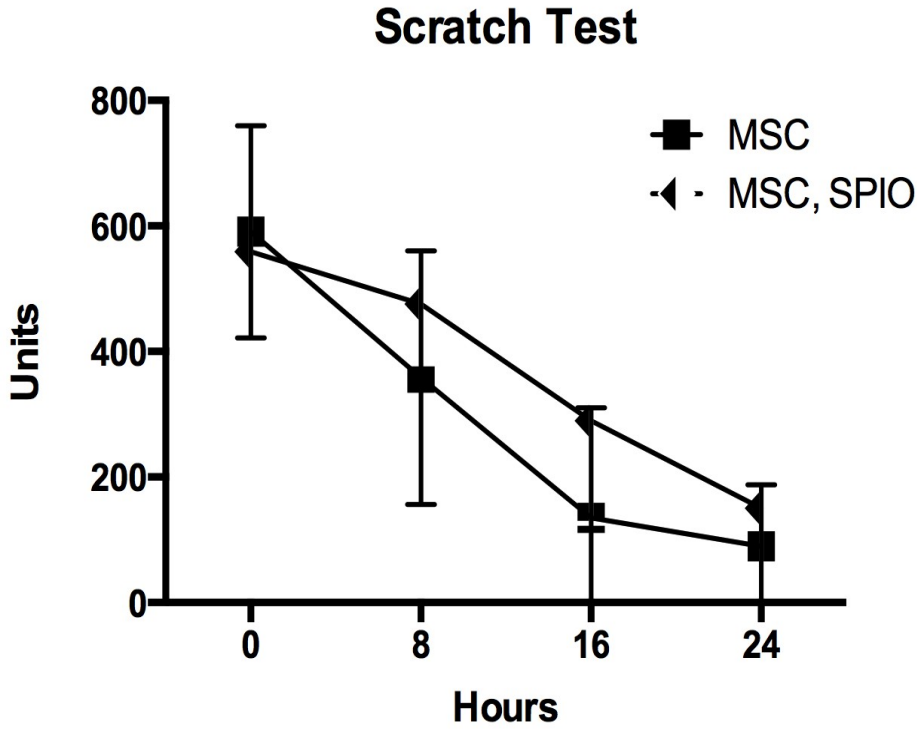

Figure 4.4. Cell migration. As measured by a scratch test over 24 hours.

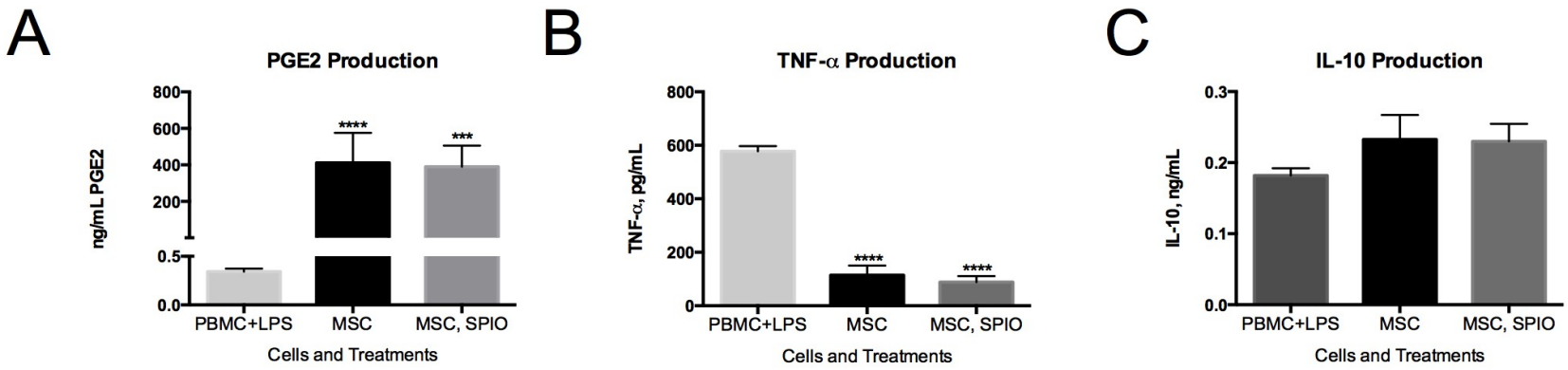

Figure 4.5. Cytokine secretion. Graphs representative of A) Prostaglandin (PG)-E2, B) tumor necrosis factor (TNF)-α, and C) interleukin (IL)-10 production in MSC co-culture with peripheral blood mononuclear cells (PBMCs) following stimulation with LPS (****$p<0.0001$, ***$p<0.01$).

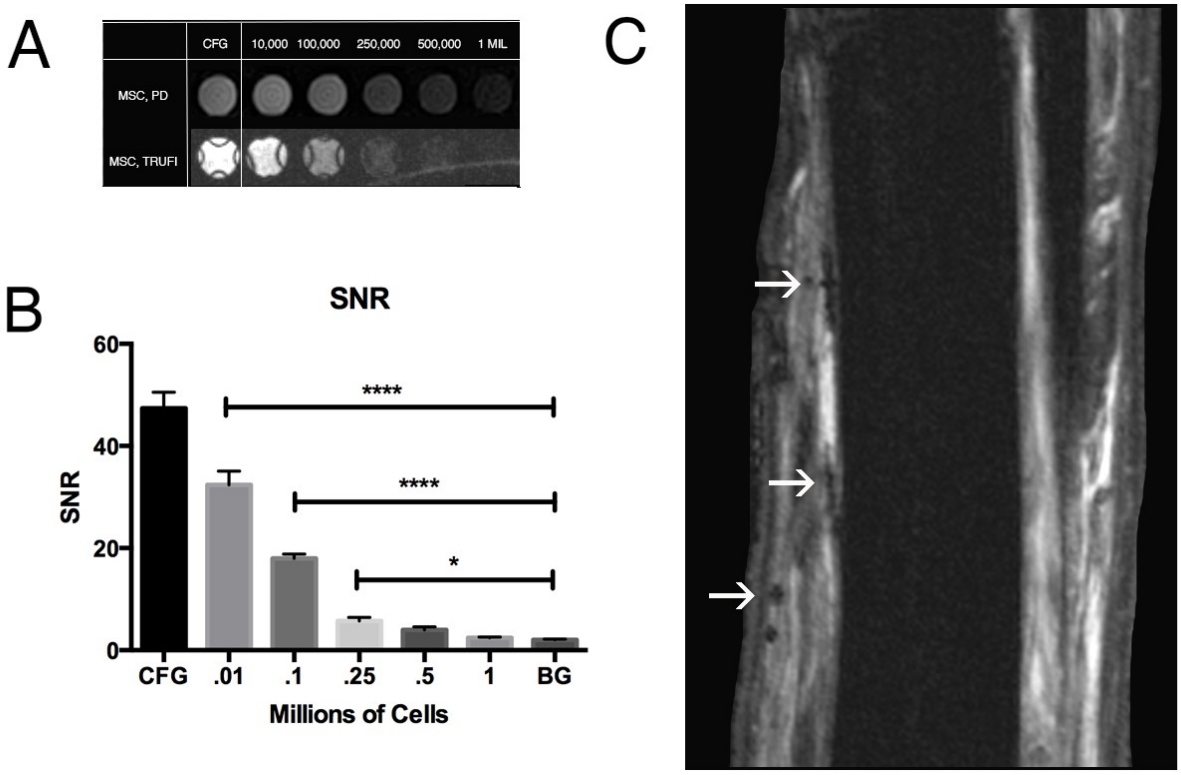

Figure 4.6. Cell phantom and cells in normal tendon. MRI data from cell suspensions in agar gel showing A) PD (top row) and TRUFI (bottom row) images ranging from cell free gel (CFG) up to $1x10^6$ cells in in a 96-well plate. B) Signal-to- noise ratios (SNR) corresponding to the TRUFI images in (A). C) Normal tendon following injection of 20, 10, 5, and $1x10^6$ SPIO-labeled MSCs from proximal to distal. SPIO-associated signal is only visible in the tissues surrounding the SDFT (arrows). (****$p<0.0001$, *$p<0.05$)

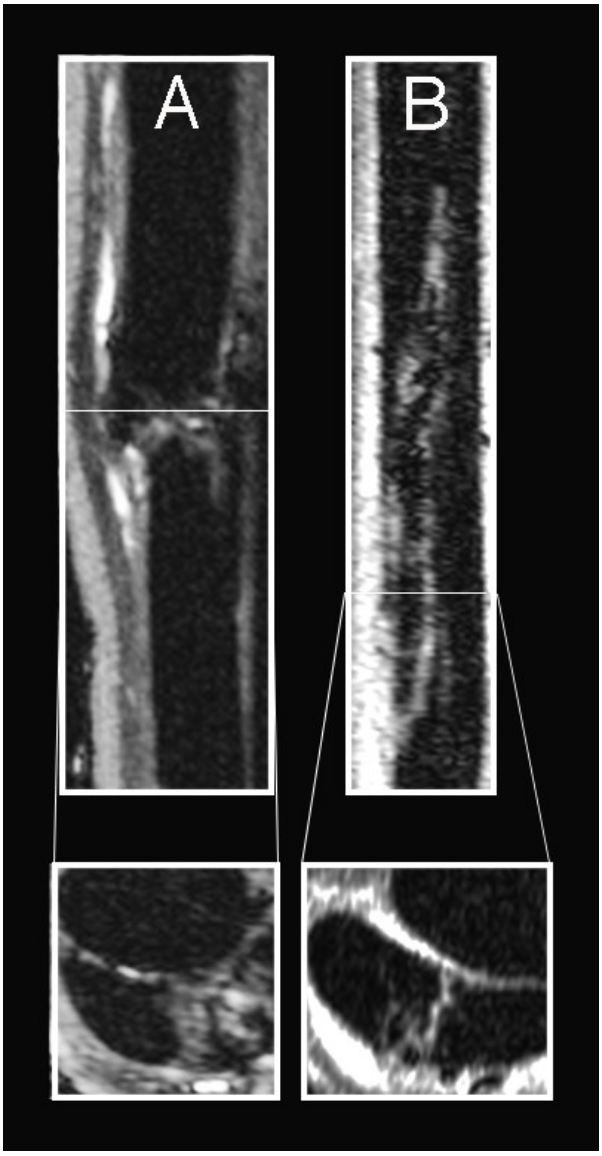

Figure 4.7. MRI of SDFT lesions. TRUFI images demonstrate a lesion A) induced immediately prior to and B) 10 days prior to injection in the sagittal (top) and transverse (bottom) planes.

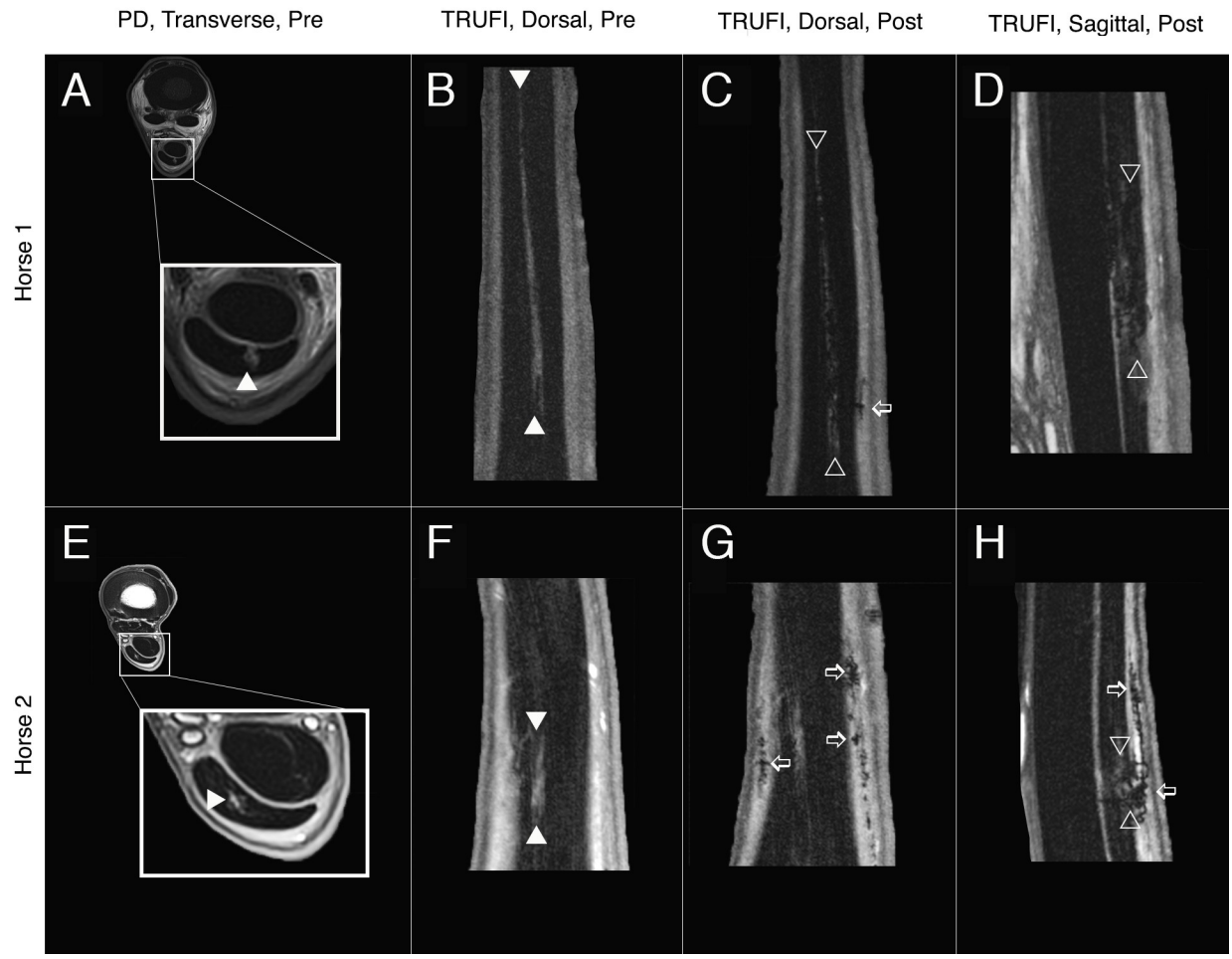

Figure 4.8. MRI of SDFT lesions before (A, B, E, F) and after (C, D, G, H) injection of SPIO-treated cells. Solid arrowheads delineate the tendon lesion in pre-injection images. Open arrowheads indicate SPIO-treated cells within the tendon lesion post-injection. The SPIO-treated cells are seen as small, heterogeneous clusters of dark signal. The open, horizontal arrows indicate SPIO-treated cells distributed throughout the tissue layers surrounding the tendon.

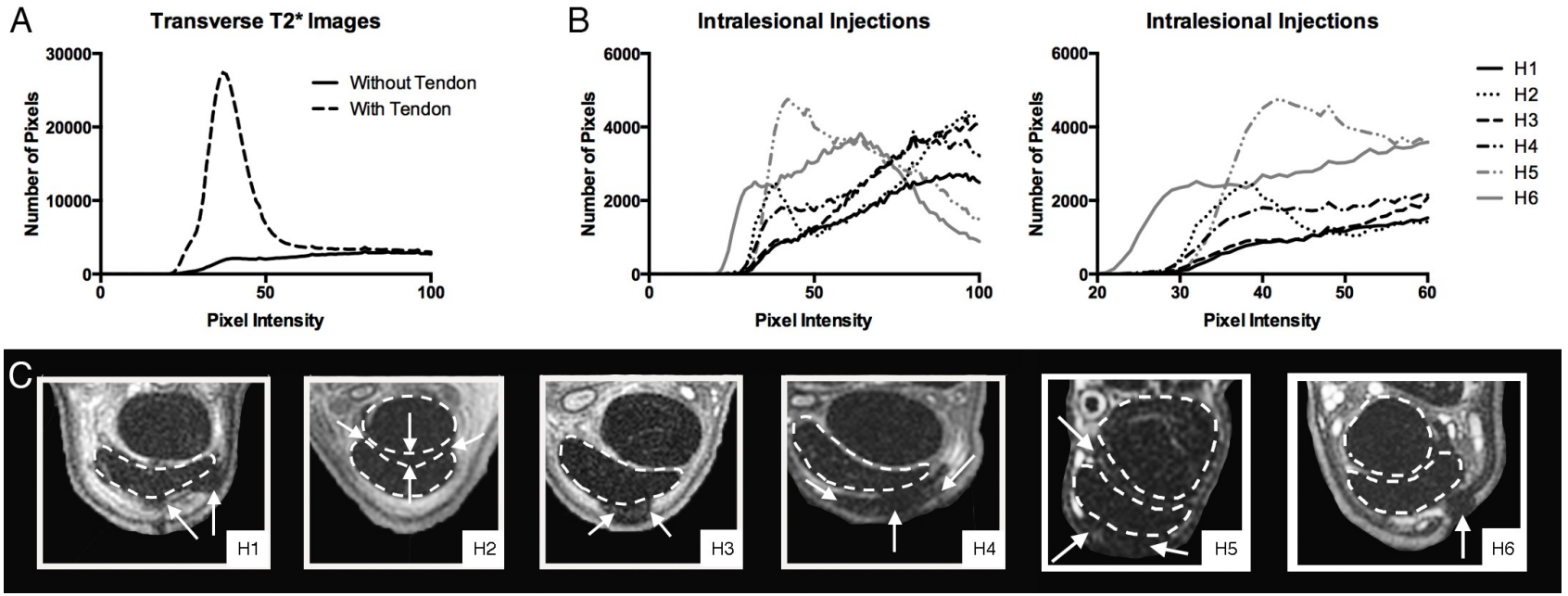

Figure 4.9. Transverse MRI of SDFT and quantification of low MRI signal. A) Graph showing summation of low signal intensity pixels before and after subtraction of DDFt and SDFT from transverse images. B) Summation of low signal intensity pixels in subcutaneous and surrounding soft tissues in all 6 subjects. C) TRUFI images demonstrating substantial efflux of cells into the paratendinous and surrounding tissues. Arrows indicate hypointense areas of MRI signal representative of SPIO-treated cells. Dotted lines estimate the boundaries of the SDFT and DDFT.

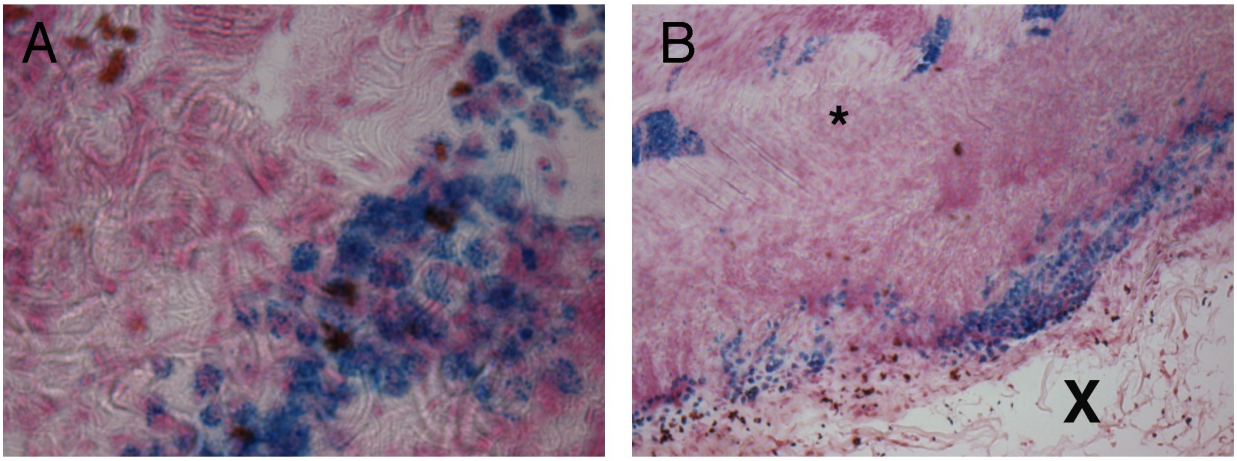

Figure 4.10. Histology of iron-labeled cells. Tissue sections demonstrate dense areas of Prussian Blue-positive, SPIO-treated MSCs lining the tendon lesion. Markers indicate the tendon lesion (X) and the tendon matrix (*). Images shown are at A) 10x and B) 40x.

References

1. Patterson-Kane JC, Becker DL, Rich T. 2012. The pathogenesis of tendon microdamage in athletes: the horse as a natural model for basic cellular research. Journal of comparative pathology 147:227-247.

2. Crovace A, Lacitignola L, Rossi G, et al. 2010. Histological and immunohistochemical evaluation of autologous cultured bone marrow mesenchymal stem cells and bone marrow mononucleated cells in collagenase-induced tendinitis of equine superficial digital flexor tendon. Vet Med Int 2010:250978.

3. Godwin EE, Young NJ, Dudhia J, et al. 2012. Implantation of bone marrow-derived mesenchymal stem cells demonstrates improved outcome in horses with overstrain injury of the superficial digital flexor tendon. Equine Vet J 44:25-32.

4. Pacini S, Spinabella S, Trombi L, et al. 2007. Suspension of bone marrow-derived undifferentiated mesenchymal stromal cells for repair of superficial digital flexor tendon in race horses. Tissue Eng 13:2949-2955.

5. Schnabel LV, Lynch ME, van der Meulen MC, et al. 2009. Mesenchymal stem cells and insulin-like growth factor-I gene-enhanced mesenchymal stem cells improve structural aspects of healing in equine flexor digitorum superficialis tendons. J Orthop Res 27:1392-1398.

6. Smith RK, Werling NJ, Dakin SG, et al. 2013. Beneficial effects of autologous bone marrow-derived mesenchymal stem cells in naturally occurring tendinopathy. PLoS One 8:e75697.

7. Carvalho Ade M, Badial PR, Alvarez LE, et al. 2013. Equine tendonitis therapy using mesenchymal stem cells and platelet concentrates: a randomized controlled trial. Stem Cell Res Ther 4:85.

8. Richardson LE, Dudhia J, Clegg PD, et al. 2007. Stem cells in veterinary medicine--attempts at regenerating equine tendon after injury. Trends Biotechnol 25:409-416.

9. Lacitignola L, Staffieri F, Rossi G, et al. 2014. Survival of bone marrow mesenchymal stem cells labelled with red fluorescent protein in an ovine model of collagenase-induced tendinitis. Vet Comp Orthop Traumatol 27:204-209.

10. Guest DJ, Smith MR, Allen WR. 2008. Monitoring the fate of autologous and allogeneic mesenchymal progenitor cells injected into the superficial digital flexor tendon of horses: preliminary study. Equine Vet J 40:178-181.

11. Guest DJ, Smith MR, Allen WR. 2010. Equine embryonic stem-like cells and mesenchymal stromal cells have different survival rates and migration patterns following their injection into damaged superficial digital flexor tendon. Equine Vet J 42:636-642.

12. Becerra P, Valdes Vazquez MA, Dudhia J, et al. 2013. Distribution of injected technetium(99m)-labeled mesenchymal stem cells in horses with naturally occurring tendinopathy. J Orthop Res 31:1096-1102.

13. Sole A, Spriet M, Galuppo LD, et al. 2012. Scintigraphic evaluation of intra-arterial and intravenous regional limb perfusion of allogeneic bone marrow-derived mesenchymal stem cells in the normal equine distal limb using (99m) Tc-HMPAO. Equine Vet J 44:594-599.

14. Geburek F, Mundle K, Conrad S, et al. 2016. Tracking of autologous adipose tissue-derived mesenchymal stromal cells with in vivo magnetic resonance imaging and histology after intralesional treatment of artificial equine tendon lesions - a pilot study. Stem Cell Res Ther 7:21.

15. Berner D, Brehm W, Gerlach K, et al. 2016. Longitudinal Cell Tracking and Simultaneous Monitoring of Tissue Regeneration after Cell Treatment of Natural Tendon Disease by Low-Field Magnetic Resonance Imaging. Stem cells international 2016:1207190.

16. Scharf A, Holmes S, Thoresen M, et al. 2015. Superparamagnetic iron oxide nanoparticles as a means to track mesenchymal stem cells in a large animal model of tendon injury. Contrast Media Mol Imaging.

17. Addicott B, Willman M, Rodriguez J, et al. 2011. Mesenchymal stem cell labeling and in vitro MR characterization at 1.5 T of new SPIO contrast agent: Molday ION Rhodamine-B. Contrast Media Mol Imaging 6:7-18.

18. Farrell E, Wielopolski P, Pavljasevic P, et al. 2008. Effects of iron oxide incorporation for long term cell tracking on MSC differentiation in vitro and in vivo. Biochemical and Biophysical Research Communications 369:1076-1081.

19. Gonzalez-Lara LE, Xu X, Hofstetrova K, et al. 2011. The use of cellular magnetic resonance imaging to track the fate of iron-labeled multipotent stromal cells after direct transplantation in a mouse model of spinal cord injury. Mol Imaging Biol 13:702-711.

20. McFadden CD, C L Mallett, and PJ Foster. 2011. Labeling of multiple cell lines using a new iron oxide agent for cell tracking by MRI. Contrast Media Mol Imaging 6:514-522.

21. Kriz J, Jirak D, White D, et al. 2008. Magnetic resonance imaging of pancreatic islets transplanted into the right liver lobes of diabetic mice. Transplant Proc 40:444-448.

22. Kraitchman DL, Kedziorek DA, Bulte JW. 2011. MR imaging of transplanted stem cells in myocardial infarction. Methods Mol Biol 680:141-152.

23. Heyn C, Ronald JA, Mackenzie LT, et al. 2006. In vivo magnetic resonance imaging of single cells in mouse brain with optical validation. Magn Reson Med 55:23-29.

24. van Buul GM, Kotek G, Wielopolski PA, et al. 2011. Clinically translatable cell tracking and quantification by MRI in cartilage repair using superparamagnetic iron oxides. Plos One 6:e17001.

25. Frank J, Miller B, Arbab A, et al. 2003. Clinically Applicable Labeling of Mammalian and Stem Cells by Combining Superparamagnetic Iron Oxides and Transfection Agents. Radiology.

26. Ko IK, Song H-T, Cho E-J, et al. 2006. In vivo MR Imaging of Tissue-engineered Human Mesenchymal Stem Cells Transplanted to Mouse: a Preliminary Study. Annals of Biomedical Engineering 35:101-108.

27. Ferreira L, Karp JM, Nobre L, et al. 2008. New Opportunities: The Use of Nanotechnologies to Manipulate and Track Stem Cells. Cell Stem Cell 3:136-146.

28. Schramme M, Hunter S, Campbell N, et al. 2010. A surgical tendonitis model in horses: technique, clinical, ultrasonographic and histological characterisation. Vet Comp Orthop Traumatol 23:231-239.

29. Schramme M, Kerekes Z, Hunter S, et al. 2010. Mr Imaging Features of Surgically Induced Core Lesions in the Equine Superficial Digital Flexor Tendon. Veterinary Radiology & Ultrasound 51:280-287.

30. Vidal MA, Kilroy GE, Johnson JR, et al. 2006. Cell growth characteristics and differentiation frequency of adherent equine bone marrow-derived mesenchymal stromal cells: adipogenic and osteogenic capacity. Vet Surg 35:601-610.

31. Liang CC, Park AY, Guan JL. 2007. In vitro scratch assay: a convenient and inexpensive method for analysis of cell migration in vitro. Nat Protoc 2:329-333.

32. Sun WC, Moore JN, Hurley DJ, et al. 2008. Adenosine A2A receptor agonists inhibit lipopolysaccharide-induced production of tumor necrosis factor-alpha by equine monocytes. Vet Immunol Immunopathol 121:91-100.

33. Crovace A, Lacitignola L, Francioso E, et al. 2008. Histology and immunohistochemistry study of ovine tendon grafted with cBMSCs and BMMNCs after collagenase-induced tendinitis. Vet Comp Orthop Traumatol 21:329-336.

34. Watts AE, Yeager AE, Kopyov OV, et al. 2011. Fetal derived embryonic-like stem cells improve healing in a large animal flexor tendonitis model. Stem Cell Res Ther 2:4.

35. Kostura L, Kraitchman DL, Mackay AM, et al. 2004. Feridex labeling of mesenchymal stem cells inhibits chondrogenesis but not adipogenesis or osteogenesis. NMR in Biomedicine 17:513-517.

36. Foldager CB, Pedersen M, Ringgaard S, et al. 2011. Chondrocyte gene expression is affected by very small iron oxide particles-labeling in long-term in vitro MRI tracking. J Magn Reson Imaging 33:724-730.

37. Farrell E, Wielopolski P, Pavljasevic P, et al. 2009. Cell labelling with superparamagnetic iron oxide has no effect on chondrocyte behaviour. Osteoarthritis and Cartilage 17:961-967.

38. Chen YC, Hsiao JK, Liu HM, et al. 2010. The inhibitory effect of superparamagnetic iron oxide nanoparticle (Ferucarbotran) on osteogenic differentiation and its signaling mechanism in human mesenchymal stem cells. Toxicol Appl Pharmacol 245:272-279.

39. Huang DM, Hsiao JK, Chen YC, et al. 2009. The promotion of human mesenchymal stem cell proliferation by superparamagnetic iron oxide nanoparticles. Biomaterials 30:3645-3651.

CHAPTER 5

LONGITUDINAL, MRI-BASED ASSESSMENT OF INTRALESIONAL MSC THERAPY AND HEALING IN AN OVINE MODEL OF TENDONITIS[1]

[1] Scharf, AM, SP Holmes, M Thoreson, M Barletta, T Lewis, A Stumpf, and J Peroni. To be submitted to *Veterinary Comparative Orthopaedics and Traumatology*.

Abstract

The aim of this study was to non-invasively monitor cell migration and survival concurrent with healing in an ovine model of acute tendon injury over 28 weeks. Iatrogenic lesions were made and injected with $10x10^6$ SPIO-labeled or unlabeled MSCs or left untreated. Short-term animals were imaged with MRI at time of injection and 6 weeks. Long-term animals were imaged with MRI at time of injection, 2 weeks and 28 weeks.

SPIO-associated signal was diffusely present throughout the soft tissues surrounding the tendon at all time points. After 6 weeks, this signal was likely associated with non-viable cells. Signal dropped off exponentially over the first 6 weeks. Non-specific differences were observed between all groups and across all time points for tendon cross-sectional area. Standard deviation (SD) of MRI signal, signal to noise ratios (SNR), and signal difference to noise ratios (SDNR) decreased over time for MSCs, SPIO-MSCs and control groups. MSC-treated tendons had lower SD, SNR and SDNR than control and SPIO-MSC treated tendons at 28 weeks. Lesion volume also appeared to contract more rapidly in MSC-treated tendons than controls.

MSC treatment appears to improve tendon healing over a period of 28 weeks in acute tendon injury as determined by MRI. Further work with biomechanical testing should be performed to confirm these results.

Introduction

Tendonitis has been studied using large animal models of injury and the results of these studies indicate that the structural and biomechanical integrity of the tendons improve following treatment with mesenchymal stem cells (MSCs).[1-3] Measures that are commonly evaluated to assess outcomes in tendon injury repair include collagen fiber orientation and crimp pattern,

immune cell infiltrate, expression of tendon-associated molecular markers, and collagen I:III ratios. *In vitro* studies suggest that MSCs may positively affect these parameters and influence healing because they are capable of both paracrine stimulation of host cells[4; 5] and direct differentiation into tendon-like precursors.[6; 7] Unfortunately, in vivo data that would help determine how to optimize the mode and timing of MCS delivery, the distribution of cells within the injury site, and ultimately assess the effect of MSCs on tendon healing over time is lacking.

Data obtained by recent cell tracking studies suggest that MSC persistence in tendon injury is short lived and therefore most of the MSC-mediated healing is likely due to early stimulation of paracrine activity rather than integration and tendon matrix regeneration.[8-12] Attempting to correlate in vitro or cell tracking data with clinical outcomes is difficult. Although anecdotal evidence for MSC use is plentiful in the clinic, well-controlled, prospective studies are not. A small number of reports on stem cell survival and migration following intra-lesional implantation exist, but they are limited by short term[13; 14] or low resolution[10; 11] imaging modalities or post-mortem analysis.[8; 9; 15] A recent study based on tracking MSCs via nuclear scintigraphy, demonstrated substantial cell related focal signal uptake after intra-lesional injection, followed by less than 24% cell retention by 24 hours.[14] Similarly, less than 5% cell retention by 10 days post-injection, was reported in a study in which treated tendons were biopsied over time for histological analysis.[9] MSC treatment may be complicated by variability in cell localization after injection. In fact, recent work in our lab demonstrated that presumed intra-lesional injection of MSCs often results in cells distributing throughout the tissues surrounding the lesion as well (*Stem Cells International,* under review).

With this study, we attempted to correlate MSC treatment with tendon healing over time. We designed experiments to monitor MSC migration and survival along with healing using MRI

techniques over 28 weeks in an acute tendon injury created in sheep. We hypothesized that tendons treated with MSCs would heal better than untreated tendons and that MSC numbers would decline rapidly within the tendons, becoming undetectable by 14 days post-treatment.

Materials and Methods

Ten, healthy, Dorset-cross adult ewes between 1 and 3 years of age were used in this study. All sheep underwent surgery to create tendon lesions and were then split into 3 groups: short term, long term, and control. All sheep tendons were imaged with MRI 3 weeks following surgery, which coincided with the time of MSC injection. Depending on the group to which the sheep were randomly assigned, they subsequently underwent MRI at 2, 6, or 28 weeks post-injection as shown by the schedule in Table 5.1. Short-term sheep were housed in box stalls in groups of 3 for the duration of the study. Long-term and control sheep were housed in box stalls for at least 4 weeks after the tendon lesion was made and then relocated to a pasture. All work of this study was performed under protocol number A2013 04-014-Y3-A6 in accordance with the University of Georgia Institutional Animal Care and Use Committee guidelines.

Deep digital flexor tendon (DDFT) lesions were created in thoracic and/or pelvic limbs of all 10 sheep and assigned to treatments in short-term, long-term, or control treatment groups according to Table 5.2. Sheep were pre-medicated with flunixin meglumine (1.1mg/kg) and ceftiofur (2.2 mg/kg) SQ and then sedated with a combination of midazolam (0.3 mg/kg) and butorphanol (0.4 mg/kg) IV. If sedation was not adequate, sheep were induced with propofol (5-10 mg/kg, to effect) IV and maintained on 2% isoflurane.

The metacarpal or metatarsal region was circumferentially clipped and aseptically prepared. The limb was desensitized with a ring block performed using 5 ml of 2% lidocaine

infused subcutaneously just distal to the carpus or tarsus. Lesions were induced using a procedure modified from Schramme et al (2010).[16] Briefly, a 1 cm incision was made on the caudal aspect of the metacarpus or metatarsus to expose the superficial and deep flexor tendons just above the proximal extent of the digital flexor tendon sheath. The DDFT was identified and a small incision made through the paratenon and into the tendon. Subsequently, a 4.5mm Steinmann pin was inserted through that incision and advanced 2.5 cm within the DDFT with slow rotational motions. The pin was extracted and replaced by a 5mm arthroscopic burr, which was activated at 2500 rpm and inserted and withdrawn within the DDFT five times. The skin incision was closed with surgical staples and the limbs were placed under a heavy bandage. Sheep received additional doses of flunixin meglumine (1.1 mg/kg) at 24 and 48 hours post-operatively.

Cryopreserved allogeneic bone marrow derived ovine MSCs (BM-MSCs) were injected under general anesthesia during the first MRI imaging procedure 3 weeks after the lesions were made. Cells were maintained in culture at 37°C and 5% CO_2, grown to 70% confluency in MSC culture medium (low glucose Dulbecco's Modified Eagle Medium (DMEM), 10% Fetal Bovine Serum, 1% L-glutamine, 50 U/mL penicillin, 50 μg/mL streptomycin), and treated with 25 μg/mL Molday ION C6Amine (Biopal, Inc.) SPIOs overnight. *In vitro* validation was performed as reported previously[17]. Unlabeled cells were prepared and cultured identically without SPIOs. Prior to use in the experiment, incubation medium was aspirated from the plates, and the cells washed with PBS and harvested after 0.25% Trypsin-EDTA (Invitrogen) treatment

MRI Assessment

Prior to anesthesia, sheep were fasted for 24 hours. A 14g intravenous jugular catheter was placed under aseptic conditions and secured to the neck with a bandage. Sheep were sedated with

a combination of midazolam (0.3 mg/kg) and butorphanol (0.4 mg/kg) IV. Anesthesia was then induced with propofol (5 to 10 mg/kg, to effect) administered intravenously as a bolus. Sheep were orotracheally intubated and maintained with isoflurane in oxygen for the duration of the procedure. Sheep were positioned in sternal recumbency for imaging forelimbs and in lateral recumbency for imaging hind limbs. Imaging was performed using a Siemens 1.5 T MRI unit with B17 software. All imaging was performed with a 15-channel transmit-receive knee coil. Sequence parameters are described in Table 5.3. Only proton density (PD) and true fast imaging with steady state precession (TRUFI) images were acquired for MSC-treated and control limbs. MRI was performed before and after injection on all limbs treated with SPIO-labeled MSCs. During the pre-injection MRI a suitable marker was placed next to the incision and guided by this marker $10x10^6$ MSCs suspended in 0.5 mL PBS were delivered intralesionally using a 20-gauge needle.

Cell Artifact Measurements

Quantitative evaluation of SPIO-associated cell artifacts included approximation of cell artifact volumes from the second echo in T2*-weighted (T2*w) MSE acquisition series in the dorsal plane. Free-hand regions of interest (ROI) were measured in Osirix, summed, and multiplied by the slice thickness to calculate approximate volumes. Transverse, T2*w images from the middle 4 cm of all SPIO-treated limbs were extracted and converted to stacks in ImageJ (NIH). Histograms of relative pixel intensity (RPI) were generated from the palmar aspect of the suspensory ligament to the most palmar aspect of the limb on every third slice. Individual histograms were also generated for the SDFT and DDFT. These histograms were subtracted from the RPI of the whole image to calculate the number of low intensity pixels in the surrounding fascia.

Statistical analysis was performed for T2* artifact volumes with one-way analysis of variance (ANOVA) and Sidak's multiple comparison test using Prism 6 software.

Tendon Measurements

Quantitative evaluation of the tendons was performed in MSC, SPIO-labeled MSC (S-MSC), and control groups. Tendon cross-sectional area, standard deviation (SD), signal-to-noise ratio (SNR), and signal-difference-to-noise ratio (SDNR) were calculated in all PD images along the longitudinal axis of the tendon lesion. Signal-to-noise ratio was calculated by measuring the mean signal intensity within the tendon divided by the standard deviation of the noise (SD_{noise}) in the background using a user-defined ROI. A modified version of SDNR as defined by Schramme et al. (2010) was calculated by measuring the maximum signal intensity minus the minimum signal intensity within the tendon divided by the SD_{noise}.[18]

For statistical analysis, normality of the data was assessed based on examination of histograms and normal Q-Q plots of the residuals. Constant variance of the data was assessed by plotting residuals against predicted values. Data were analyzed using linear mixed-effects modeling with sheep modeled as random effects and treatment group and time modeled as fixed nominal effects. Two-way interactions were also included in the model. Model fit was assessed using Akaike information criterion values. For all analyses, $p < 0.05$ was considered significant. Analyses performed on ln-transformed data to satisfy assumptions of normality and equal variances

Lesion Measurements

A boarded veterinary radiologist performed quantitative evaluation of cross-sectional area of tendon lesions using free-hand ROIs in transverse plane of PD images. The same number of slices were monitored serially and were unique to each affected limb, as determined by the extent

of the lesion. Areas were summed and multiplied by the slice thickness. Statistical analysis was not performed due to variability in appearance of lesion quality and difficulty performing repeated measures. Data is graphically represented to observe trends only. Sequential MRI images were qualitatively interpreted to assess overall lesion quality and iron-associated signal in relation to the location and the change of the lesion over time.

Histology

At 6 weeks (short-term) and 28 weeks (long-term), animals were euthanized and flexor tendons were collected following MRI. Each DDFT was excised in approximately 3.5 cm sections centered at the lesion site, embedded in OCT compound (Tissue-Tek®), and longitudinally sectioned on a cryostat (Leica) at 12 μm. Hematoxylin and eosin (H&E) staining and enzymatic immunohistochemistry for Collagen I was performed. After incubation with serum free protein block (DAKO), sections were incubated with monoclonal mouse type I collagen primary antibody (mab3391, Millipore). The sections were washed with PBS-tween 20 and blocked with 10% hydrogen peroxide. Next, incubation with the secondary biotinylated goat anti-mouse IgG antibody (BA-9200, Vector labs) was performed, slides were rinsed and incubated with streptavidin-horseradish peroxidase (HRP, Vector labs). For development, a DAB peroxidase (HRP) substrate kit (Vector labs) was used according to the manufacturer's instructions. Counterstain with hematoxylin was performed. Slides were dehydrated in an ethanol series, cleared in xylene, mounted and dried. Normal tendon was also similarly prepared and evaluated.

Prussian Blue staining was performed on 6-week sections only. For Prussian blue, sections were mounted, fixed with 4% paraformaldehyde, incubated with Prussian Blue reagents (Biopal, Inc) to evaluate the presence of iron nanoparticles, and counterstained with Nuclear Fast Red to visualize tissue morphology with light microscopy.

Results

Cell Artifact Measurements

Larger numbers of pixels with low (dark) intensity were present and distributed more focally in the tissues surrounding the DDFT and SDFT at the time of injection (TOI). The signal decreased and became more diffuse over 4 months (Figure 5.1A). The total volume of hypointense, cell-associated artifacts on T2*w images decreased in an exponential fashion, demonstrating significant decrease between the time of injection and 2 weeks ($p<0.05$). A downward trend continued until 6 weeks and stabilized between 6 and 28 weeks (Figure 5.1B).

Tendon Measurements

All tendon measurements reflect data acquired from PD and transverse images. Tendon lesions were identified by focal increases in signal intensity on PD and TRUFI sequences (Figure 5.2). Non-specific trends and changes were observed between all groups and across all time points for tendon CSA (Figure 5.3A). The CSA of MSC tendons were not different from S-MSC ($p=0.248$) or control ($p=0.115$) tendons at 2 weeks. Lesions in the MSC tendons were smaller at 6 weeks as compared to those in S-MSC tendons ($p<0.05$), but not smaller than control lesions ($p=0.127$). Lesions in the MSC tendons were larger than both lesions in S-MSC and control tendons at 28 weeks ($p<0.05$). Those in MSC tendons decreased in size from 2 to 6 weeks ($p<0.05$) and increased in size from 6 to 28 weeks ($p<0.05$). Those in control and S-MSC tendons did not change from 2 to 6 weeks ($p=0.484, 0.485$), but both decreased in size from 6 to 28 weeks ($p<0.05$).

Standard deviation within transverse cross-sections of tendon decreased over time for all groups (Figure 5.3B). The control group was more homogeneous at week 2 compared to the MSC group ($p<0.05$). The tendons treated with MSCs were more homogeneous than both the

control ($p<0.05$) and S-MSC ($p<0.05$) treated tendons at 28 weeks. Control tendons did not change from 2 to 6 weeks ($p=1$), but they improved from 6 to 28 weeks ($p<0.05$). The MSC treated tendons demonstrated improvement over 2 to 6 weeks ($p<0.05$) and 6 to 28 weeks ($p<0.05$).

Signal difference to noise ratios decreased over time for all groups (Figure 5.3C). The control tendons had a lower SDNR as compared to the MSC ($p<0.05$) and S-MSC ($p<0.05$) groups at 2 weeks. At 28 weeks the MSC-treated tendons had significantly lower SDNR than the S-MSCs treated ones ($p<0.05$). The MSC-treated tendons had lower SDNR than controls, but the result was not significant ($p=0.104$). Signal difference to noise ratios decreased from 2 to 6 weeks in the MSC treated tendons only ($p<0.05$) and from 6 to 28 weeks in both the MSC treated tendons ($p<0.05$) and control tendons ($p<0.05$).

Signal to noise ratios decreased over time for all groups (Figure 5.3D). The control tendons had a lower SDNR than the S-MSC treated tendons ($p<0.05$), but was not different from the MSC treated tendons ($p=0.454$) at 2 weeks. The control and MSC treated tendons were not different at 6 weeks ($p=0.469$). However, the MSC treated tendons had a lower SDNR than both the S-MSC treated tendons ($p<0.05$) and control tendons ($p<0.05$) at 28 weeks. Signal to noise ratios of the MSC treated and control tendons both decreased from 6 to 28 weeks ($p<0.05$).

Lesion Measurements

Lesion volume increased from 0-6 weeks in control tendons, whereas lesion volume decreased from 2-6 weeks in MSC treated tendons. All lesions were resolved by observation on PD transverse images at 28 weeks (Figure 5.4).

Qualitative Assessment

Labeled cells did not likely migrate into the area of injury over time (Figure 5.5).

Histology

Staining with H&E in treated and untreated tendons demonstrated increased cellularity, fibrous scar deposition, fiber disruption, and decreased crimp pattern at both 6 and 28 weeks compared to normal tendon (Figure 5.6). Collagen I staining appeared to be more focal and evenly distributed in treated lesions (Figure 5.7). No qualitative differences were appreciated between control and treated tendons at 28 weeks. Prussian blue staining showed SPIO-associated, blue staining throughout the connective tissue lining the site of injury and within collagenous tendon fibers. More staining was evident in the loose connective tissue and fascia (Figure 5.8).

Discussion

This study represents a novel assessment of MSC migration and disappearance over time in conjunction with the resolution of acute tendon injury. It is also the first implementation of a surgical, non-transection based model of tendon injury in the ovine species. Our ovine model demonstrates characteristics similar to those of its equine counterpart described in Schramme et al. (2010), showing the most pronounced contrast in PD images. Our data shows decreasing trends in SDNR and SNR over time, similar to those data reported in MSDR calculated from a low field MRI scanner.[18] Greater improvements in both SDNR and SNR are seen in MSC-treated limbs, which are excellent indicators of the efficacy of MSC therapy.

Morphological parameters such as tendon CSA, lesion volume, and signal intensity are commonly used to monitor tendon health.[2; 18; 19] Together, reductions in SNR, SDNR, and SD over 28 weeks indicate a trend towards more homogenous signal intensity, similar to normal tendon. Our results demonstrate significant improvement in SDNR, SNR, and SD in MSC treated animals as compared to controls, indicating less localized edema and improvement in

fiber organization. These data highlight the ability of MSCs to improve the structural integrity of tendons over time. Although significant differences were observed between treatment groups for tendon CSA, the absence of an overall downward trend in CSA over 28 weeks indicates these changes may not be associated with a decrease in swelling and inflammation. Absence of significance in tendon CSA has been observed in another report[19] and CSA is not considered as a negative indicator of treatment for this study.

Interestingly, trends between MSC and SPIO-MSC treated tendons were not consistent. As SPIOs are associated with conspicuous areas of dark signal intensity on most MRI sequences, they may confound measurements of data like SNR and SDNR, therefore data must be interpreted with care. However, it would be expected that SNR and SDNR for SPIO-treated tendons would decrease due to the higher proportion of low signal intensity in these limbs. At 28 weeks, SPIO-MSC treated tendons had significantly higher SNR and SDNR as compared to MSC-treated limbs. It is possible that SPIOs induce a low-grade inflammatory response and may impede healing. This should be investigated further prior to the implementation of this technology into the clinical setting.

Well-controlled studies are needed to confirm that MSCs offer a superior alternative to conservative treatment and that their therapeutic advantages are sustained over time. Many studies assess tendon repair at relatively short time periods, following subjects out for approximately 2 months. Reports have shown significant differences following treatment over a range of 6-10 weeks using ultrasound and MRI-based imaging modalities.[10; 19-21] Although reports of improvement in MSC tendons have been reported at 6 months as measured by ultrasound analysis[2], a recent study suggests ultrasound may overstate improvements in tendon quality as

compared to MRI.[11] The results of our study emphasize the importance of long-term follow-up, showing a larger magnitude of difference in healing at 6 weeks as compared to 28 weeks.

Magnetic resonance imaging offers the ability to track MSCs and tendon healing simultaneously within the same patient. Although some patients are only assessed with one-time diagnostic imaging panel in the clinic, studies have highlighted the need for recheck MRI to refine and confirm prognosis[22]. Recent progress in imaging has also led to more robust assessment of tendon and ligament injuries via MRI that have been shown to correlate with histological scoring methods[18; 23] and long term outcome.[22] Measurement of tendon lesion CSA using MRI has been previously validated with an approximate underestimation of -1.4%, which was not clinically significant. Our study shows a faster decrease in of tendon lesion volume in MSC-treated patients, which may be associated with the ability of MSCs to mediate the transition from granulation tissue to fibrous deposition in the proliferative phase of wound healing. This stage is predominated by macrophage infiltration[24] and the ability of MSCs to influence the transition from M1 to anti-inflammatory M2 macrophages is widely documented.[25-27]

Interestingly, some lesions were more conspicuous in TRUFI images in the dorsal and sagittal planes. This may be due to the inclusion of T1 contrast,[18] gradient echo type sequences, as well as the improved resolution in these 3D images. T1w sequences are more likely to show mature scar tissue within a core lesion, whereas they may appear to resolve completely on T2w sequences. We used T2w images to accentuate iron-labeled cell artifacts, which also demonstrated early closure of the tendon gap. These observations are likely associated with a transition from immature granulation tissue to fibrous scar. As histology revealed large amount of disorganized, fibrous scar tissue at 28 weeks in both treated and control groups, it is unlikely

that the low MSI observed on T2w sequences correlated to restored tendon function. Without T1w sequences it is difficult to comment on the chronicity of these lesions, but it would be useful to assess in the future. Although our measures of MRI signal detected significant differences compared to controls, we believe that biomechanical measurements and additional sequences that account for the development of naïve scar tissue may be needed to confirm these findings. This may help to define long-term characteristics that vary between control and MSC-treated lesions.

New research efforts have been made to investigate the benefits of systemic or regional, intravenous delivery of MSCs to exploit their effects on injury modulation.[28] This is particularly relevant in light of the data suggesting relatively low survival and retention rates following direct injection into an orthopedic lesion.[8; 9] A study in a murine model of femoral fracture showed proportionally less apoptotic MSCs were found after systemic delivery compared to local delivery.[28] The change in signal intensity change between 2 and 6 weeks suggests some cells persist beyond 14 days, which contradicts the notion that <5% of the initial population remains by this time.[9; 15; 17] This may be due to the peripheral localization of the MSCs in the nutrient rich fascia.

Major findings from this study include that MSCs do not likely migrate into the lesions over time, and that lesions appear to resolve with greater improvement at 6 weeks in treated groups. However both treated and untreated groups appear to achieve equal lesion resolution at 28 weeks. Movement of SPIO-associated signal form the peripheral soft tissues into the lesioned area was not seen, suggesting that cells that are not initially delivered within the tendon lesion will not migrate to this location at later time points. This data agrees with other studies regarding cell migration. Following injection of $10x10^6$ MSC into an equine model with bilateral SDFT

injuries, no migration into the contralateral limb was observed.[29] Additionally, scintigraphy studies have demonstrated minimal retention into tendon lesions following regional limb perfusion.[12-14] Our data also suggest that cells survive up to 6 weeks at the maximum. Studies have demonstrated that SPIO-labeled, apoptotic cells are characterized by a constant area of T2w signal,[30] which we observed between 6 and 28 weeks. From this data we can conclude that few viable cells remain or persist beyond 6 weeks.

The high load of intracellular iron or the use of allogeneic cells may have influenced cell survival and healing. The safety of SPIO-labeling cells has been debated, although our previous work found no differences in SPIO-labeled and unlabeled MSCs.[17] This study utilized allogeneic MSCs, which may be an important factor in cell survival and healing. Although studies exist demonstrating the utility of allogeneic MSCs,[31; 32] other studies suggest preferential improvement in models treated with autologous cells.[33; 34] The safety[9; 32] and efficacy[31; 32] of allogeneic cell injections has been shown, but they have the potential to produce a low-grade immunogenic response *in vivo* which may limit the quality of healing.[35; 36] A study by Park et al. showed a significant decrease in cell survival of allogeneic MSCs as compared to autologous MSCs,[34] which may contribute to decreased healing over time. Overall, the degree of healing seen in this study may be enhanced by the use of autologous MSCs. In future tracking studies, we suggest the use of a lower iron load per cell or the use of a smaller percentage of labeled cells per dose.

N=10 animals	-3 weeks	T0	2 weeks	6 weeks	28 weeks
Long Term (N=4)	Lesion Induction	MRI	MRI		MRI, euthanasia
Short Term (N=3)	Lesion Induction	MRI	(n=1)	MRI, euthanasia	
Control (N=3)	Lesion Induction	MRI	(n=1)	MRI	MRI, euthanasia

Sheep	1, LT	2, LT	3, LT	4, LT	5, ST	6, ST	7, ST	8, C	9, C	10, C
Forelimb	S-M	No cells	M	M	M	M	M	___	___	No cells
Hindlimb	M	S-M	S-M	S-M	S-M	S-M	S-M	No cells	No cells	No cells

Long term: n_{SPIO}= 4; n_{MSC}= 3
Short term: n_{SPIO}= 3; n_{MSC}= 3
Control: n= 5

Table 5.1 (top). Schedule for MRI of treatment groups.

Table 5.2 (bottom). Schedule for MSC injections of individual sheep.

Sequence, plane	PD, sagittal	PD, transverse	TRUFI, sagittal and dorsal	T2*, transverse	MSE T2, sagittal
TR (ms)	1830	4010	11.8	695	400
TE (ms)	56	53	5	22.5	4.8, 13, 21.3, 29.6, 37.8
Slice thickness (mm)	2.5	3.0	0.3	2.5	2.5
Flip angle	150	143	28	30	60
FOV (cm)	16x16	12x12	11x16	12.2x15	11.4x14
Matrix size	320x320	256x256	352x512	260x320	260x320

Table 5.3. MRI parameters of relevant MRI sequences.

CSA		lnCSA		actual CSA, mm^2	
Treatment	Time (weeks)	Mean	Std. Error	95% Confidence Interval	
				Lower Bound	Upper Bound
control	2	3.483	0.09	27.221	38.939
	6	3.610	0.039	34.022	40.165
	28	3.437	0.036	28.789	33.582
MSC	2	3.688	0.043	36.598	43.598
	6	3.483	0.045	29.696	35.659
	28	3.732	0.051	37.751	46.247
S-MSC	2	3.640	0.033	35.623	40.772
	6	3.723	0.054	37.114	46.155
	28	3.452	0.035	29.371	33.954

Table 5.4. Tendon cross sectional area data

SD		lnSD		actual SD	
Treatment	Time (weeks)	Mean	Std. Error	95% Confidence Interval	
				Lower Bound	Upper Bound
control	2	4.181	0.215	42.606	100.585
	6	4.161	0.16	45.559	90.288
	28	3.593	0.151	26.233	50.400
MSC	2	4.744	0.146	84.690	156.022
	6	3.968	0.168	37.040	75.490
	28	2.969	0.16	14.027	27.058
S-MSC	2	4.632	0.165	73.113	144.315
	6	.#	.		
	28	3.533	0.136	25.559	45.833

Table 5.5. Standard deviation data. (#, This level combination of factors is not observed, thus the corresponding population marginal mean is not estimable)

SNR		lnSNR		actual SNR	
Treatment	Time (weeks)	Mean	Std. Error	95% Confidence Interval	
				Lower Bound	Upper Bound
control	2	1.810	0.201	4.088	9.143
	6	1.753	0.154	4.170	7.988
	28	1.352	0.146	2.832	5.270
MSC	2	2.073	0.14	5.936	10.644
	6	1.905	0.163	4.773	9.450
	28	.716	0.152	1.498	2.795
S-MSC	2	2.334	0.159	7.448	14.296
	6	.#	.		
	28	1.010	0.133	2.071	3.636

Table 5.6. Signal to noise ratio (SNR) data. (#, This level combination of factors is not observed, thus the corresponding population marginal mean is not estimable)

SDNR		lnSDNR		actual SDNR	
Treatment	Time (weeks)	Mean	Std. Error	95% Confidence Interval	
				Lower Bound	Upper Bound
control	2	3.515	0.26	19.866	56.940
	6	3.439	0.219	19.590	49.501
	28	3.029	0.21	13.210	32.362
MSC	2	4.248	0.195	46.109	106.166
	6	3.769	0.227	26.950	69.756
	28	2.581	0.207	8.551	20.389
S-MSC	2	4.467	0.218	55.257	137.277
	6	.#	.		
	28	3.182	0.192	15.943	36.416

Table 5.7. Signal difference to noise ratio (SDNR) data. (#, This level combination of factors is not observed, thus the corresponding population marginal mean is not estimable)

A.

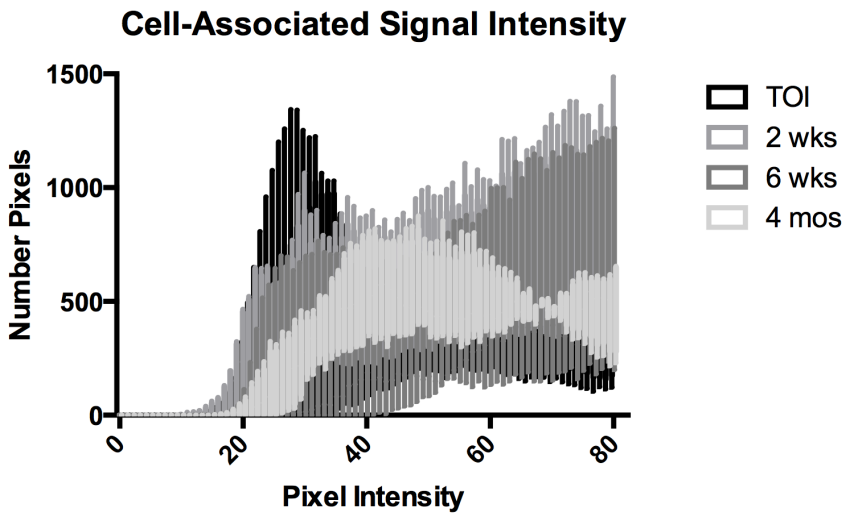

B.

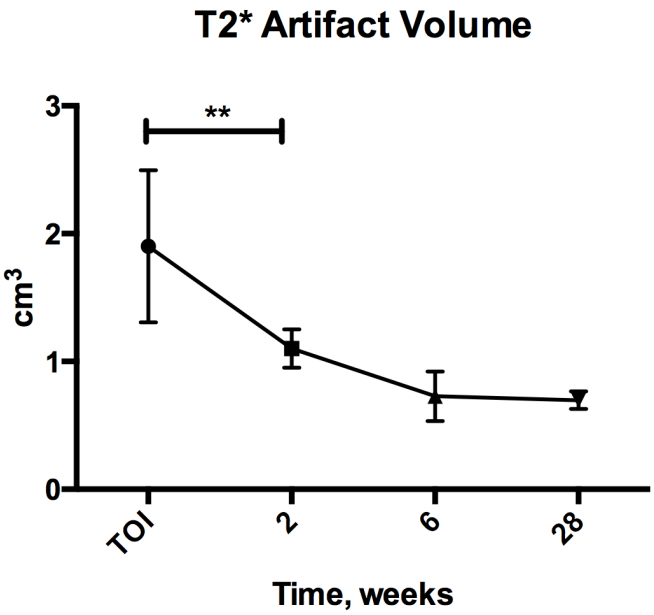

Figure 5.1. Quantification of MRI-associated artifacts. A) Cell artifacts from T2*w, transverse images in tissue surrounding tendon become smaller and more diffuse over time. Pixel intensity representative of a scale from 1-255, 255 is white and 1 is black. Lowest values likely associated with iron-labeled cells, but may also include hemorrhage or other low intensity tissue characteristics. B) Artifact changes from dorsal T2*w, MSE images show that cells diminish over 28 weeks with most rapid changes over first 2 weeks (**$p<0.01$). 6 to 28 weeks does not appear to change and likely indicates residual signal from dead cells or exocytosed iron particles.

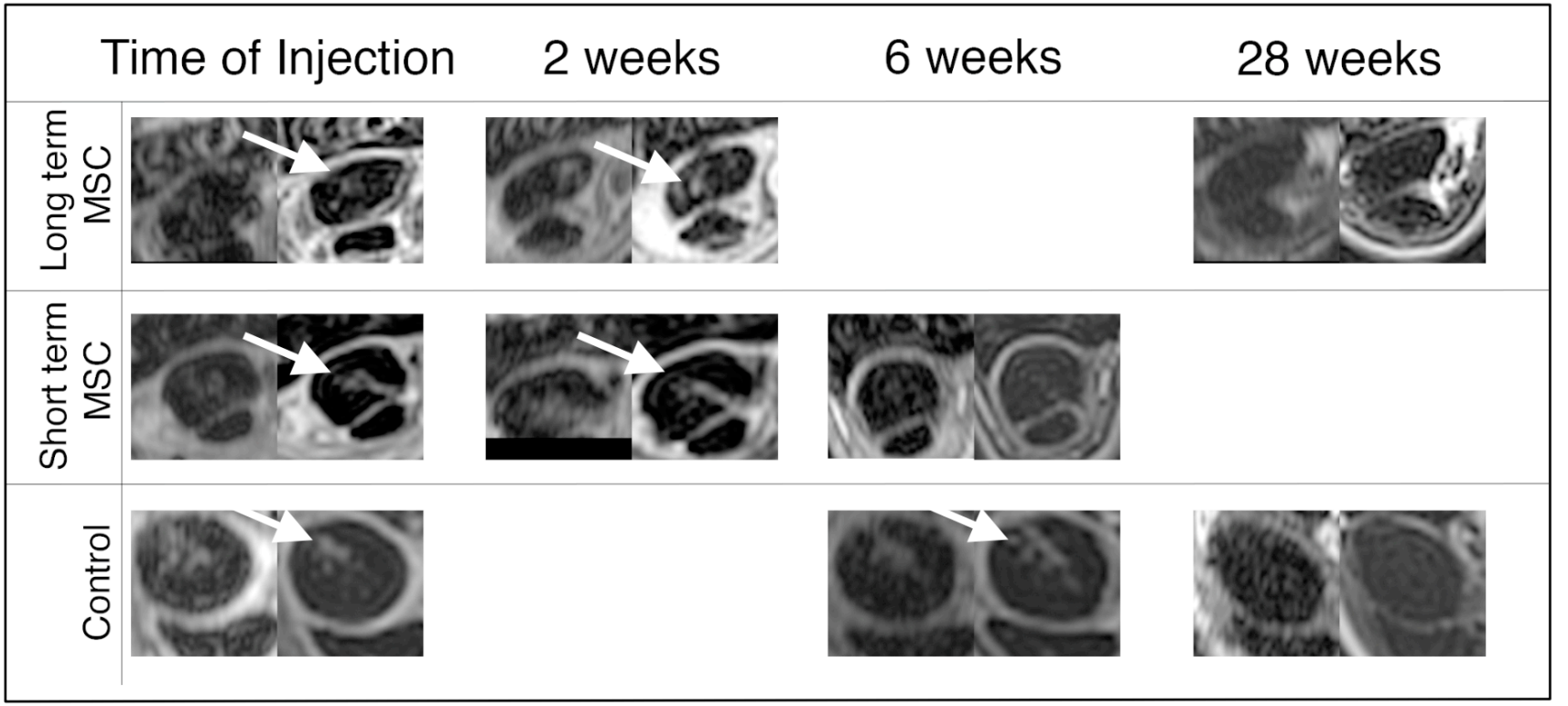

Figure 5.2. Examples of DDFT lesions over time. Lesions are visible as bright areas within the DDFT (arrows). TRUFI images are on the left, and PD images are on the right. Leions appear more conspicuous in PD images. Control lesions tend to persist longer than treated lesions and were more evident at 6 weeks. Lesions are not discernible in control or treated tendons at 28 weeks.

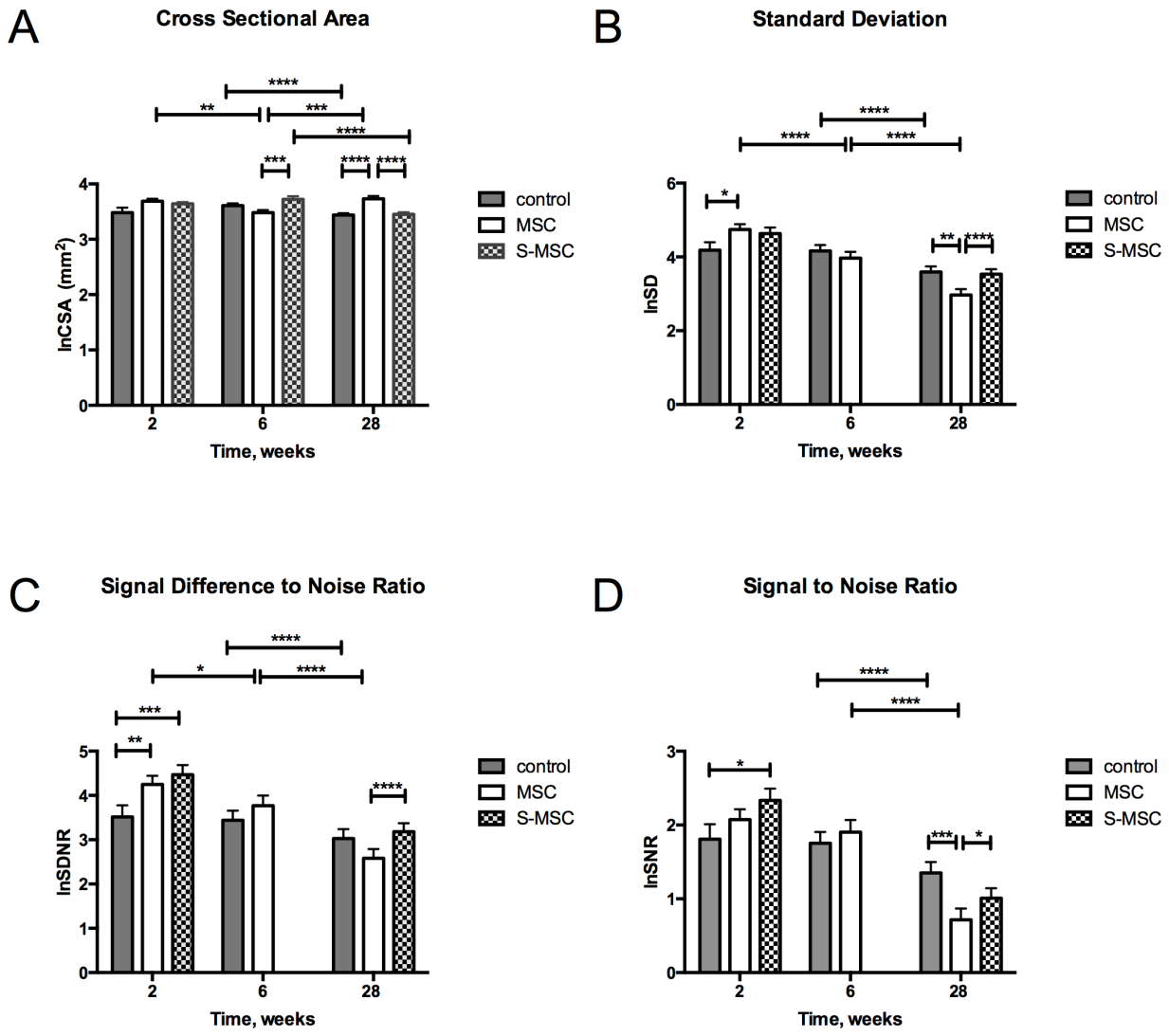

Figure 5.3. Tendon measurements. A) cross-sectional area, B) standard deviation, C) signal difference to noise ratios, and D) signal to noise ratios over time in control cells, MSCs, and SPIO-labeled MSCs (S-MSC). (*p<0.05, **p<0.01,***p<0.001,****p<0.0001)

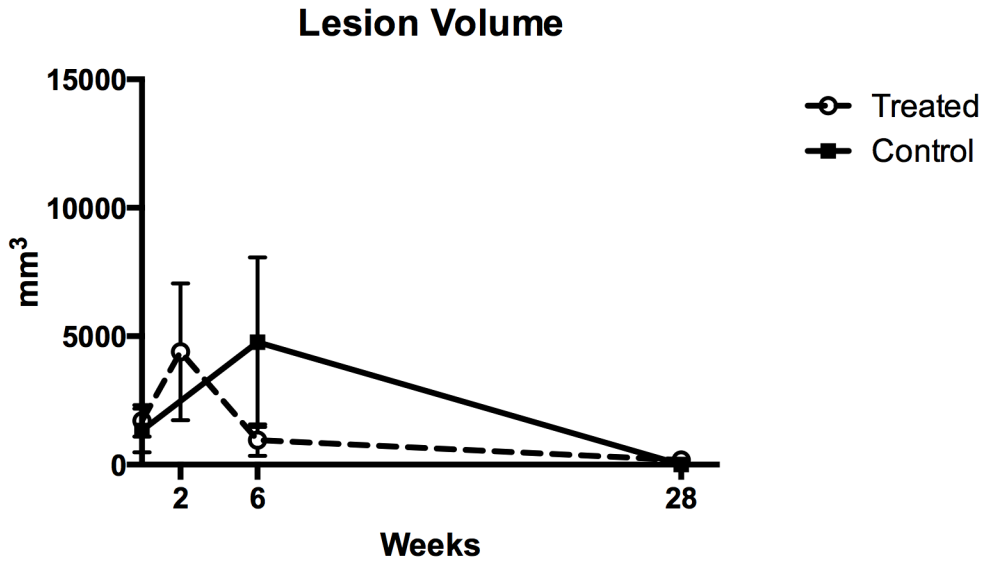

Figure 5.4. Lesion volume measurements.

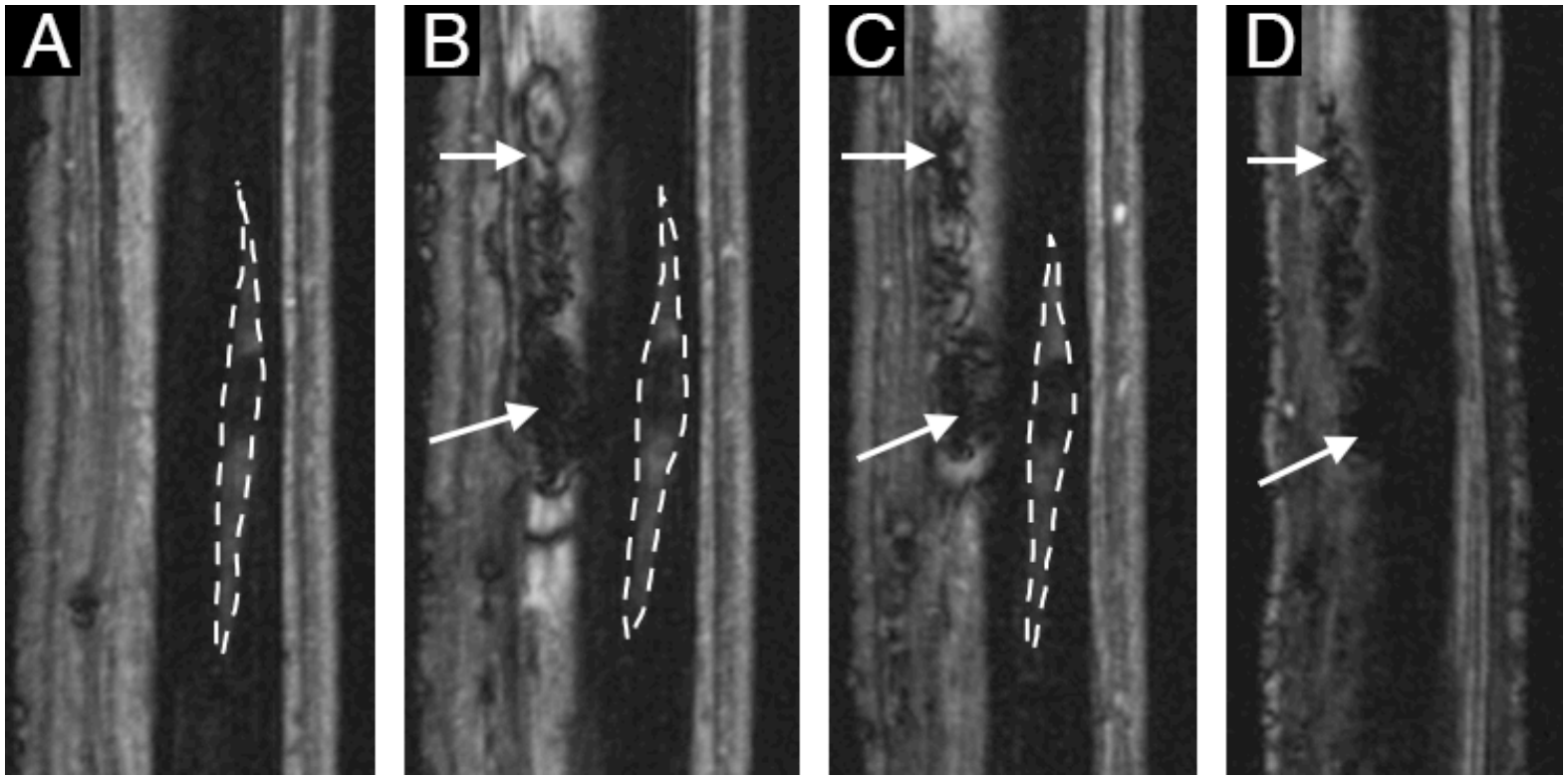

Figure 5.5. MRI of cell migration. Sequential TRUFI images representative of a long-term, treated sheep A) pre-injection, B) immediately post-injection, C) 2 weeks, and D) 28 weeks following treatment. Lesion is outlined by the dotted line and is not differentiable from surrounding, normal tendon at 28 weeks. Cell artifact does not appear to re-distribute from surrounding fascia into tendon lesion at 2 weeks. Arrows indicate proximal and distal sections of iron-

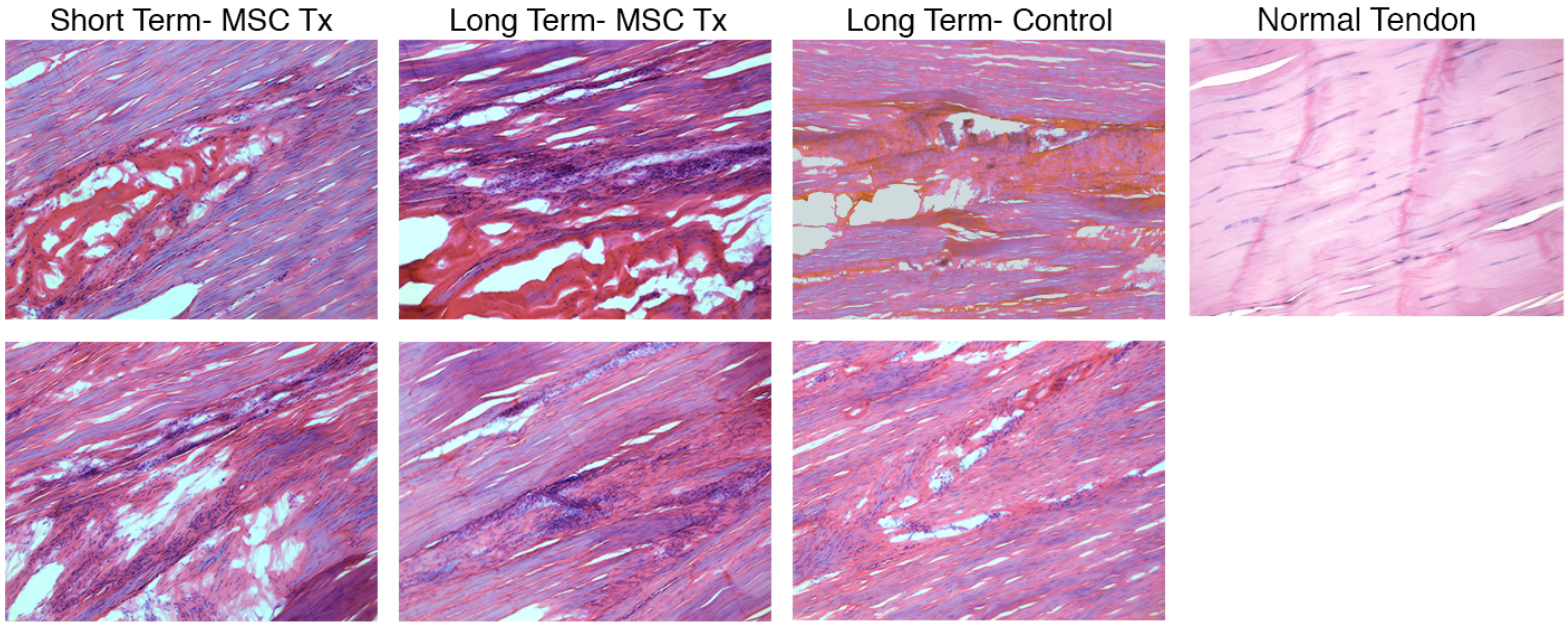

Figure 5.6. H&E histological sections. Representative of 6 (short-term) and 28 weeks (long-term and control) at 10x, demonstrating more focal (top) and more diffusely characterized lesions (bottom). Substantial collagenous disruption and increased cellularity is visible in all sections.

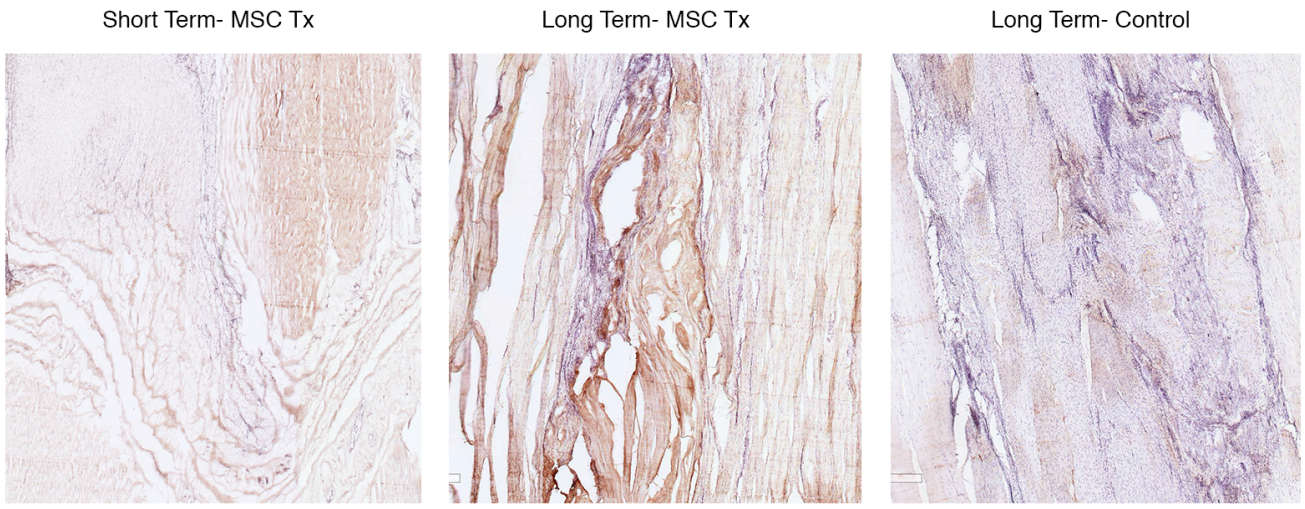

Figure 5.7. Collagen I immunohistochemistry. Representative of 6 weeks (short-term) and 28 weeks (long-term and control). Substantial collagen I deposition is seen at all time points, but may be increased in treated groups and at later time points.

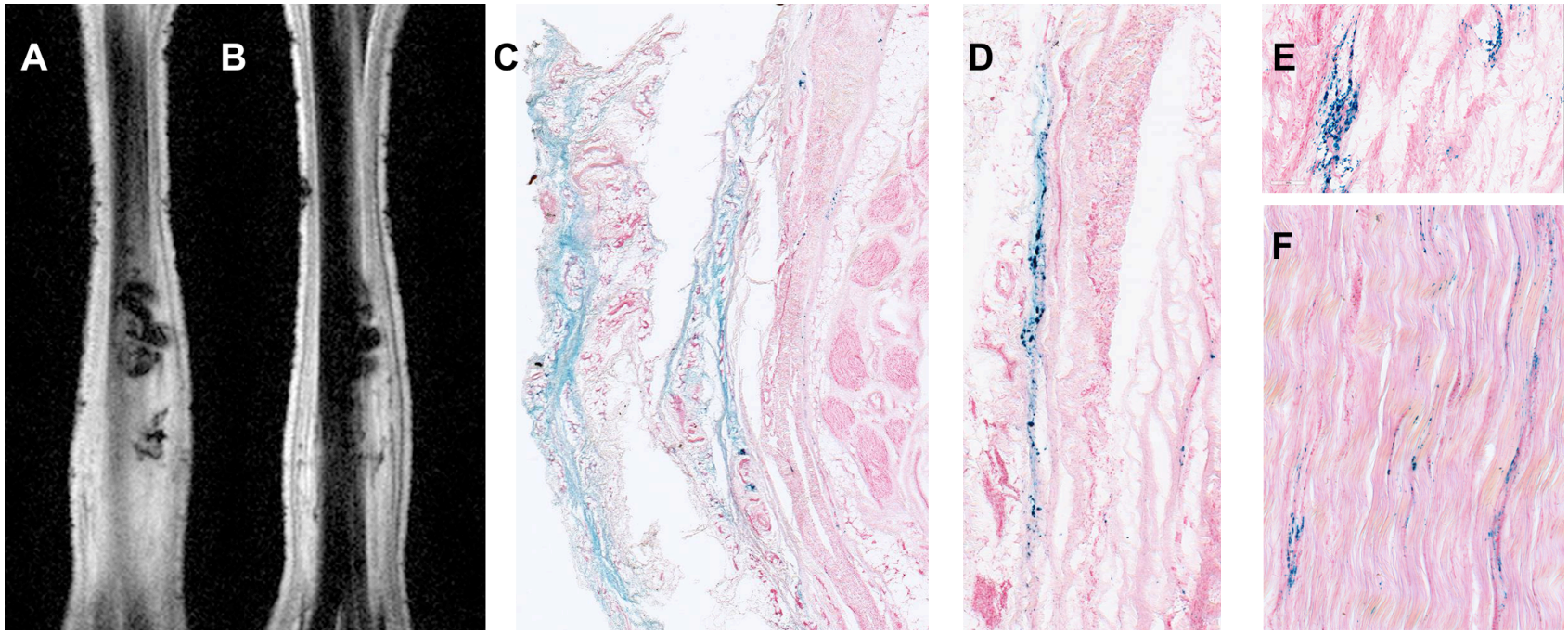

Figure 5.8. Prussian blue histology. Staining associated with iron-labeled cells at 6 weeks post-injection. MRI images on left demonstrate artifact in A) surrounding fascia and B) tendon and corresponding histology in C,D,E) surrounding fascia and F) tendon.

References

1. Crovace A, Lacitignola L, Rossi G, et al. 2010. Histological and immunohistochemical evaluation of autologous cultured bone marrow mesenchymal stem cells and bone marrow mononucleated cells in collagenase-induced tendinitis of equine superficial digital flexor tendon. Vet Med Int 2010:250978.

2. Smith RK, Werling NJ, Dakin SG, et al. 2013. Beneficial effects of autologous bone marrow-derived mesenchymal stem cells in naturally occurring tendinopathy. PLoS One 8:e75697.

3. Crovace A, Lacitignola L, Francioso E, et al. 2008. Histology and immunohistochemistry study of ovine tendon grafted with cBMSCs and BMMNCs after collagenase-induced tendinitis. Vet Comp Orthop Traumatol 21:329-336.

4. Mareschi K, Castiglia S, Sanavio F, et al. 2015. Immunoregulatory effects on T lymphocytes by human mesenchymal stromal cells isolated from bone marrow, amniotic fluid, and placenta. Experimental hematology.

5. Nasef A, Chapel A, Mazurier C, et al. 2007. Identification of IL-10 and TGF-beta transcripts involved in the inhibition of T-lymphocyte proliferation during cell contact with human mesenchymal stem cells. Gene expression 13:217-226.

6. Tan SL, Ahmad RE, Ahmad TS, et al. 2012. Effect of Growth Differentiation Factor 5 on the Proliferation and Tenogenic Differentiation Potential of Human Mesenchymal Stem Cells in vitro. Cells Tissues Organs.

7. Violini S, Ramelli P, Pisani LF, et al. 2009. Horse bone marrow mesenchymal stem cells express embryo stem cell markers and show the ability for tenogenic differentiation by in vitro exposure to BMP-12. BMC Cell Biol 10:29.

8. Guest DJ, Smith MR, Allen WR. 2010. Equine embryonic stem-like cells and mesenchymal stromal cells have different survival rates and migration patterns following their injection into damaged superficial digital flexor tendon. Equine Vet J 42:636-642.

9. Guest DJ, Smith MR, Allen WR. 2008. Monitoring the fate of autologous and allogeneic mesenchymal progenitor cells injected into the superficial digital flexor tendon of horses: preliminary study. Equine Vet J 40:178-181.

10. Geburek F, Mundle K, Conrad S, et al. 2016. Tracking of autologous adipose tissue-derived mesenchymal stromal cells with in vivo magnetic resonance imaging and histology after intralesional treatment of artificial equine tendon lesions - a pilot study. Stem Cell Res Ther 7:21.

11. Berner D, Brehm W, Gerlach K, et al. 2016. Longitudinal Cell Tracking and Simultaneous Monitoring of Tissue Regeneration after Cell Treatment of Natural Tendon Disease by Low-Field Magnetic Resonance Imaging. Stem cells international 2016:1207190.

12. Trela JM, Spriet M, Padgett KA, et al. 2014. Scintigraphic comparison of intra-arterial injection and distal intravenous regional limb perfusion for administration of mesenchymal stem cells to the equine foot. Equine Vet J 46:479-483.

13. Spriet M, Buerchler S, Trela JM, et al. 2015. Scintigraphic tracking of mesenchymal stem cells after intravenous regional limb perfusion and subcutaneous administration in the standing horse. Vet Surg 44:273-280.

14. Becerra P, Valdes Vazquez MA, Dudhia J, et al. 2013. Distribution of injected technetium(99m)-labeled mesenchymal stem cells in horses with naturally occurring tendinopathy. J Orthop Res 31:1096-1102.

15. Lacitignola L, Staffieri F, Rossi G, et al. 2014. Survival of bone marrow mesenchymal stem cells labelled with red fluorescent protein in an ovine model of collagenase-induced tendinitis. Vet Comp Orthop Traumatol 27:204-209.

16. Schramme M, Hunter S, Campbell N, et al. 2010. A surgical tendonitis model in horses: technique, clinical, ultrasonographic and histological characterisation. Vet Comp Orthop Traumatol 23:231-239.

17. Scharf A, Holmes S, Thoresen M, et al. 2015. Superparamagnetic iron oxide nanoparticles as a means to track mesenchymal stem cells in a large animal model of tendon injury. Contrast Media Mol Imaging.

18. Schramme M, Kerekes Z, Hunter S, et al. 2010. Mr Imaging Features of Surgically Induced Core Lesions in the Equine Superficial Digital Flexor Tendon. Veterinary Radiology & Ultrasound 51:280-287.

19. Watts AE, Yeager AE, Kopyov OV, et al. 2011. Fetal derived embryonic-like stem cells improve healing in a large animal flexor tendonitis model. Stem Cell Res Ther 2:4.

20. Schnabel LV, Lynch ME, van der Meulen MC, et al. 2009. Mesenchymal stem cells and insulin-like growth factor-I gene-enhanced mesenchymal stem cells improve structural aspects of healing in equine flexor digitorum superficialis tendons. J Orthop Res 27:1392-1398.

21. Pacini S, Spinabella S, Trombi L, et al. 2007. Suspension of bone marrow-derived undifferentiated mesenchymal stromal cells for repair of superficial digital flexor tendon in race horses. Tissue Eng 13:2949-2955.

22. Vanel M, Olive J, Gold S, et al. 2012. Clinical significance and prognosis of deep digital flexor tendinopathy assessed over time using MRI. Veterinary radiology & ultrasound : the official journal of the American College of Veterinary Radiology and the International Veterinary Radiology Association 53:621-627.

23. Fukawa T, Yamaguchi S, Watanabe A, et al. 2015. Quantitative Assessment of Tendon Healing by Using MR T2 Mapping in a Rabbit Achilles Tendon Transection Model Treated with Platelet-rich Plasma. Radiology 276:748-755.

24. Marsolais D, Cote CH, Frenette J. 2001. Neutrophils and macrophages accumulate sequentially following Achilles tendon injury. J Orthop Res 19:1203-1209.

25. Manning CN, Martel C, Sakiyama-Elbert SE, et al. 2015. Adipose-derived mesenchymal stromal cells modulate tendon fibroblast responses to macrophage-induced inflammation in vitro. Stem Cell Res Ther 6:74.

26. Cho DI, Kim MR, Jeong HY, et al. 2014. Mesenchymal stem cells reciprocally regulate the M1/M2 balance in mouse bone marrow-derived macrophages. Experimental & molecular medicine 46:e70.

27. Abumaree MH, Al Jumah MA, Kalionis B, et al. 2013. Human placental mesenchymal stem cells (pMSCs) play a role as immune suppressive cells by shifting macrophage differentiation from inflammatory M1 to anti-inflammatory M2 macrophages. Stem Cell Rev 9:620-641.

28. Huang S, Xu L, Sun Y, et al. 2015. The fate of systemically administrated allogeneic mesenchymal stem cells in mouse femoral fracture healing. Stem Cell Res Ther 6:206.

29. Carvalho AM, Yamada AL, Golim MA, et al. 2014. Evaluation of mesenchymal stem cell migration after equine tendonitis therapy. Equine Vet J 46:635-638.

30. Henning TD, Gawande R, Khurana A, et al. 2012. Magnetic Resonance Imaging of Ferumoxide-Labeled Mesenchymal Stem Cells in Cartilage Defects: In Vitro and In Vivo Investigations. Mol Imaging 11:197-209.

31. Arinzeh TL, Peter SJ, Archambault MP, et al. 2003. Allogeneic mesenchymal stem cells regenerate bone in a critical-sized canine segmental defect. J Bone Joint Surg Am 85-a:1927-1935.

32. Van Loon VJ, Scheffer CJ, Genn HJ, et al. 2014. Clinical follow-up of horses treated with allogeneic equine mesenchymal stem cells derived from umbilical cord blood for different tendon and ligament disorders. The Veterinary quarterly 34:92-97.

33. Hare JM, Fishman JE, Gerstenblith G, et al. 2012. Comparison of allogeneic vs autologous bone marrow-derived mesenchymal stem cells delivered by transendocardial injection in patients with ischemic cardiomyopathy: the POSEIDON randomized trial. Jama 308:2369-2379.

34. Jung DI, Ha J, Kang BT, et al. 2009. A comparison of autologous and allogenic bone marrow-derived mesenchymal stem cell transplantation in canine spinal cord injury. Journal of the neurological sciences 285:67-77.

35. Tano N, Kaneko M, Ichihara Y, et al. 2016. Allogeneic Mesenchymal Stromal Cells Transplanted Onto the Heart Surface Achieve Therapeutic Myocardial Repair Despite Immunologic Responses in Rats. Journal of the American Heart Association 5.

36. Poncelet AJ, Vercruysse J, Saliez A, et al. 2007. Although pig allogeneic mesenchymal stem cells are not immunogenic in vitro, intracardiac injection elicits an immune response in vivo. Transplantation 83:783-790.

CHAPTER 6

CONCLUSION

The overall objective of this study was to establish a safe and effective means of tracking MSCs in equine and ovine models of tendonitis with the potential for clinical translation. The first two studies focused on validating the SPION labeling method in both ovine and equine MSCs prior to use *in vivo.* Differences in cell health were present between the two species, most notably due to varying degrees of uptake. This emphasizes the need to validate individual cell lines with each labeling product. Following treatment with 25 μg SPIONs/mL overnight, ovine cells were recorded to carry 10 pg/cell, whereas equine cells carried 19 pg/cell. Equine cells with 19 pg/cell demonstrated inferior cell characteristics as compared to controls, so the incubation time was reduced to 4 hours. This resulted in approximately 4 pg Fe/cell and no differences between labeled equine MSCs were noted as compared to controls.

On MRI, susceptibility artifacts were disproportionately large within ovine tendon following the injection of $10x10^6$ cells labeled with 10 pg/cell (Chapter 5). Artifacts overlapped tendon lesions and obscured substantial amounts of anatomical detail. We suggest maintaining a lower dose of iron (<5 pg) per cell, as susceptibility artifacts were more appropriate in equine tendons containing cells labeled with 4 pg/cell. Another option is to only label a portion of the injected cells. Interestingly, increased SNR and SDNR were observed in SPION-MSC tendons in the final sheep study and further encourage the cautionary use of high SPION loads *in vivo.* As

conflicting reports on chondrogenic differentiation exist, the potential for tenogenic impairment should not be ignored.

Through this study, we learned that MSCs are highly delocalized following injection and undergo minimal migration *in vivo*. Movement of SPION-associated signal from the peripheral soft tissues into the lesioned area was not seen, suggesting that cells that are not initially delivered within the tendon lesion do not make it to this location at later time points. Cell signal in the peripheral soft tissues did not change after 6 weeks, suggesting no survival beyond this point. The signal flux between 2 and 6 weeks brings to question if there are substantial numbers of MSCs remaining at this time. If so, previous reports of little to no cell retention beyond 14 days may apply only to the intratendinous, collagenous zones and not to the surrounding tissue.

Regardless of low migration and survival, the cells were still able to improve several parameters of healing as measured by MRI. Allogeneic MSCs may provide substantial therapeutic benefits to acute tendon injuries. Biomechanical testing is likely the most important missing component of finalizing these conclusions in large animals, and was unfortunately omitted due to the use of large tissue sections for histology. Further comparisons of MRI data to histological and biomechanical data can help support the development of robust, longitudinal methods for measuring patient outcomes and reduce the number of terminal studies needed.

Our models demonstrate several deficits of using SPIONs to track cells within tendon and support the exploration of alternative tracking methods. Firstly, the inherent low signal intensity of tendon makes it extraordinarily difficult to discern tendon fibers from SPION signal within the lesion, particularly at later time points. Fortunately, an inadvertent discovery in this work was that many cells reside in the tissues surrounding the tendon as opposed to within the lesion following injection. These cells likely engage in chemical signaling and host cell recruitment to

promote healing as opposed to differentiating into tenocytes or acting through direct cell-cell contact at the site of injury. Secondly, the signal from SPIONs cannot be quantified and correlated to cell number and becomes dissociated from live cells at an indeterminate time point *in vivo* through cell death or exocytosis. Lastly, our long term study demonstrated that a high dose of SPIONs may cause low-grade inflammation within the host tissue and may associated with retardation of healing.

Alternative labeling methods such as GFP and optical dyes that require histological evaluation have been used with some success. However with the broad delocalization of cells, large tissue biopsies and labor intensive sectioning and staining are required, especially in large animals. Radionuclide labeling has also been tried, but is only effective for very short-term studies, requires specialized equipment and high safety precautions, and demonstrates higher cell toxicity than SPIONs. Optical and fluorescent imaging has been performed in mice, but the thickness of the skin and size of the animal makes these technically difficult, if not impossible in larger animals.

Future tendon studies would benefit from the use of positive, MRI contrast media, as MRI has proven to be an excellent tool for measuring tendon healing concurrently with cellular behavior. Our lab briefly pursued a Gd-based detection method, but free ions were associated with fibrotic events within the injured tendons and the technique was abandoned due to safety concerns. Other Gd-based products have been met with some success and this may be particularly relevant in tendon where the bright, T1 contrast can easily be distinguished from other tissues. Overall, SPIONs offered an acceptable approach for monitoring MSCs, but an alternative such as a positive contrast, MRI-based reporter gene will likely prove to be a superior option. These types of studies can be performed on clinical scanners with readily available

equipment at a low-risk to the patient. The ultimate goal is to monitor cell behavior in veterinary patients, providing preclinical data for human trials as well as data to veterinarians and clientele about the behavior of cells and mechanisms of healing *in vivo.*

Future studies should also rely more heavily on the non-terminal study of veterinary patients with naturally occurring disease. Although iatrogenic models provide an excellent means to study tendon injuries, there are several deficits. Collagenase-injection models produce an enzymatic degradation of collagen fibers that spans an undefined time period that may continue on as therapeutic efforts are made. The tendency of collagenase to melt the fibers also produces a unique, inflammatory response that is not characteristic of the localized, inflammatory infiltrate found in acute disease or the lack of any inflammatory components in chronic disease. Mechanical models produce a pathologic process more similar to acute disease, although natural disease is often preceded by some degree of degeneration and matrix breakdown. Mechanical models also require an entry point through the skin and tendon perimeter. This provides a theoretical point of exit for any therapies that are applied at a later time and asymmetrically weakens the mechanical integrity of the edge.

In the clinic, conservative treatments are often applied first. Patients are not seen until healing processes are underway and a generous amount of scar tissue has already been produced. Regenerative treatments are not usually applied as the first line of treatment, although this is changing. However, it is still rare for patients to be injected 1-2 weeks post-injury. Although studies indicate that injection at these early time points leads to MSC repair and healing, injections at more realistic time points of 30-45 days post-injury are needed. These patients have a unique micro-environment for the MSCs, where degenerative processes from overuse, matrix

breakdown, and inflammatory infiltrate occur simultaneously. This combination may change the results and changes we see in current models.